UNIVERSITY OF BIRMINGHAM

A Modelling Study of the Atmospheric Role of Iodine in the Coastal Marine Boundary Layer

Master of Philosophy

Lucy Jane Concannon-Banner

September 2009

Abstract

This study modelled the concentration of iodine species using results obtained from a field measurement campaign called POMORIS (Point Measurements of Reactive Iodine Species). These measurements were obtained from the coastal marine environment of Mace Head, Ireland in Summer 2007.

The modelled results have shown that in such an environment, the presence of iodine species has a significant impact upon the oxidising capacity of the troposphere, especially in the first minute following I_2 emission. This result has implications for the interpretation of field measurements of HO_x, NO_x and related species at the Mace Head site, and the modelling approach which is required to interpret such data. This is contrary to previous findings where the effect was only determined at intervals of 15 minutes and more.

For My Loving Family.

Acknowledgements

Firstly I would like to thank my supervisor Dr William Bloss for the endless support throughout this project. Bill introduced me to this area of chemistry and I have thoroughly enjoyed my research.

Thank you to everyone who worked on the NAMBLEX campaign for allowing me to use your data, especially Roisin Commane and Steve Ball.

I'd like to thank Kate and Salim for your continuous patience and willingness to help; trips to your office were always entertaining!

I have learnt many important facts from Dr Ruth Harrison, I am very grateful for your help!

My many thanks to office 412 (and Emma who should have been in our office!); you have been fun to work with. Special thanks to Vivien and Charlie who always managed to sort out my computer problems. You've been great.

A massive thank you to my fantastic friends: Harpreet, Nagina, Tanz and Yasmin. Your help and support is always appreciated.

Lastly, the most important people to thank are my family. You have made this year possible for me. Thank you for your guidance and for always listening to me (not that you have choice sometimes!). You always show an interest in what I do and support me 100%. A special thank you to my husband, David, you're my rock.

Contents

1 INTRODUCTION 1

1.1 Regions of the Atmosphere 3

1.1.1 Chemical Composition of the Troposphere 5

1.2 Pollution in the Troposphere 7

1.2.1 The Role of OH in Oxidation Reactions 15

1.3 The Presence of Halogen Species in the Troposphere 17

1.3.1 The Presence of Chlorine in the Troposphere 18

1.3.2 The Presence of Bromine in the Troposphere 19

1.3.3 The Presence of Iodine in the Troposphere 21

1.4 Recent Measurements of Iodine Species 24

1.4.1 Measurements of Iodine Species during NAMBLEX 26

1.4.2 Measurements of Iodine Species during POMORIS 28

2 METHODS 30

2.1 The Use of Modelling in Atmospheric Chemistry 30

3 RESULTS 45

3.1 Modelled Data during the Daytime 50

3.1.1 Scenario A1: Low low tide, the Whole Emission Zone 50

3.1.2 Scenario A2: Low low tide, the Concentrated Emission Zone 55

3.1.3 Scenario B: High low tide, the Whole Emission Zone 58

3.2 Modelled Data during the Night 60

3.2.1 Scenario C1: Low low tide, the Whole Emission Zone 60

3.2.2 Scenario C2: Low low tide, the Concentrated Emission Zone 63

4 SENSITIVITY STUDY 66

4.1 Additional Reactions used in the Sensitivity Study 66

4.2 Changes to the Total Aerosol Surface Area 69

4.3 A Change in Photolysis Yield for the reaction of OIO 71

4.4 Altering the Rate of Photolysis of $IONO_2$ 73

4.5 Alternative Products for the Reaction IO + CH_3O_2 74

4.6 Investigating the Thermal Stability of $IONO_2$ 77

4.7 Summary of Sensitivity Study 78

5 DISCUSSION 83

5.1 Previous Modelling Studies 84

5.2 The Models Ability to Replicate Observations 86

5.3 The Impact of Iodine Species on HO_x and NO_x 88
5.4 The Evolution of Iodine Species 91
5.5 An Environment with Higher Concentrations of NO_x 92
5.6 Estimating the Global Iodine Emission 94
5.7 Iodine Species in the Aerosol Phase 95
5.8 Limitations of This Study 96
5.9 Further Work 97
6 CONCLUSION 99
7 REFERENCES 100
8 Appendices 103
8.1 DMS Oxidation 103
8.2 Halogen Reaction Scheme 105
8.3 Photolysis rates 110
8.4 Heterogeneous Processes 111
8.5 Sections of the Model Used in this Study 119

List of Figures

Figure 1.1: The regions of the atmosphere showing how temperature varies with altitude. [2].....3
Figure 1.2: Oxidation processes in the atmosphere for CH_4 and CO. (Adapted from Bloss 2007).[11] 9
Figure 1.3: Production rate of Ozone 11
Figure 1.4: Primary and secondary aerosol sources.[13] 13
Figure 1.5: The release of halogens from the ocean.[18] 19
Figure 1.6: Oxidation processes in the troposphere, including iodine chemistry. (Adapted from Bloss 2007).[11].....23
Figure 1.7: An aerial photograph of Mace Head (taken by R. M. Purvis) and the observation station (taken by D. E. Heard).[41].....25
Figure 1.8: Top: The location of Croaghnakeela Island. Bottom: The layout of the site at Mace Head. 27
Figure 1.9: Instruments employed at Mace Head, (courtesy of Anna Hollingsworth University of Leicester). 29
Figure 2.1: Pie chart to show the percentage contribution of each VOC to OH loss. 34
Figure 2.2: Illustration of the Solar Zenith Angle (SZA). 36
Figure 2.3: Model scenario. 110 m is the distance from the start of the emission zone (i.e lowest low-tide mark) to the observation station. 50 m indicates the estimated extent of the whole potential emission zone and 10 m indicates the estimated concentrated emission zone (see below). 38
Figure 2.4: Spin-up time. 39
Figure 2.5: Spin-up time; simulation results after one hour (3600 seconds).....40
Figure 2.6: The difference between low low tide and high low tide.....43
Figure 3.1: Modelled Data for HO_x and NO_x at Midday with no Iodine. 45
Figure 3.2: Modelled Data for HO_x and NO_x at Midnight with no Iodine 46
Figure 3.3: IO concentrations and tide height recorded at Mace Head, Ireland (Courtesy of Roisin Commane University of Leeds). 47
Figure 3.4: Measured I_2 data from POMORIS (courtesy of Steve Ball, University of Leicester).....47
Figure 3.5: Measured I_2, IO and I atom data from POMORIS. The black dotted line indicates the point at midday on 29/08/07 which was used for the model simulations.[51] 48
Figure 3.6: Measured IO and Tide Height Data from Mace Head, Ireland during POMORIS. 49
Figure 3.7: Modelled Iodine species for Simulation A1. 50
Figure 3.8: Modelled HO_x and NO_x Species Concentrations for Simulation A1. 52
Figure 3.9: Modelled Data of OH and I_2 for Simulation A1. 53
Figure 3.10: Modelled HO_2 and HOI Data for Simulation A1. 53
Figure 3.11: Modelled Data for the Production Pathway of HOI. 54
Figure 3.12: Modelled Iodine Species in the Aerosol Phase for Simulation A1. 55

Figure 3.13: Modelled Iodine Species for Simulation A2. 56
Figure 3.14: Modelled HO_x and NO_x Concentrations for Simulation A2. 56
Figure 3.15: Comparing HO_x and NO_x Data for Scenarios A1 and A2. 57
Figure 3.16: Modelled Data for Other Iodine Species. 58
Figure 3.17: Modelled Iodine Species Concentrations. 59
Figure 3.18: Modelled HO_x and NO_x Concentrations for Simulation B. 60
Figure 3.19: Modelled Iodine Concentrations for Simulation C1. 61
Figure 3.20: Modelled HO_x and NO_x Species Concentrations for Simulation C1. 62
Figure 3.21: Modelled Data for Simulation C1. 62
Figure 3.22: Modelled Concentrations for Iodine Species for Simulation C2. 63
Figure 3.23: Modelled NO_3 Data for Simulation C2. 65
Figure 3.24: Modelled Iodine Species Concentrations for Scenario C2. 65
Figure 4.1: Modelled Concentrations of I and IO including addition reactions 20-23. I (A1) and IO (A1) show the original values without the addition of any reactions. 67
Figure 4.2: Modelled Concentrations of HO_x including addition reactions 20-23. (A1) indicate the original levels of HO_x. 68
Figure 4.3: Modelled PI Data with Additional Reactions 20-23. (A1) indicate the original levels of PI. 68
Figure 4.4: Modelled Concentration of I and IO with a change in Aerosol Surface Area. (A1) indicate the original levels of I and IO. 69
Figure 4.5: Modelled Concentration of HO_x with a change in Aerosol Surface Area. (A1) indicate the original levels of HO_x. 70
Figure 4.6: Modelled PI Data with a change in Aerosol Surface Area. (A1) indicates original levels of PI. 71
Figure 4.7: Modelled I and IO Concentrations with a Change on Photolysis Yield. 72
Figure 4.8: Modelled HO_x Concentrations for the Change in Photolysis Yield. 72
Figure 4.9: Modelled PI Data for the Change in Photolysis Yield. 73
Figure 4.10: Modelled Data for I and IO Concentration with the Change in Photolysis Rate. (A1) indicate the original levels of I and IO. 74
Figure 4.11: Modelled Concentrations for I and IO for the Alternative Rates and Products for the reaction IO + CH_3O_2. 75
Figure 4.12: Modelled Concentrations for HO_x for the Alternative Rates and Products for the reaction IO + CH_3O_2. 76
Figure 4.13: Modelled PI Data for the Alternative Rates and Products for the reaction IO + CH_3O_2. 77
Figure 4.14: Modelled I and IO Data for the Investigation in Thermal Stability of $IONO_2$. 78
Figure 5.1: Measured I_2, IO and I atom data from POMORIS with Modelled Data for the Whole emission zone shown as a single point, (scenario A1). 87
Figure 5.2: Measured I2, IO and I atom data from POMORIS with Modelled Data for the Concentrated emission zone shown as a single point, (scenario A2). 88
Figure 5.3: Extended Time of Scenario A1 to 30 minutes in order to see the evolution of IO_x and PI Species. 92

Figure 5.4: Modelled Data Showing the affect of an Increased level of NO_x (100 ppb) which would be found in Polluted Environments such as Cities and many more populated coastal locations. 93
Figure 5.5: Modelled Data for Scenario A1 using 50 ppt NO_x. 94
Figure 5.6: Density (g cm^{-3}) of Aerosol Particles from NAMBLEX 2002 (courtesy of W. Bloss). 95

1 INTRODUCTION

This thesis explores the role of iodine in the lower atmosphere in a coastal marine environment. Its effects on the atmosphere's oxidising capacity are investigated.

Exploring the weather and factors influencing air quality has been of interest to scientists for several hundred years. Air quality in Britain changed dramatically at the end of the 18th and early 19th Century due to the industrial revolution. The invention and manufacture of machines soon spread throughout the world. These new processes required the use of fossil fuels such as coal which began to pollute the atmosphere in a number of ways. The most common and noticeable pollutant at this time was smog (smoke and fog), resulting in the reduction of the quality of air. This problem interested scientists encouraging them to study what might be happening to the atmosphere.[1]

A common concern for atmospheric scientists is the hole in the polar ozone layers which was first discovered in 1985.[2] This urgently required a solution to prevent the hole from getting bigger and consequently attracted much attention from scientists, the government and the media. With the ban of CFCs and some halogenated compounds this problem appears to be under control. Today, with the presence of greenhouse gases, a constant media reference to air pollution, climate change and our global carbon footprint, understanding the chemistry of our atmosphere is a key issue and main focal point for scientists. In order to assess the long term effects on our planet will be, it is essential that the chemical processes are understood in order to provide solutions and preserve the Earth.

The potential impact of halogens upon atmospheric chemistry has been recognised most commonly in association with the hole in the stratospheric ozone layer as mentioned previously. This problem occurs mostly due to chlorine containing compounds (such as Chlorofluorocarbons (CFCs)) and bromine species (such as methyl bromide (CH_3Br)). However this project is concerned with another halogen, iodine, and its importance in the troposphere. It has been suggested that the principal source of iodine to the troposphere is from seaweed emissions in marine environments.[3] Iodine was discovered in the early 19th century and shortly afterwards, it was obtained from seaweed and used to treat certain medical conditions. It continues to be used today in the drug thyroxin which is used to treat thyroid gland problems.[4]

Recent measurements confirm that iodine is emitted from seaweed at periods of low tide.[3, 5] These iodine species have short lifetimes of several seconds so the effects of these species are limited to the boundary layer. Photolysis of molecular iodine releases constituent I atoms which react with O_3 to form IO radicals. Reactions of the IO radicals may lead to the loss of O_3 which could affect the oxidising capacity of the atmosphere. Reactions of IO could also lead to the formation of particulate matter which may affect the climate.[6]

The aim of this project is to use computer modelling studies to investigate the effect of iodine species present in the troposphere upon atmospheric chemistry. Data which has been taken in previous field studies will be used to constrain the model in order to determine the behaviour of iodine species in the troposphere. This chapter will introduce the background to key physical and chemical properties of the atmosphere.

The atmospheric role of iodine compounds in the coastal marine boundary layer is also introduced.

1.1 Regions of the Atmosphere

The Earth's atmosphere is made up of the layer of gases that surround it. The atmosphere can be divided into four main regions known as the troposphere, stratosphere, mesosphere and thermosphere. These regions are separated by three boundaries: the tropopause, stratopause and mesopause which are illustrated in Figure 1.1. These regions can be defined in terms of their temperature profile.

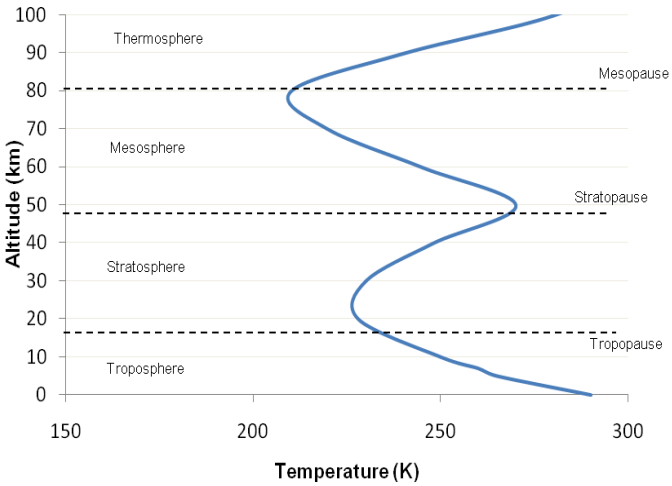

Figure 1.1: The regions of the atmosphere showing how temperature varies with altitude. [2]

In the troposphere and mesosphere temperature decreases as air expands. In these two regions this behaviour can be explained due to dynamic instability. Vertical mixing occurs rapidly, resulting in cooling as the altitude increases. [7] In the troposphere heat is transferred from the earth's surface which directly influences the air in the lower area of the troposphere.[8] At ground level the atmosphere is warmest

due to energy being emitted from the earth. The temperature profile in this region relies largely on the convection and mixing of air which occurs due to heat rising from the earth's surface.[9] However, in the stratosphere temperature generally increases with altitude. This occurs due to the presence of stratospheric ozone which absorbs sunlight and results in heating. Temperature is difficult to record in the thermosphere due to its high altitude.[2]

The troposphere is the closest region to the earth's surface with an altitude of 0-15 km. The stratosphere lies above this from 15-50 km above the earth.[8] The stratosphere contains the ozone layer which is important as the ultra violet (UV) radiation emitted by the sun is harmful to human health. The ozone layer absorbs this dangerous radiation preventing it from penetrating the troposphere.

The stratosphere is the most stable region of the atmosphere and when pollutants are transported to the stratosphere they stay there for a long time. A substance that is not normally present in the atmosphere or a substance that is present at excessively high concentrations can be described as a pollutant. Any pollution present lower down in the troposphere has a direct effect on human health and pollutants can get trapped, allowing them to build up. Emission of species such as I_2 from the earth's surface directly influences the troposphere's chemistry.

The troposphere is described as being wet in contrast to the stratosphere which is dry. This is due to the presence of water in the troposphere and this is the region where weather occurs. The troposphere, in particular the boundary layer, will be the main focus of this project.

There are two regions in the troposphere: the planetary boundary layer (PBL) and the free troposphere. The PBL is the lowermost region of the troposphere with an altitude of 100-3000 m. As the PBL is directly above the earth's surface, it is influenced by earth's very presence and the chemistry of the PBL can change and respond to the conditions (such as temperature or emissions) at the surface. The free troposphere is directly above the PBL. The PBL's thickness varies from hundreds of metres to a few kilometres. The thickness can be defined by temperature and turbulence; as the temperature of the earth's surface changes, transport processes that occur in the PBL also change and this causes turbulence. The free troposphere has a slow response to changes at the earth's surface, unlike the PBL which can respond after a few seconds.[8]

The PBL is the region of the atmosphere where all humans live; this is why tropospheric chemistry is of interest to scientists as any build up of pollution in the PBL could have serious consequences.[10]

1.1.1 Chemical Composition of the Troposphere

The main components of the atmosphere are nitrogen, oxygen, argon and water vapour. Table 1.1.1 shows the percent volume of these and other gases present in the troposphere. Species with a low percent volume such as ozone are known as trace gases. Trace species are usually represented in parts per million (ppm, 1 part in 10^6), billion (ppb, 1 part in 10^9), or trillion (ppt, 1 part in 10^{12}). It is these trace species that govern the chemistry of the atmosphere.[11] For example, methane (CH_4) is present in air at 1800 ppb and is considered a trace species; it may have a small

concentration (compared to nitrogen) but it has an important impact upon atmospheric chemistry, in contrast to nitrogen which is unreactive.

Gas Name	Concentration
Nitrogen (N_2)	78.08 % (in dry air)
Oxygen (O_2)	20.95 % (in dry air)
Water (H_2O)	0 – 4 %
Argon (Ar)	0.93 %
Gas Name	**Concentration**
Carbon Dioxide (CO_2)	390 ppm
Methane (CH_4)	~1800 ppb
Hydrogen (H_2)	550 ppb
Nitrous Oxide (N_2O)	310 ppb
Ozone (O_3)	10 – 150 ppb

Table 1.1.1: Chemical composition of the troposphere.[12]

The most important and reactive trace species are gas phase radicals. A radical is a molecular fragment with an unpaired electron. Atmospheric radicals are fast reacting species whose concentrations in the troposphere are low. They play an important role in the atmosphere's oxidising capacity.[13] The hydroxyl radical (OH) is the most important radical present in the troposphere. The main production pathway for OH radicals is *via* ozone photolysis, so highest concentrations of OH are observed during the day with the presence of sunlight. OH is a highly reactive species with a lifetime of ~0.1-2 seconds.[14] OH initiates the breakdown of most species that are released into the atmosphere. The lifetimes of a chemical species present in the troposphere are primarily calculated with respect to the concentration of OH radicals, [OH]. Essentially, [OH] governs the lifetime of some chemical pollutants present in the

atmosphere (such as CH_4). The following equation is used to calculate the lifetime of a species: $\tau = \frac{1}{k_{speciesx+OH}[OH]}$

τ = Lifetime (seconds)

k = Rate constant of the reaction of species X + OH ($molec^{-1}\ cm^3\ s^{-1}$)

$[OH]$ = Average concentration of OH radicals ($1x10^6$ molec cm^{-3})[15]

In the case of CH_4, the calculation would be:

$$\tau_{CH_4} = \frac{1}{\left(5.56\times10^{-15}\right)\left(1\times10^{6}\right)}$$

resulting in a lifetime of 5.7 years. The lifetime of a species can be defined as the time taken for the species concentration to decrease by a factor of 1/e where e is the exponential of 1 (2.718, therefore the concentration of a species decreasing by 37 %). The troposphere is a wet environment containing H_2O which gives rise to a higher concentration of OH radicals in the troposphere. This is through ozone photolysis, as it occurs in the presence of water as shown in reactions 1-2. This allows the OH radical to be used on the understanding of tropospheric chemistry.[11]

$O_3 + h\nu \rightarrow O\left(^1D\right) + O_2$ Reaction 1

$O\left(^1D\right) + H_2O \rightarrow 2OH$ Reaction 2

1.2 Pollution in the Troposphere

Environmental problems occur due to the presence of pollutants in the atmosphere. Some of these pollutants can cause health problems which is why they are studied in great detail. Changes in our environment can arise from anthropogenic activities but,

not all changes occur due to this human activity. Climate changes such as global warming have occurred due to an increase of carbon dioxide (CO_2) and other greenhouse gas (CH_4, N_2O) emissions.[7] A greenhouse gas is a gas such as CO_2 or Chlorofluorocarbons (CFCs) that absorb solar radiation in the region 5-50 μm, where most terrestrial radiation is emitted. The Earth emits infrared (IR) radiation, some of which is absorbed and re-emitted by greenhouse gases. This results in a warming of the atmosphere, known as the greenhouse effect.

There are many other different atmospheric pollutants that contribute to health problems and environmental changes. They each have a variety of sources and sinks where they can be destroyed or chemically altered. These pollutants can also affect the OH budget which could lead to dramatic changes in the atmosphere's cleansing capacity. Hence, these pollutants need to be considered.

There are many oxidation processes taking place in the troposphere as OH is highly reactive and a key oxidising agent.[1] An oxidative process is when a chemical species reacts with an electrophile (electron loving species) that wishes to gain electrons from, for example, oxygen, chlorine or bromine. The chemical species that reacts with the electrophile loses electrons, hence becoming oxidised. Oxidation processes are important in our understanding of atmospheric chemistry. Figure 1.2 summarises these processes showing the oxidation of methane. OH radicals cleanse the atmosphere of pollutants and consequently understanding OH abundance is a key goal for atmospheric chemists.

Figure 1.2 is an example of the simplest volatile organic compound (VOC) chemistry which shows the oxidation of CH_4 and CO. A VOC is an organic species that has a high vapour pressure allowing it to vaporise significantly and enter the atmosphere. The high vapour pressure refers to an initial boiling point of a species which is less than or equal to 250 °C with an atmospheric pressure of 101.3 kPa.[16]

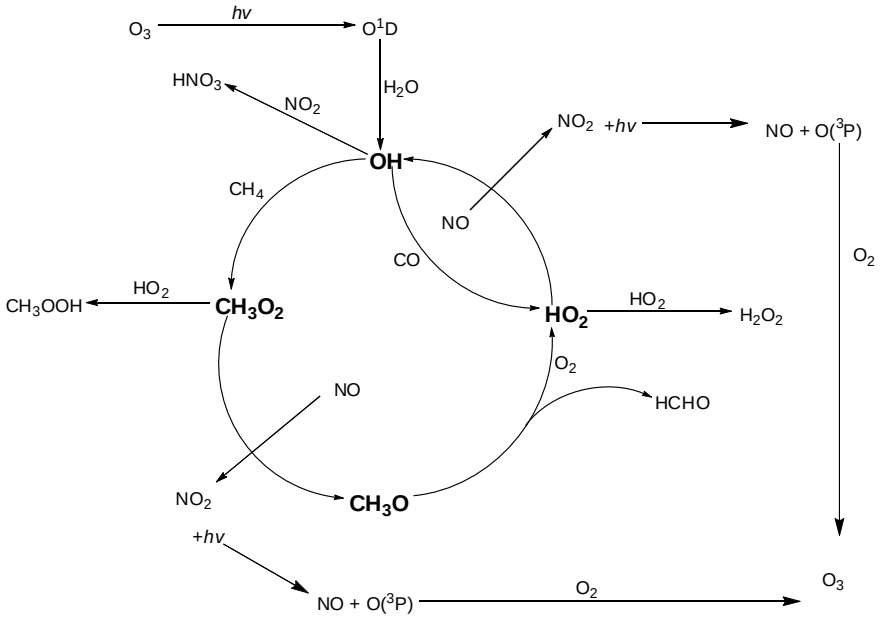

Figure 1.2: Oxidation processes in the atmosphere for CH_4 and CO. (Adapted from Bloss 2007).[11]

Knowledge and understanding of this cycle is essential in order to understand atmospheric chemistry. In particular it is important to understand how VOCs contribute to the OH budget along with the removal of pollutants from the troposphere and the formation of O_3. It is therefore critical to understand possible

impacts of species such as iodine compounds upon OH. This makes it possible to explore the role of iodine in coastal marine environments.

An important factor affecting OH radicals occurs from the reactions of nitric oxide (NO) and nitrogen dioxide (NO_2), referred to collectively as NO_x.

Emissions from road traffic provide the main source of NO to the atmosphere. In cities there is significantly more NO (10-50 ppb compared to 10-100 ppt in a marine environment) due to the release from cars where nitrogen from air reacts with oxygen at high temperatures during combustion (producing NO).[11] NO can react with peroxy radicals (such as HO_2, CH_3O_2) to produce ozone as shown in reactions 3-5.

$$HO_2 + NO \rightarrow NO_2 + OH$$ reaction 3

$$NO_2 + h\nu \rightarrow NO + O\left(^3P\right)$$ reaction 4

$$O\left(^3P\right) + O_2 \xrightarrow{M} O_3$$ reaction 5

NO_2 is an atmospheric pollutant whose major source is from the oxidation of NO with O_3. Another source is the oxidation of nitrogen gas (N_2) in the air within combustion engines (not in the ambient air).

Soil and micro-organisms provide a natural source of NO_x along with lightning.[17] NO_x is a pollutant which is harmful to human health and it removes important radicals from the atmosphere. NO_x reacts with OH forming nitric acid (HNO_3), a process which is

illustrated in Figure 1.2. HNO_3 is soluble in water and it may therefore be deposited as acid rain, an additional pollutant.[7]

Sunlight initiates chemical reactions between VOCs and NO_x which leads to the formation of O_3. O_3 is both formed and acts as a pollutant in the troposphere. As mentioned previously ozone is essential in the stratosphere to absorb harmful UV radiation; however its presence in the troposphere can be harmful to human health so it is considered to be a pollutant. A small amount of ozone is transported to the troposphere from the stratosphere but most is produced in the troposphere.

Figure1.3 illustrates the relationship of O_3 concentration with NO_x. As the concentration of NO_x increases, the production rate of O_3 increases. This occurs until a certain point (indicated by the dotted line) and then O_3 starts to decrease. This is due to NO_2 reacting with OH producing nitric acid (HNO_3). This reaction dominates at high levels of NO_x resulting in a reduction of O_3 production.

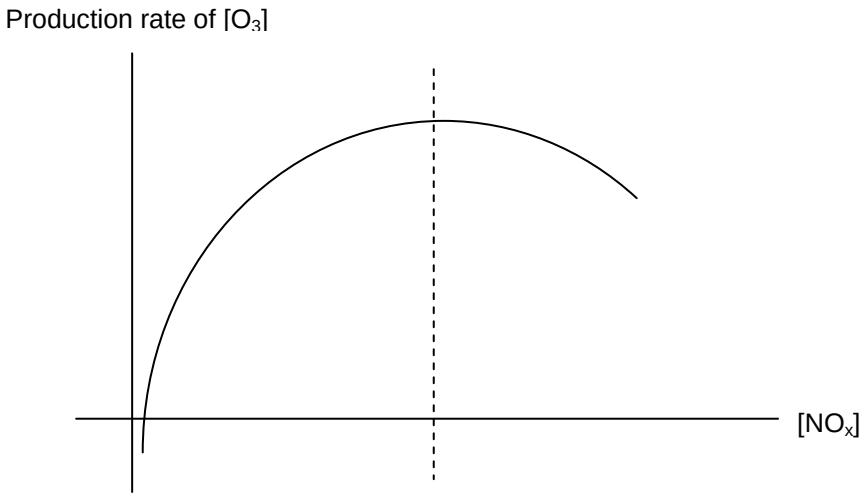

Figure 1.3: Production rate of Ozone

NO_2 can react with ozone (O_3) to produce the nitrate radical (NO_3) which is known as the night-time radical as it is a highly reactive species which is only significantly present during hours with no sunlight. During darkness it can react with pollutants such as alkenes (unsaturated hydrocarbons) or aldehydes (RCHO) and act as a sink for them, much like the OH radical does during daylight. During the day, NO_3 has a very short lifetime as it is photolysed quickly forming NO_x.

The concentration of O_3 varies annually, usually the highest amount is observed in late spring to early summer.[18] High concentrations of ozone (40-100 ppb) are generally found downwind of urban areas compared with much lower concentrations (less than 40 ppb) in a marine environment.[2]

When an environment (such as urban areas), contain high levels of NO_x (10-50 ppb), it is described as a polluted atmosphere. In contrast to this, marine environments contain significantly lower levels of NO_x (10-100 ppt) and this is described as a clean environment. With low levels of NO_x, peroxy radicals react with themselves as shown in reaction 6 and form peroxides that have lifetimes of a few days which are then removed by wet deposition.[19]

$$HO_2 + HO_2 \xrightarrow{M} H_2O_2$$ reaction 6

Although the main chemical species considered here are VOCs, NO_x and O_3, there are numerous other compounds also present in the atmosphere, for example isoprene (C_5H_8) which is emitted naturally from plants and trees. When released into the atmosphere it reacts with ozone to provide a source of the pollutant carbon

monoxide (CO).[20],[7] Isoprene oxidation also leads to the formation of ozone and secondary organic aerosols (SOA) which has important implications for tropospheric chemistry as SOAs are pollutants. OH oxidises isoprene to give SOA therefore affecting the OH budget of the troposphere.[21]

An aerosol is defined as a collection of particles which can be present as a single phase or a mixture of phases (solid, liquid), and these particles are suspended in a gas (air).[10] Aerosols can cause respiratory problems. When emitted directly they are known as primary aerosols; when an aerosol forms as a result of a chemical reaction, it is known as a secondary aerosol. Figure 1.4 shows many sources of primary and secondary aerosol particles.

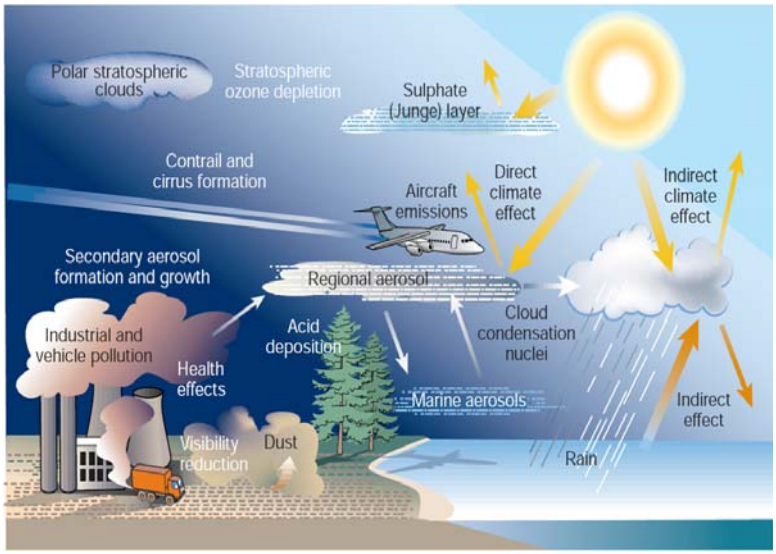

Figure 1.4: Primary and secondary aerosol sources.[13]

Another pathway leading to the formation of aerosol particles is through the reaction of the VOC dimethyl sulphide (DMS). DMS is produced by marine phytoplankton; they need sunlight in order to actively release DMS. When DMS reacts with OH, sulphur dioxide (SO_2) is produced.[20] SO_2 is a harmful pollutant. It can be removed

from the atmosphere by rainfall and dry deposition to the ground.[22] DMS can also be removed from the atmosphere by reacting with OH. This reaction of DMS oxidation (in the presence of OH) leads to an aerosol being formed.[23] In an urban environment exhaust emissions and photochemical smog contain aerosol particles. Photochemical smog occurs when hydrocarbons are mixed with NO_x which photolyses producing O_3, this effect can physically be seen as smog (particles in smog are also a cause of the visible haze).

In contrast to urban areas, primary marine aerosols result from the spray of sea salt; however marine organisms (such a phytoplankton) which emit gaseous pollutants such as DMS provide a source of secondary aerosols. Aerosols can have an indirect effect on climate change.[24] In marine environments, aerosol particles, particularly those containing salts such as iodate, can form cloud condensation nuclei (CCN). The presence of CCN in the atmosphere can lead to clouds being formed because CCN attract small water droplets. The presence of additional clouds leads to the reflection of more solar radiation.[25] It has been suggested that coastal regions are the areas where bursts of new particles are formed in the marine boundary layer.[6]

Ozone's presence in the atmosphere as a pollutant in its own right and as a reactant involved in the formation of other pollutants is central in tropospheric chemistry. Of particular importance is its role in providing the main production pathway for OH radicals *via* ozone photolysis.[26]

1.2.1 The Role of OH in Oxidation Reactions

OH is the most important gas phase radical in the troposphere as it cleanses the atmosphere of pollutants.[2, 11]

Figure 1.2 displays the various sources of OH which are summarised in reactions 7 to 9; these are simply a few examples and by no means exhaustive. Ozone photolysis is the dominant source of OH radicals in the troposphere (in polluted areas the reaction of NO and HO_2 would be the dominant OH source).

$O_3 + h\nu + H_2O \rightarrow\rightarrow OH$ reaction 7

$HO_2 + NO \rightarrow OH + NO_2$ reaction 8

$H_2O_2 + h\nu \rightarrow 2OH$ reaction 9

As shown in figure 1.2 ozone absorbs a photon (*hv*, a quantum of light energy). The bonds in ozone then break; this process is referred to as photolysis giving $O(^1D)$ which is an excited state of oxygen that can react rapidly with water to produce OH radicals. OH radicals oxidise hydrocarbons such as methane which produce methyl peroxy radicals (CH_3O_2). Formaldehyde (HCHO) is also produced when methane is oxidised and it is found throughout the troposphere.[7] In polluted environments the cycle is driven round to the formation of CH_3O and HO_x radicals (HO_2 and OH). In these environments, high NO_x concentrations result in reaction 10 occurring in preference to reaction 11, resulting in a decrease in the production of ozone.

$$OH + NO_2 \xrightarrow{M} HNO_3$$ reaction 10

$$OH + CH_4 \rightarrow CH_3 + H_2O$$ reaction 11

As well as providing a sink for OH, CH_4 itself is an atmospheric pollutant and (excluding water) it is the second most important greenhouse gas after CO_2. The amount of CH_4 in the atmosphere has risen dramatically since the industrial revolution and is now present at ~1800 ppb compared to previous levels of 750 ppb which makes it the most abundant greenhouse gas.[27] There are many sources of CH_4 which result from human activity and natural processes in animals such as ruminants and termites who release methane during enteric fermentation. Decomposition of organic material in landfill sites, combustion, rice cultivation and natural gas leakage all contribute to the emission of methane in the troposphere. Microbes in the soil provide a small sink for methane as they use it as a source of carbon and energy.[7]

As a major sink of OH, CH_4 produces peroxy radicals (CH_3O_2). In a clean environment this radical would react with HO_2 forming CH_3OOH (methyl hydroperoxide). In polluted environments however, the presence of NO_x forces the cycle round to the formation of more radicals, CH_3O, alkoxy radical and HO_2 which can be seen in Figure 1.2.

A further compound affecting the OH budget is carbon monoxide (CO) which is present in urban environments as a result of car exhausts and incomplete combustion of fuel. CO provides another sink for OH through a reaction resulting in the formation of hydroperoxyl radicals (HO_2). In a polluted environment, HO_2 radicals can provide a source of OH when reacted with NO_x. In contrast to this, marine environments contain (much lower levels of) CO due to the oxidation of VOCs. OH can also react with CO to form H and CO_2. In a clean atmosphere, HO_2 will primarily react with itself forming H_2O_2.[20]

There are many different processes affecting the ability of OH to provide a natural 'detergent' for the atmosphere. This project focuses on the role of iodine in the troposphere and how it may affect the atmosphere's oxidising capacity and ability to cleanse itself of pollutants. Iodine is a member of the halogens. Halogens have mostly been of interest to atmospheric scientists due to their role in the depletion of stratospheric ozone. However, in the troposphere, it has been suggested that halogens may form new ultra-fine particles; which could contribute to tropospheric pollution.[5, 6, 19, 28] Halogens may also take part in the chemistry of HO_x and NO_x species which may affect climate change.[29]

1.3 The Presence of Halogen Species in the Troposphere

A halogen is an element of group 7 in the periodic table. In terms of atmospheric chemistry, the most important members of this group, in ascending order of molecular weight, are chlorine, bromine and iodine. Halogens are important to the chemistry of the troposphere because they can influence the oxidation processes.[23, 30] When the role of halogen chemistry in the atmosphere was first explored, they

were of interest to scientists due to their ability to destroy ozone in the stratosphere.[29] However, it has also been suggested that the presence of halogens in the troposphere could significantly alter the chemistry of HO_x and NO_x species.[29, 31] Halogens can lead to O_3 loss in the troposphere which in turn can affect its oxidising capacity. In particular iodine oxide (IO) has been suggested to have a significant impact upon the depletion of tropospheric O_3.[30, 32] New particles can also be formed as a result of the presence of iodine in the troposphere. These new particles are a source of particulate matter which can lead to the formation of aerosols, a harmful pollutant.[33] As discussed in section 1.2 this could have significant impacts upon climate change.

1.3.1 The Presence of Chlorine in the Troposphere

The most well known halogen in the atmosphere is chlorine which has been widely studied.[32] Chlorofluorocarbons (CFCs) are extremely stable materials produced anthropogenically (such as CF_2Cl_2).[2] CFCs are chlorine containing compounds which have been used as solvents and refrigerants. Due to the long lifetime of CFCs (more than 50 years) they can travel to the stratosphere where they are destroyed leading to ozone depletion which creates a hole in the protective ozone layer. Due to CFCs being an ozone depleting substance, their use has been phased out. The main natural source of chlorine is found in coastal marine environments when the sea sprays into the air with waves. This process is illustrated in Figure 1.5.

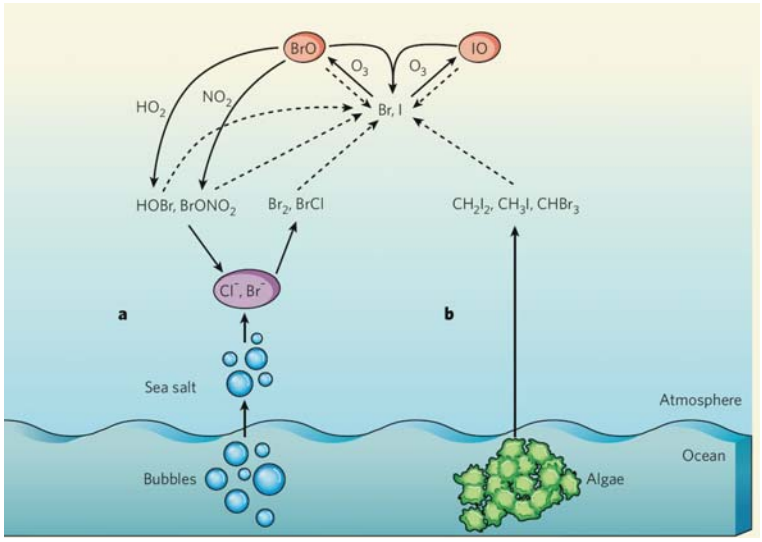

Figure 1.5: The release of halogens from the ocean.[18]

Chlorine is present in sea salt and when this is released into the atmosphere chlorine and bromine may react together forming BrCl.[23, 34] Sunlight initiates the breakdown of BrCl into Br and Cl atoms.

1.3.2 The Presence of Bromine in the Troposphere

As shown in Figure 1.5, bromine (Br) can be released naturally from sea salt in the form of sea spray. Br leads to tropospheric O_3 destruction as it can react with O_3 to form the halogen oxide BrO.[18, 35] The presence of halogen oxides such as BrO during the day can affect HO_x and NO_x ratios which could have serious consequences for the atmosphere.[5, 31] This could in turn affect the oxidising capacity of the troposphere.[5, 31]

A further source of bromine in the troposphere originates from methyl halides (CH_3X where X represents the halogen). In rural areas, CH_3X are released into the

atmosphere by biomass burning and the use of pesticides. Methyl bromide (CH_3Br) is considered to be one of the most efficient pesticides as it can control many pathogens and insects. The key feature of CH_3Br which allows it to be such a successful pesticide is its high vapour pressure (1,420 mm Hg at 20 °C), permitting CH_3Br to travel easily through the soil and reach pests. 60,000 metric tonnes of CH_3Br were produced in 1991, 48,000 of which were used for fumigation, suggesting it to be a significant source of bromine in the atmosphere.[36]

CH_3Br is classified as an ozone depleting chemical.[37] Bromine can react with stratospheric ozone to break it down. Bromine atoms are up to 40 times more effective at destroying ozone than chlorine radicals (from CFCs).[37, 38] CH_3Br is not photolysed in the troposphere and is quite stable with an average lifetime of 1.7 years, therefore it can alter tropospheric chemistry by reacting with important radicals such as OH.[34] Due to the stability of CH_3Br, its effect on tropospheric chemistry is not significant.

Bromine can be removed from the atmosphere by wet deposition (the ocean), degradation in soil and uptake by plants.[38] Due to CH_3Br destroying stratospheric ozone there have been investigations into the compound since 1970.[36] The US Environmental Protection Agency (EPA) classified CH_3Br as a “Restricted Use Pesticide” so it was phased out and eventually banned in 2005. Now it is only used for emergency and critical exemptions which follow the Montreal Protocol.[39]

1.3.3 The Presence of Iodine in the Troposphere

The main source of iodine emission to the troposphere is from seaweed, which is the focus of this project and Figure 1.5 illustrates the emission of iodine from seaweed beds.[3] Small amounts of iodine are present in sea water and hence salt spray but the concentration is so small that this is not considered to be a major source of iodine.[18] The new pesticide methyl iodide (CH_3I) also provides a source of iodine to the troposphere.[37]

It has been suggested that molecular iodine (I_2) is the source of the majority of atmospheric iodine in coastal regions.[29] I_2 is released into the atmosphere by macroalgae (seaweeds) and microalgae (phytoplankton).[3] Iodine compounds build up in seaweed, most notably a type called Laminaria (a form of kelp) which leads to the emission of I_2 into the atmosphere when the seaweed beds are exposed at low tide.[29] Observations have been recorded which clearly indicate the presence of iodine species at periods of low tide, confirming the nature of the seaweed emission.[29]

There are many alkyl iodides present in the atmosphere (RI, such as CH_2I_2, CH_2ICl, CH_3I) which may originate from the ocean. These RI species are photolysed rapidly which can lead to the formation of I atoms.[40]

Following the emission of I_2 into the atmosphere, it is rapidly photolysed (with a lifetime of around 15 seconds) releasing iodine atoms (I) which can react with O_3 leading to the production of iodine oxide, IO.[29] Due to its fast photolysis I_2 is not a

stratospheric ozone depleting species as the lifetime is simply much too short to permit transport to the stratosphere. However, as previously mentioned, IO may react with tropospheric O_3 which could lead to a significant impact upon the production of OH.[27]

When iodine compounds react in the troposphere, their higher iodine oxide (for example OIO) vapours can condense readily which leads to the formation of aerosol particles; this can have an important impact on climate change (see section 1.2).[24, 29, 40]

It has been suggested that IO can react with HO_x and NO_x species which consequently alters the ratios of these important radicals.[35] This could disturb the chemistry in the troposphere, altering the processes dealing with pollution. The proposed mechanism for iodine species in the troposphere is illustrated in Figure 1.6.

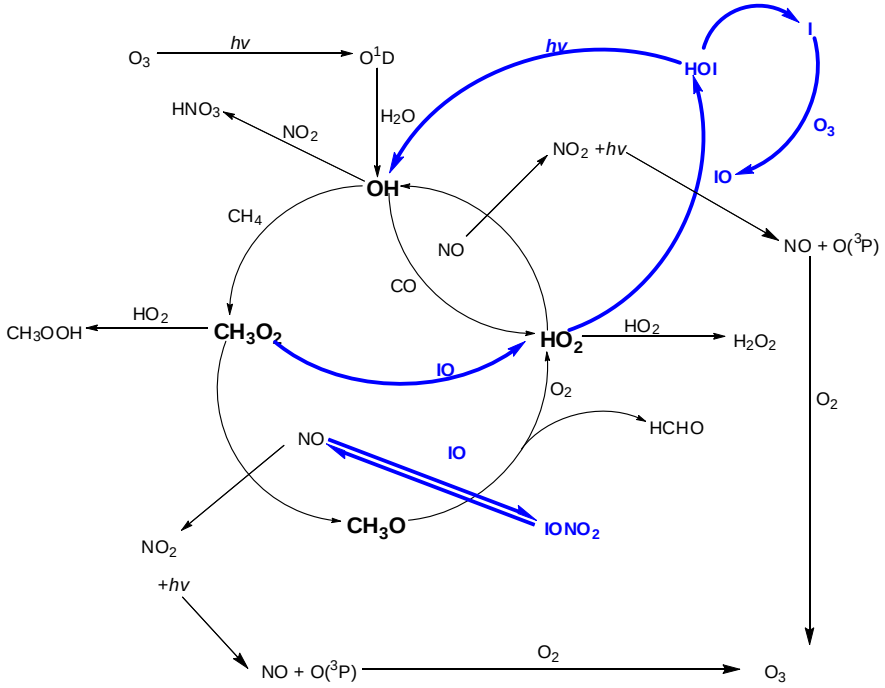

Figure 1.6: Oxidation processes in the troposphere, including iodine chemistry. (Adapted from Bloss 2007).[11]

Little is understood as to the atmospheric role of iodine in the coastal marine boundary layer. This current project focuses on measurements taken from field campaigns at Mace Head in Galway, Ireland. One of the campaigns is known at the North Atlantic Marine Boundary Layer Experiment, carried out in summer 2002 (NAMBLEX see section 1.4) and this provided the general chemical background to the modelling, with limited measurements of iodine species, IO, and I_2 which showed a higher concentration of these species during periods of low tide. Another campaign also at Mace Head is known as Point Measurements of Reactive Iodine Species (POMORIS, conducted in summer 2007). POMORIS provided more detailed measurements of iodine species, notably at point locations near to the coast and also measured I atoms for the first time.

Computer modelling studies will be used in order to determine the amount (flux) of I_2 emitted from seaweed at low tide. This will be carried out by replicating the measurements of iodine species observed at Mace Head. How iodine species interact with the chemistry of HO_x and NO_x species will then be investigated using the model.

Exactly how the presence of iodine species in the atmosphere affect tropospheric chemistry is relatively unknown due to little being studied. Therefore much attention has been focussed on this in recent years.

1.4 Recent Measurements of Iodine Species

The NAMBLEX campaign was a field experiment carried out from July to September in 2002.[41] The project took place in a remote setting at Mace Head, Galway on the west coast of Ireland as illustrated in Figure 1.7. The observation station is located 110 metres away from the coast; this station is also shown in Figure 1.7.

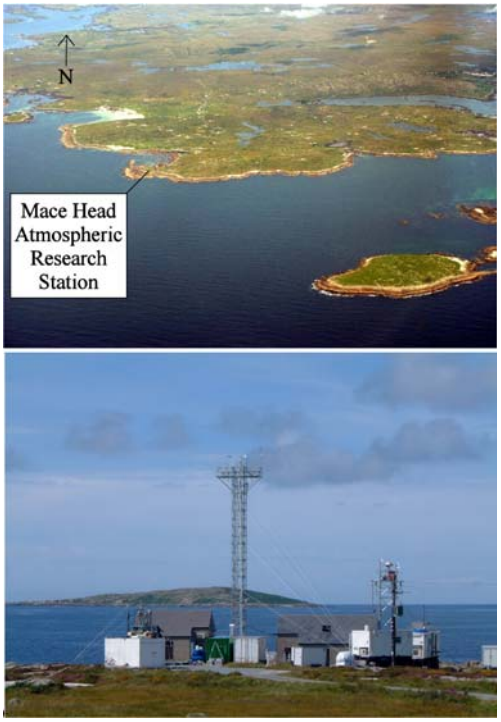

Figure 1.7: An aerial photograph of Mace Head (taken by R. M. Purvis) and the observation station (taken by D. E. Heard).[41]

Over 50 scientists took part in the campaign, the aim of which was to investigate the chemical processes in the marine boundary layer including atmospheric composition and structure. Mace Head is located in the Northern Hemisphere and when the wind is in the prevailing direction of 180-300°, the air has passed over the open Atlantic ocean. This air is considered to represent clean air that is unpolluted and representative of the Northern Hemisphere. In order to try and understand this chemistry, measurements of iodine species have been taken at various locations using a variety of methods such as gas chromatography – mass spectroscopy (GC-MS) and differential optical absorption spectroscopy (DOAS).[42]

During this campaign (NAMBLEX), radicals which have short lifetimes, such as OH, and long lived species, such as HCHO, were measured and compared to model simulations. Instrumentation used for the measurements of these species were located in laboratories 110 metres away from the coast. Data recorded from

NAMBLEX has been used in this project to determine the models' initial conditions, (this is discussed in more detail in chapter 2).

1.4.1 Measurements of Iodine Species during NAMBLEX

During the NAMBLEX campaign, various instruments were used for the detection of atmospheric species. One method employed was DOAS which was used for the detection and measurements of IO, OIO and I_2. These species absorb light in the visible region which allows their detection via this method. I_2 is detectable at 535-575 nm and IO can be detected at 430-460 nm.[5, 35] I_2 has been measured from 5 ppt to night time levels of 93 ppt. I_2 photolyses readily giving I atoms. These I atoms can then react with O_3 to give IO and OIO. At night however, IO and OIO have been measured at ~2-10 ppt which suggests I_2 reacts with NO_3 providing a source of iodine oxides. [29, 40] Model simulations carried out during NAMBLEX support this idea of I_2 + NO_3 yielding iodine oxides.[29] The DOAS instrument requires a retro-reflector which was situated on an island, Croaghnakeela, 4.2 km west of Mace Head.[40] The disadvantage with using DOAS is that the measurements taken are averaged over the DOAS path which here is a total of ~8 km. As I_2 is emitted from seaweed at the coast, these measurements are not an accurate representation of the levels of I_2 that may be emitted in to the atmosphere at any point. Also, due to I_2 having a short lifetime in the troposphere it can be difficult to measure, especially using methods such as DOAS where the observations will be averaged over such a long path.[6]

Figure 1.8 indicates the location of Croaghnakeela Island and the DOAS path is shown in red. It also shows the layout of the site at Mace Head which shows the positions of the buildings and instruments used.

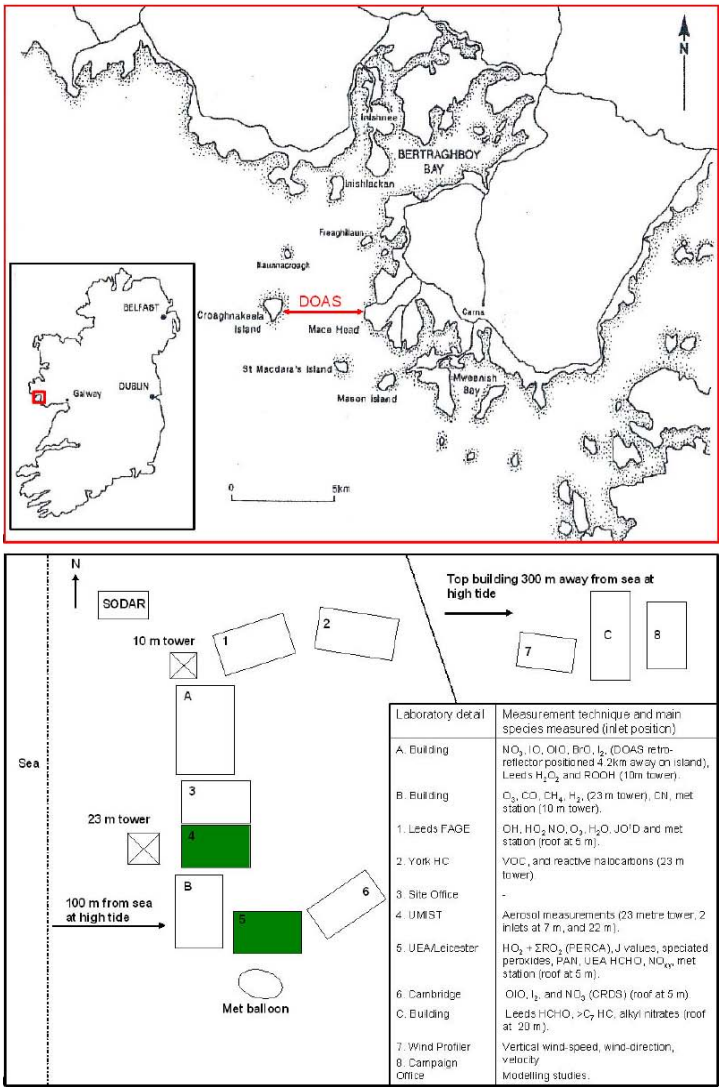

Figure 1.8: Top: The location of Croaghnakeela Island. Bottom: The layout of the site at Mace Head.

As NAMBLEX data is taken from a coastal observation station it is unknown whether iodine is also active over the open ocean. If so, this could have significant impacts on tropospheric chemistry, given the global extent of sea coverage.

1.4.2 Measurements of Iodine Species during POMORIS

The campaign POMORIS was conducted in 2007 again at Mace Head, Ireland. Significant levels of IO have been determined by DOAS but employing methods such as broadband cavity-enhanced absorption spectroscopy (BBCEAS), which have also measured iodine species, allow for point measurements to be taken which indicates how much I_2 is emitted from the source.[35] During this campaign IO, I and I_2 data were recorded using point iodine instruments (i.e. those that measured the levels at a specific point, rather than as a 4-km average) such as BBCEAS, laser induced fluorescence (LIF) and resonance fluorescence (RF). LIF was used to detect IO, RF measured I atoms and BBCEAS measured I_2. This campaign had the advantage over its predecessor NAMBLEX (2002) as the instruments employed allowed point measurements of iodine species to be made. This represents a more accurate picture of the emissions into our atmosphere as measurements were recorded of I_2 directly over the coast instead of an average of their concentration over several kilometres. However, supporting instrumentation for VOCs and HOx species were not available. This project uses measurements taken from POMORIS for iodine species and from NAMBLEX for the supporting levels of NO_x, O_3 and VOCs.

Figure 1.9 shows instruments that have been employed at the Mace Head site. The top photograph shows the dual channel BBCEAS instrument and the lower photograph shows the RF instrument.

Figure 1.9: Instruments employed at Mace Head, (courtesy of Anna Hollingsworth University of Leicester).

2 METHODS

In order to gain a deeper understanding of atmospheric chemistry, numerical models can be employed. They are advantageous as they allow us to simulate real life situations occurring in the atmosphere. Models can also be used to make predictions about the behaviour of certain species, for example if the concentration of a potential pollutant is increased, the model could tell us what might happen to the concentration of OH radicals as a result of the pollutant being present. For this thesis a numerical model was used to simulate the gas-phase composition of the atmosphere. This composition varied as a theoretical parcel of air travelled across the coastal margin and had a burst of iodine added to it. A number of simulations were performed to explore the dependence of the predicted concentrations upon several factors such as background conditions (location, temperature), chemical reaction rates and iodine source strength.

2.1 The Use of Modelling in Atmospheric Chemistry

There are several different types of atmospheric chemistry models that can be of use; the simplest of which are zero-dimensional box-models. For this box-model it is assumed that the box of air is well mixed. The box-model is used to study short lived chemical species (such as OH and I_2), but is constrained to observed levels of long lived species.[1, 26]

Models can also contain 1, 2 and 3-dimensions, however due to computational limitations they contain simplified chemical schemes and mechanisms.[1] Another type of box model, Eulerian, contains simple chemical schemes and includes transportation of the chemical species within the box of air. A Lagrangian box model is employed when examining the evolution of an air parcel.[2, 43] This current project uses a simple zero-dimensional atmospheric box model which is also Lagrangian as the model simulates an air parcel travelling over the open ocean and passing over seaweed, an emission source of I_2. The chemistry inside the air parcel evolves as the parcel continues to travel to an observation station. The air parcel passes over the coastal region to a land-based shoreline observation point.

Box models need a computer program in order to simulate situations and generate results. FACSIMILE is a program which runs in Windows and has been used for this project. FACSIMILE integrates the features of the model, such as the chemical and differential equations.[44]

In order to construct the box model used in this project, the Master Chemical Mechanism (MCM) provided the basic chemical schemes.[15] The MCM is a chemical mechanism containing chemical and photochemical mechanisms for reactions which occur in the troposphere. Version 3.1 was used which was constructed by Sam Saunders, Mike Jenkin and Claire Bloss; the database is updated periodically and is based on laboratory data.[15] This is an ongoing project which requires tests against field observations and emissions data in order to get a full, accurate picture of oxidation processes occurring in the troposphere.

The MCM provides a detailed mechanism for 124 volatile organic compounds (VOCs) which undergo oxidation in the troposphere. The MCM combines some elementary processes where these are rapid and consecutive in the atmosphere, for example reactions 12-13 would be shown as reaction 14 by the MCM. This is because forming HO_2 (reaction 13) is a rapid reaction; H almost instantaneously reacts with O_2 in the atmosphere so for simplicity this step is not shown.

$OH + CO \rightarrow H + CO_2$ Reaction 12

$H + O_2 \xrightarrow{M} HO_2$ Reaction 13

$OH + CO \rightarrow HO_2$ Reaction 14

For the box model used for this investigation, the chemical schemes taken from the MCM were CH_4, CH_3OH, HCHO and CH_3CHO oxidation along with inorganic thermal gas phase reactions. The rationale for this choice of VOCs is given below. The model was constrained to concentrations of the long lived species: CO_2, H_2O, N_2, O_3, NO_x and O_2. This formed the backbone of the model.

Data taken from the NAMBLEX campaign was used to determine the initial conditions in the model, the temperature and the concentration of species such as O_3 and NO_x. NAMBLEX data was also used to identify a subset of VOCs to use in the model. There are many thousands of possible VOCs that could be used; however it is only practical to include a small number in the model. VOCs are an important consideration for the box-model as they contribute to the loss of OH in the

atmosphere. Based on NAMBLEX data a definitive list of VOCs were selected which account for ~95% of the measured OH loss.[45]

NAMBLEX data provided the concentration of each chemical species (present in ppb) listed in Table 2. In a previous study, 80% of the species contributing to the OH budget were considered. In this study 95% of species contributing to the OH budget were accounted for.[45] The concentration of each species was converted from ppb to molecules cm^{-3} in order to calculate the contribution to OH loss. The rate constant (k) for each reaction was taken from the MCM database. From that the cumulative percentage was calculated in order to choose the appropriate VOCs to include in the model. VOCs which were used in this modelling study were: CH_4, CH_3CHO, HCHO, CH_3OH and DMS which together accounted for 95% of the total OH loss, but allowed the model chemical mechanism to be kept to a manageable size. CO and H_2, which contribute to the OH budget, were also included. Table 2 and Figure 2.1 show which chemical species were used to calculate the percentage contribution to OH loss.

Chemical Species	Concentration (PPB)	k (Chemical species with [OH])[15]	Concentration (molecules cm^{-3})	concentration*k	Cumulative %
CO	110	1.57E-13	2.75E+12	0.43175	38.85
CH_4	1844	6.18E-15	4.61E+13	0.284898	64.48
Ethanal (CH_3CHO)	0.26843	1.58E-11	6.71E+09	0.10602985	74.02
HCHO	0.6065	6.33E-12	1.52E+10	0.095978625	82.65
H_2	512	6.70E-15	1.28E+13	0.08576	90.37
Methanol (CH_3OH)	1.16456	9.44E-13	2.91E+10	0.027483616	92.84
Acetone	0.72496	1.35E-12	1.81E+10	0.0244674	95.04
DMS	0.16909	6.30E-12	4.23E+09	0.026631675	97.44
Ethene	0.03506	9.00E-12	8.77E+08	0.0078885	98.15
Propene	0.01098	3.00E-11	2.75E+08	0.008235	98.89
Isoprene	0.0139	1.65E-11	3.48E+08	0.00573375	99.41
Toluene	0.01442	3.94E-13	3.61E+08	0.000142037	99.42
Benzene	0.02621	4.29E-13	6.55E+08	0.000281102	99.44
Ethyne	0.06193	8.97E-13	1.55E+09	0.00138878	99.57
Propane	0.09881	2.96E-13	2.47E+09	0.000731194	99.64
Ethane	0.649	2.50E-13	1.62E+10	0.00405625	100.00
Data taken from Leeds GC NABLEX **(Species to consider)**					

Table 2: Spreadsheet for the calculation of VOCs contribution to OH loss.[15]

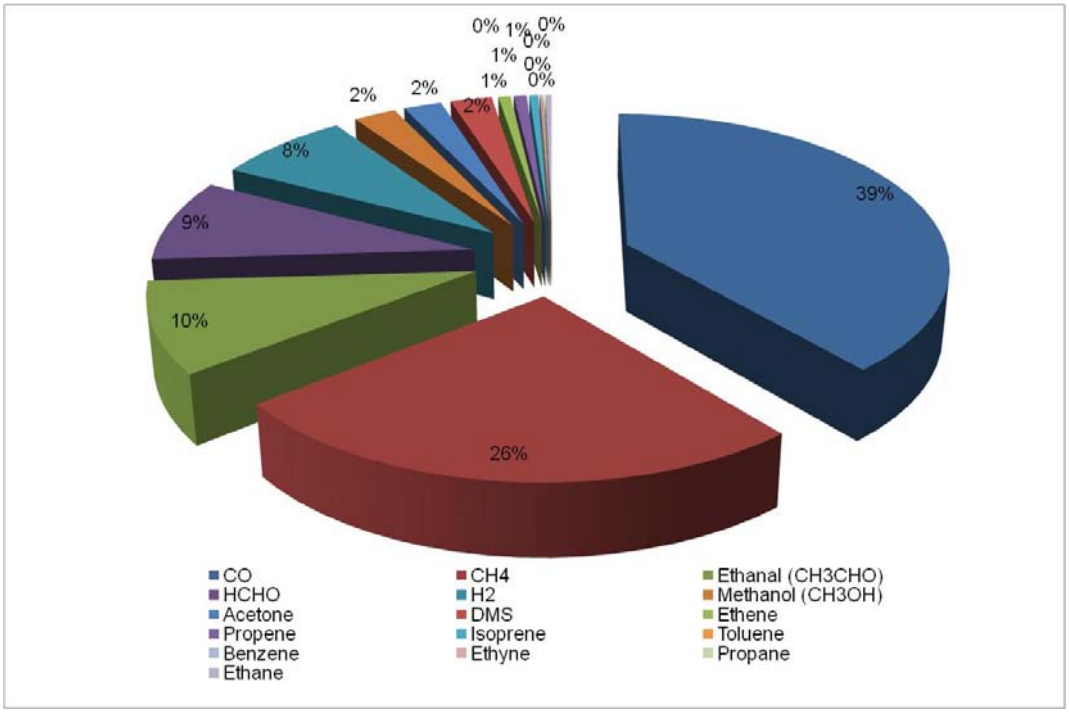

Figure 2.1: Pie chart to show the percentage contribution of each VOC to OH loss.

In conjunction with the MCM, additional sources were used to provide aspects of the chemical schemes. The mechanism for DMS was taken from Sommariva, 2005; there were halogen-mediated DMS oxidation steps added for this model (see Appendix 8.1 for details).[1]

Mechanisms for the detailed iodine inorganic and organic chemistry included in the model can be seen in Appendix 8.2. This includes photolysis reactions, thermal kinetic processes, heterogeneous uptake and deposition for iodine species. Gas phase kinetic parameters were taken from the literature using the NASA/JPL and IUPAC evaluations.[46, 47] Some estimation had to be made due to poor understanding and a lack of recorded data for a number of the kinetic and photochemical parameters. This mechanism was taken from W. Bloss (private communication).[48] Due to the uncertainty of these estimations and potential variations in the rates and products of some key iodine reactions, a sensitivity study was undertaken to assess the importance of these estimations (see chapter 4).

The model includes other algorithms essential for it to function and generate accurate data. For certain species, such as O_3, photolysis rates are important. The photolysis rate of reaction 15 would be calculated for the speed at which the bonds in ozone break to form O (^{3}P).

$O_3 + h\nu \rightarrow O\left(^3P\right) + O_2$ Reaction 15

Photolysis rates are calculated in terms of the solar zenith angle (SZA) which uses a global position (entered into the model) and calculates the angle of the sun to the earth's surface for a certain time of day and date. This is illustrated in Figure 2.2.

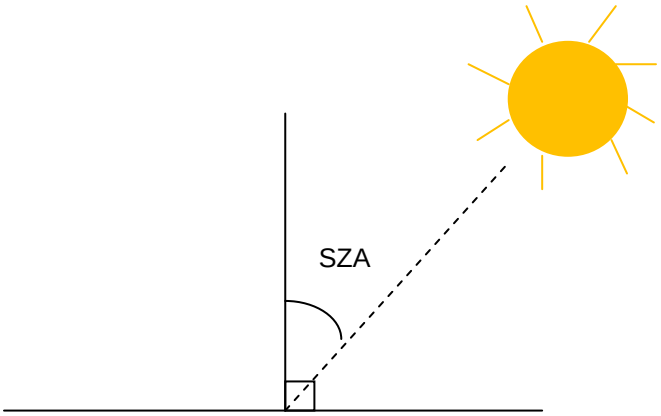

Figure 2.2: Illustration of the Solar Zenith Angle (SZA).

This is important in explaining and understanding behaviour of certain species; in the case of reaction 15 we would expect to see a high concentration of OH radicals at midday compared to a low concentration in the evening when there is limited sunlight. In addition to the standard MCM photolysis rates for HO_x, NO_x and VOCs, species which are not included in the MCM (photolysis rates for iodine species) which were calculated according to the algorithms of Hough *et al.*, can be seen in Appendix 8.3.[49]

Certain chemical species (for example iodine oxides, IO and OIO) experience heterogeneous loss to aerosol. Iodine oxides are thought to polymerise by the addition of iodine oxides with themselves and higher iodine oxides. Knowledge of the mechanism for the removal of iodine oxides into the condensed phase is poorly

understood. The assumptions made in this study are discussed in Appendix 8.2 note 7. In the model this is calculated as a loss rate. This calculation involves the surface area of the aerosol particles present. The surface area of the aerosol used in this model was 5 x 10^{-6} cm^2 cm^3.[31] This value was based upon observations during the NAMBLEX campaign. Appendix 8.4 shows the reaction probabilities used for the iodine mechanism.

Another sink to consider is when species are lost by dry deposition. This is again accounted for in the model using a calculation where the height of the PBL is important.

When iodine is emitted from seaweed, it is initially emitted at the very bottom of the PBL. However, as the iodine emission travels downwind the region of air that it comes into contact with changes. This is the iodine plume, the volume of air that iodine is affecting increases as the plume travels with the wind and grows by mixing and dispersion. This effect was implemented in the model to give accurate predictions of the effect iodine species may have on the atmosphere.

The box model used in this project simulates an air parcel travelling across the open ocean (representing ‘clean’ air), crossing a coastal margin and continuing on to an observation station 110 m away from the coast. At the coastal margin the air passes over seaweed beds where, at low tide, iodine is emitted. This air parcel, therefore,

receives an injection of iodine. This process is illustrated in Figure 2.3, where the plume boundary is also shown (however, the angle is exaggerated for illustration purposes). Here, iodine is emitted at the lowermost region of the atmosphere and as the iodine plume travels downwind the volume of air it affects evolves (it grows vertically). Hence the importance of the iodine plume in the model.

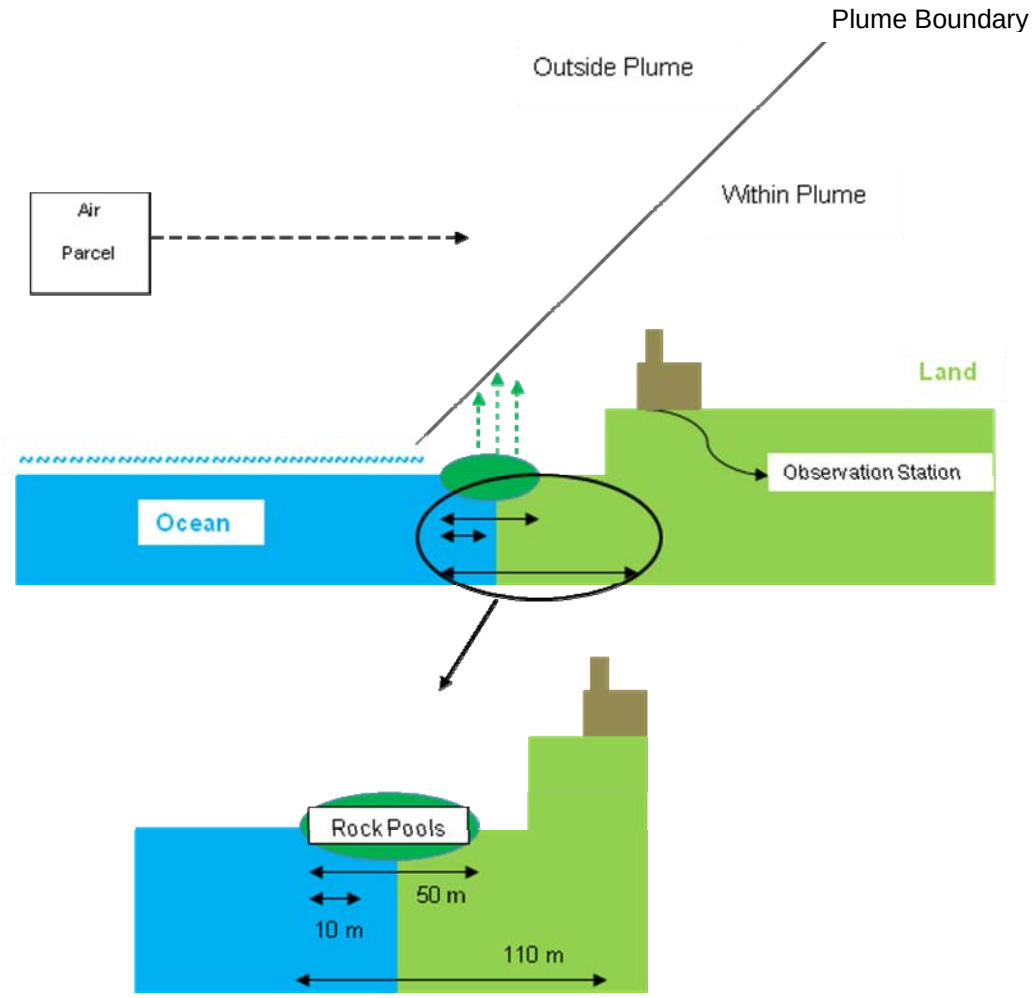

Figure 2.3: Model scenario. 110 m is the distance from the start of the emission zone (i.e lowest low-tide mark) to the observation station. 50 m indicates the estimated extent of the whole potential emission zone and 10 m indicates the estimated concentrated emission zone (see below).

The evolution (the variation in height with distance) of the iodine plume depends on the wind speed observed at the time of low tide.

In order to simulate an accurate situation, the model requires a period of time in which to allow calculated concentrations of intermediate species (for example HO_2, CH_3O_2) to reach steady state according to the conditions that have been set. This is referred to as the 'spin-up' time. Figure 2.4 indicates the importance of spin-up time as the first eight minutes of the simulation (prior to the dotted line) do not truly represent the activity of the selected chemical species. Their concentrations are adjusting to the conditions set in the model, from their initial values (zero) to reach equilibrium. Constant levels are never actually reached due to the loss of species such as NO_x which will react to form HNO_3 and changing photolysis rates along with other contributing factors.

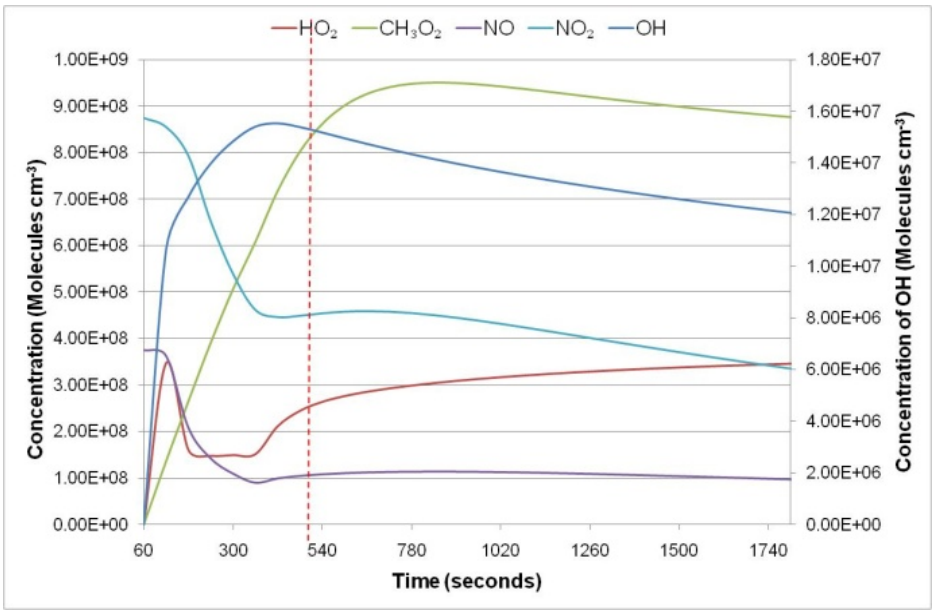

Figure 2.4: Spin-up time.

The simulation generating these data began at midday; one would not expect to see such a fluctuation in these chemical species. For example at midday, there would be a steady peak of OH (as OH is produced *via* O_3 photolysis) and this is not shown in Figure 2.4. Hence the importance of accounting for spin-up time, without which results generated by the model would not be accurate. Figure 2.5 displays results after the model running for one hour (3600 seconds) after beginning at midday, After 30 minutes (1800 seconds, marked with a dotted line) the model had adjusted to the set conditions and the chemistry represented a real-life situation in the atmosphere. Therefore when running all simulations, the first 30 minutes was allowed for spin-up time and no analysis was conducted for this period as is does not produce accurate, reliable data. The ongoing slow changes apparent in the model after 30 minutes reflect net chemical losses (for example of NO_x, O_3) which in this simulation are not counterbalanced by mixing from an overlying troposphere. However the focus of this work is upon the few seconds after an air parcel crosses the coastal margin – compared with which the trends apparent in Figure 2.5 are not significant.

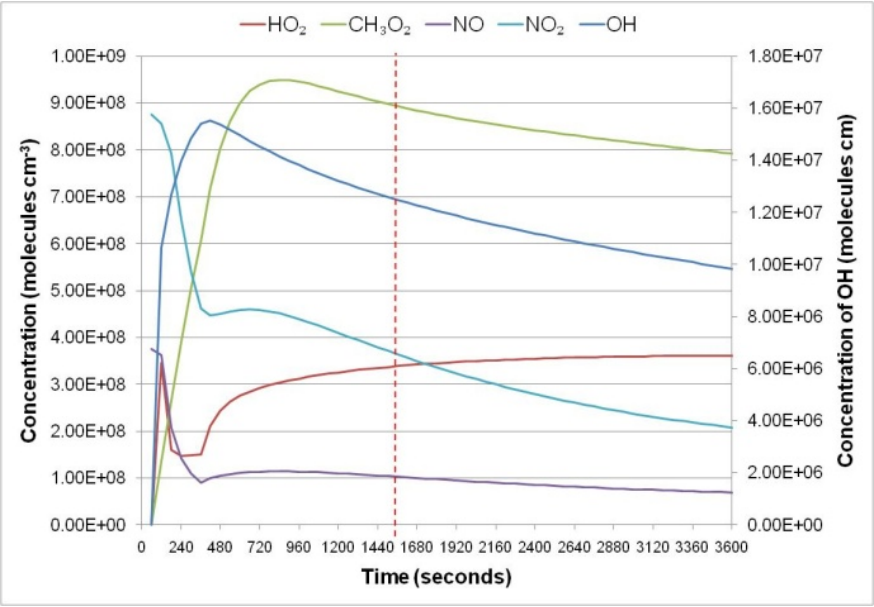

Figure 2.5: Spin-up time; simulation results after one hour (3600 seconds).

With the backbone of the model in place, a routine was added for the addition of iodine. This routine allowed iodine to be injected after the spin-up period and for the emission to be stopped after the air parcel had passed over the iodine source. The iodine source strength and spatial extent, (intertidal region), were optimised, as described below in order to reproduce observed IO data. Wind speed data collected during POMORIS (courtesy of Roisin Commane, University of Leeds) was reported at 9 m s^{-1}. This was added to the model along with Pasquill-Gifford stability class D parameters in order for the plume height to be calculated.[50] Subsequent HO_x and NO_x evolution was recorded from the modelled data.

As previously mentioned, the model was constrained to measured data from NAMBLEX which were concentrations of long lived species. However this data was only indicative of one type of air mass travelling to the observation station. The VOCs accounting for ~95% of the OH budget were used and these provided the models initial concentrations. IO data (provided courtesy of Roisin Commane, University of Leeds), I and I_2 data (courtesy of Steve Ball and Anna Hollinsworth, University of Leicester) were used for the specific day of 29/08/07. This was the only day available for I atom data.

The model was run, firstly without iodine, for day and night to provide base case results in which to compare any changes in HO_x and NO_x species induced by the iodine emissions. Three different situations were used with the addition of iodine to replicate the IO data during the day. Two simulations also looked at night time levels

of I_2, these scenarios are summarised in Table 3. Components of the model used in this study can be seen in Appendix 8.5.

Scenario	Tide	Emission Zone	Time of Day	Total I_2 Added
A1	Low, low tide	Whole emission zone (50 m)	Midday	90 ppt
A2	Low, low tide	Concentrated emission zone (10 m)	Midday	260 ppt
B	High, low tide	Whole emission zone (20 m)	15.00	30 ppt
C1	Low, low tide	Whole emission zone (50 m)	Midnight	360 ppt
C2	Low, low tide	Concentrated emission zone (10 m)	Midnight	360 ppt

Table 3: Summary of scenarios used in the model.

The emission zone employed in each scenario was estimated based on the observation site being 110 m away from the coast. The terms ‘low low’ tide and ‘high low’ tide refer to periods of low tide. However as Figure 2.6 indicates, on the 20/08/07 the tide height at low tide (indicated by the dashed line) was much higher than that of 29/08/07 (indicated by the solid line).

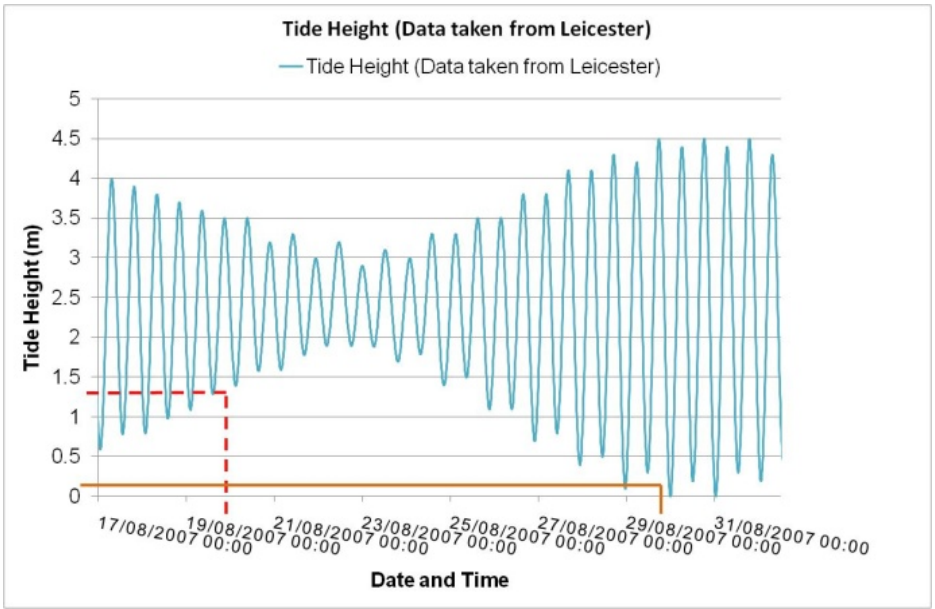

Figure 2.6: The difference between low low tide and high low tide.

These different tide heights would correspond to different seaweed exposures, and different spatial extents for the intertidal iodine emissions region: 50m in width for the lowest low tides (scenarios A1, C1) and 20 m in width for the highest low tides (scenario B). As a further test, the assumption that iodine was only significantly emitted by the seaweed species exposed at the lowest reaches of the tide was also considered – scenarios A2 and C2, corresponding to a 10-m emission zone at the lowermost edge of the low tide region. This approach was supported by the observations, which only showed appreciable levels of I_2 or IO when the lowest tide heights were reached (chapter 3, Figure 3.3), and by observations of the distribution of seaweed species (W. Bloss, personal communication).

For scenarios A1, A2 and B, the addition of I_2 was manually adjusted in the model in order to replicate the observed IO data taken from POMORIS. Once the data was successfully replicated, corresponding HO_x and NO_x data was analysed. Scenarios

C1 and C2 were used to look at night time levels of I_2 and to see if any other species were affected by its presence during the night (IO was below the instrument detection limit at night, and I_2 was below the detection limit during the day).

The observation station at Mace Head was a shoreline cottage which, at periods of low low tide, was situated 110 m away from the coast. Therefore, at a wind speed of 9 m s^{-1} (which was recorded during POMORIS) it would take 12 seconds for the air parcel to reach the station hence travelling 110 m. Scenario A1, A2, C1 and C2 are all periods of low low tide. For these simulations, it takes the air parcel 12 seconds to travel from the start of the iodine source to the observation station. For scenario B however, this is considered at a period of high low tide. This means that from the initial emission of I_2, then travelling to the observation station, travelling this 80 m would result in the air parcel reaching the observation station at 9 seconds.

During the whole emission zone of 50 m, as used in scenario A1 and C1, it would take 6 seconds for the air parcel to pass over the emission source. Hence I_2 was added for 6 seconds in the model simulation so a total of 90 ppt I_2 was added in the case of scenario A1 and 360 ppt I_2 in the case pf scenario C1. However, during the concentrated emission zone of 10 m, as used in scenario A2 and C2, it would take 2 second for the air parcel to travel over the emission source. Hence I_2 was added for 1 second. This was a total of 260 ppt I_2 for scenario A2 and 360 ppt I_2 for scenario C2.

3 RESULTS

In order to investigate the affect of iodine species upon HO_x and NO_x the model ran two simulations which did not include the addition of iodine, one was modelled during the day and one at night, these cases will be referred to base day and base night respectively. In both cases, except for the addition of iodine, the conditions of the model are the same as scenario A1 (midday) and C1 (midnight). The results of which can be seen in Figure 3.1and Figure 3.2.

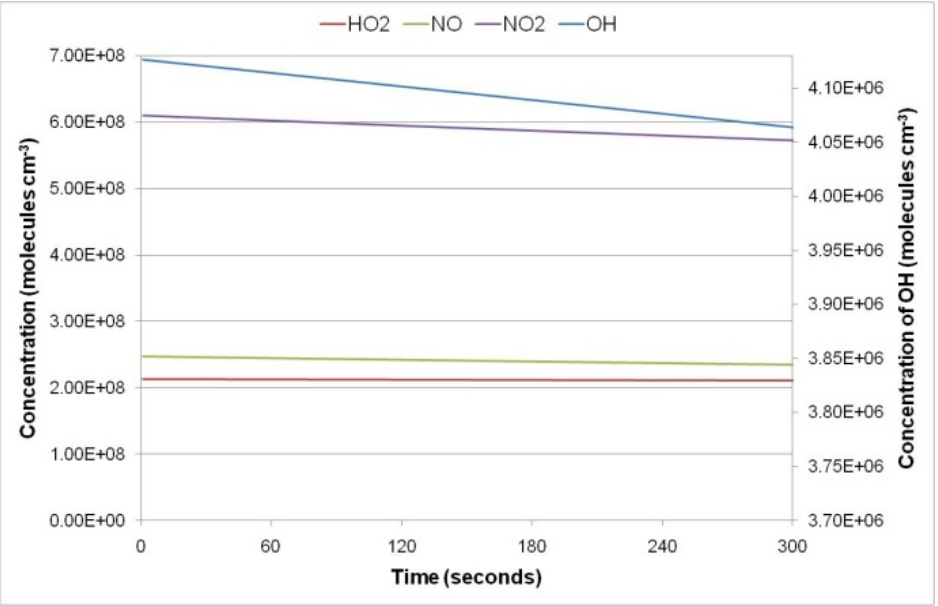

Figure 3.1: Modelled Data for HO_x and NO_x at Midday with no Iodine.

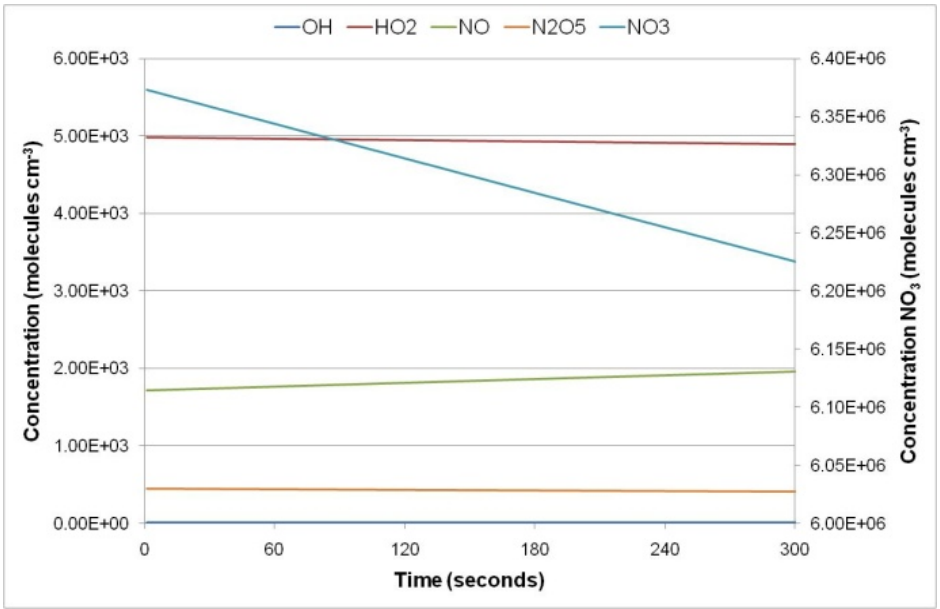

Figure 3.2: Modelled Data for HO_x and NO_x at Midnight with no Iodine

The time axis in these figures corresponds to the model time elapsed since the air passed the coastal margin at the low tide point - i.e. the observation station (Mace Head) is reached at a time of 12 seconds for scenarios A to C.

During the POMORIS campaign, the concentration of iodine monoxide (IO) was measured for the period 14/08/07 – 31/08/07. Figure 3.3, Figure 3.4 and Figure 3.5 show the available IO, I and I2 data, together with tide height.

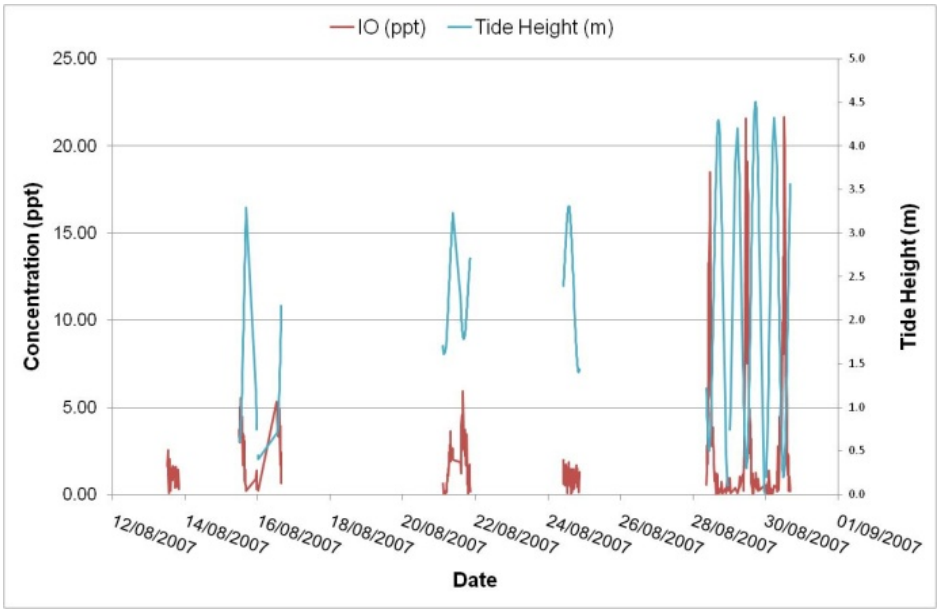

Figure 3.3: IO concentrations and tide height recorded at Mace Head, Ireland (Courtesy of Roisin Commane University of Leeds).

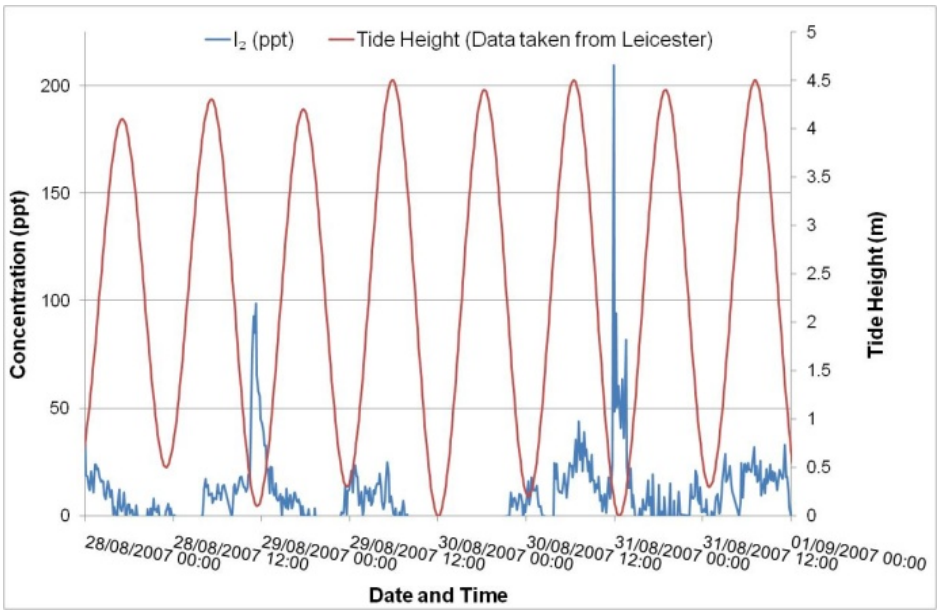

Figure 3.4: Measured I_2 data from POMORIS (courtesy of Steve Ball, University of Leicester)

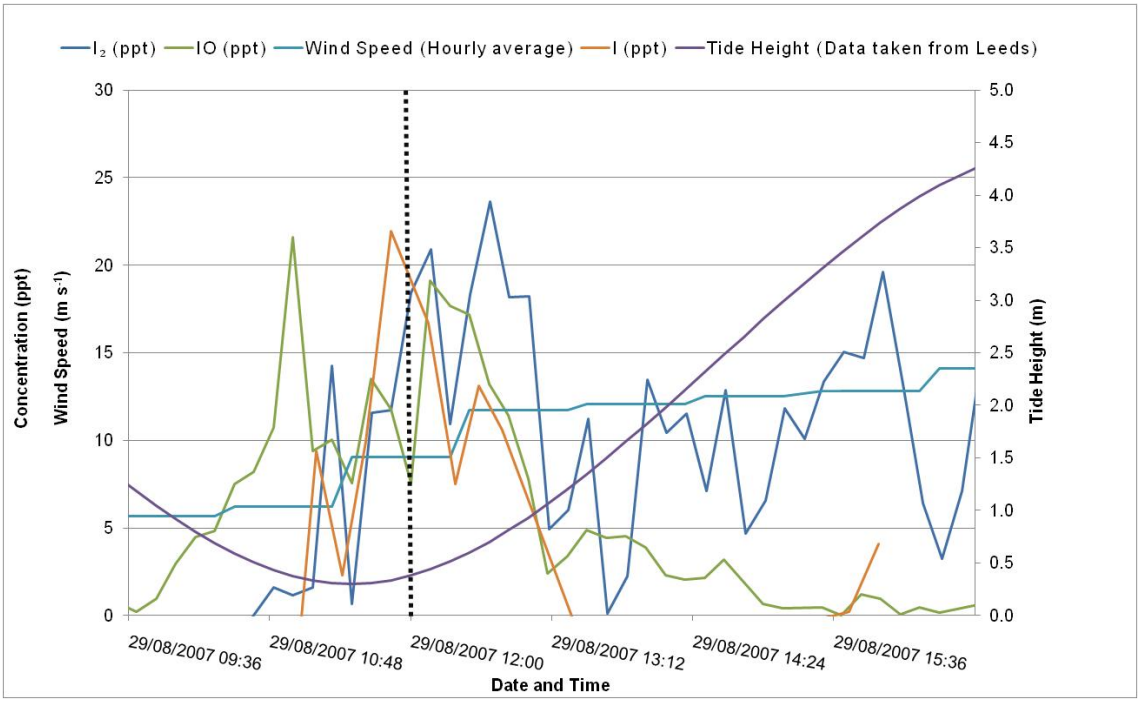

Figure 3.5: Measured I_2, IO and I atom data from POMORIS. The black dotted line indicates the point at midday on 29/08/07 which was used for the model simulations.[51]

These measured data for I_2, IO and I for 29/08/07 were used as a guideline for the modelling studies. Figure 3.5 shows a summary of this data, with wind speed and tide height. These data were used to constrain the model during scenarios A1, A2 and B.

At periods of low tide, a high concentration of IO is observed, thus supporting the idea that iodine is emitted from exposed coastal seaweed. Figure 3.6 shows measured data for IO on 28/8/07 to 30/8/07. This clearly indicates at low tide only, iodine species are present.

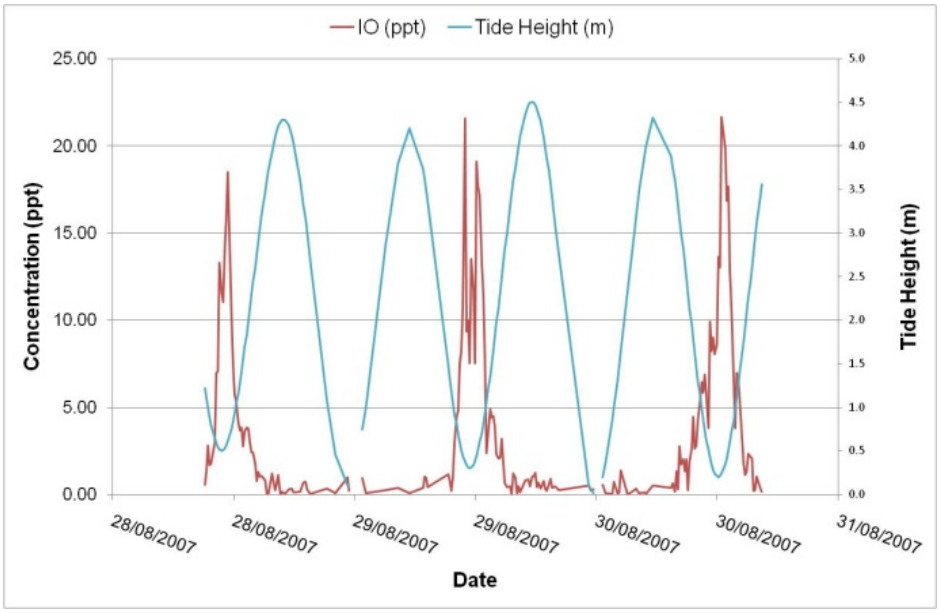

Figure 3.6: Measured IO and Tide Height Data from Mace Head, Ireland during POMORIS.

As previously mentioned, the model was set to the 29/08/07 and the addition of I_2 was adjusted manually in order to replicate observed levels of IO. Replicating these data allows the investigation of the influence of iodine species upon HO_x and NO_x species. HO_x and NO_x were looked at for each simulation of A1-C2. The wind speed is of particular importance as it indicates that the model output at a specific time will correspond to the levels of iodine species expected at the Mace Head (shoreline) site. As discussed in 2.1 it takes 12 seconds for the air parcel to travel from the start of the emission source, at a period of low low tide, to the observation station. The approach used previously in modelling studies operated on a 15-minute time step and integration period.[52] This meant the appropriate level of IO was set in the model and then species such as HO_x and NO_x were allowed to reach steady state. However, the transit time from the iodine source to the observation site is a few

seconds, not 15 minutes as modelled, so this is not a correct treatment resulting in over- (and under-) estimates of the effects of the iodine chemistry.

3.1 Modelled Data during the Daytime

3.1.1 Scenario A1: Low low tide, the Whole Emission Zone

Figure 3.7 shows the modelled data for iodine species for scenario A1, at a period of low low tide during midday. A total of 90 ppt of I_2 was injected into the air parcel during this simulation. At 12 seconds, the point at which iodine species would reach the observation station, Figure 3.7 shows the levels of modelled iodine species and if compared to Figure 3.5 the range of IO concentration has been replicated. As this situation represents day, only a few ppt of I_2 would be detected at the observation station due to its fast photolysis.

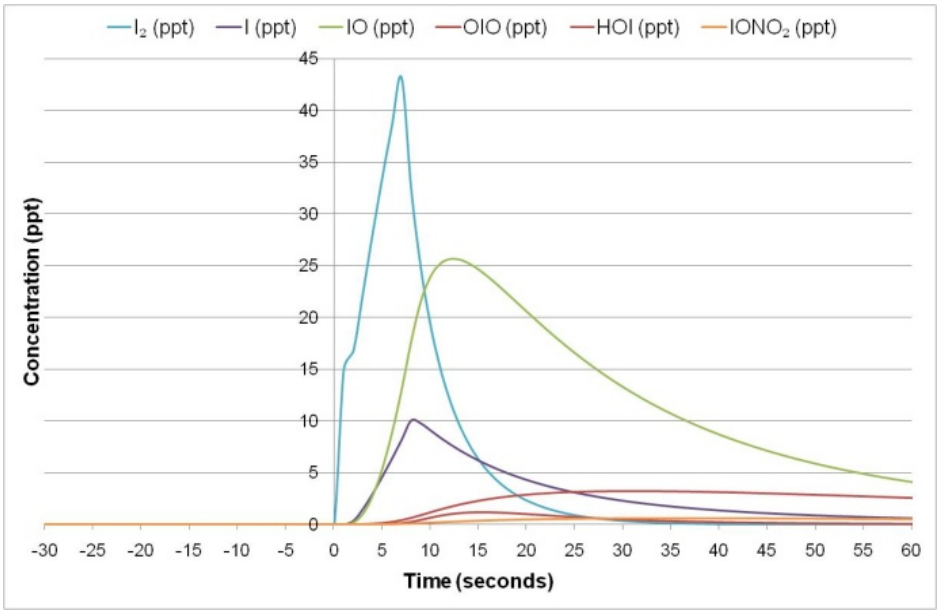

Figure 3.7: Modelled Iodine species for Simulation A1.

In Figure 3.7, -30 to -1 seconds refers to the time passed before the emission of I_2.The emission point of iodine is at time = 0. The concentration of iodine atoms can be seen in Figure 3.7, which shows a peak of ~10 ppt 8 seconds after the addition of I_2 to the model. This is due to the rapid photolysis of I_2 yielding I atoms. After 12 seconds there is a rapid decrease of I atom concentration, suggesting that I atoms are reacting in the troposphere very quickly.

The loss of I atoms are dominated by their reaction with O_3 shown in reaction 16. However, I atoms also react with HO_2 and NO_x yielding various products which are summarised in reactions 17 to 19. (See conclusion for discussion comparing I atom measurements and modelled data).

$I + O_3 \rightarrow IO + O_2$ reaction 16

$I + HO_2 \rightarrow HI + O_2$ reaction 17

$I + NO_2 \rightarrow INO_2$ reaction 18

$I + NO \rightarrow INO$ reaction 19

Figure 3.7 confirms that I_2 is photolysed rapidly in the troposphere as after just 25 seconds, almost all of the I_2 had gone. Figure 3.8 indicates the affect of iodine species on HO_x and NO_x during midday on 29/8/07. During the first 60 seconds all species decrease in concentration, the most rapid is the concentration of OH. This behaviour could be explained due to the reaction of OH and I_2 which can form HOI.

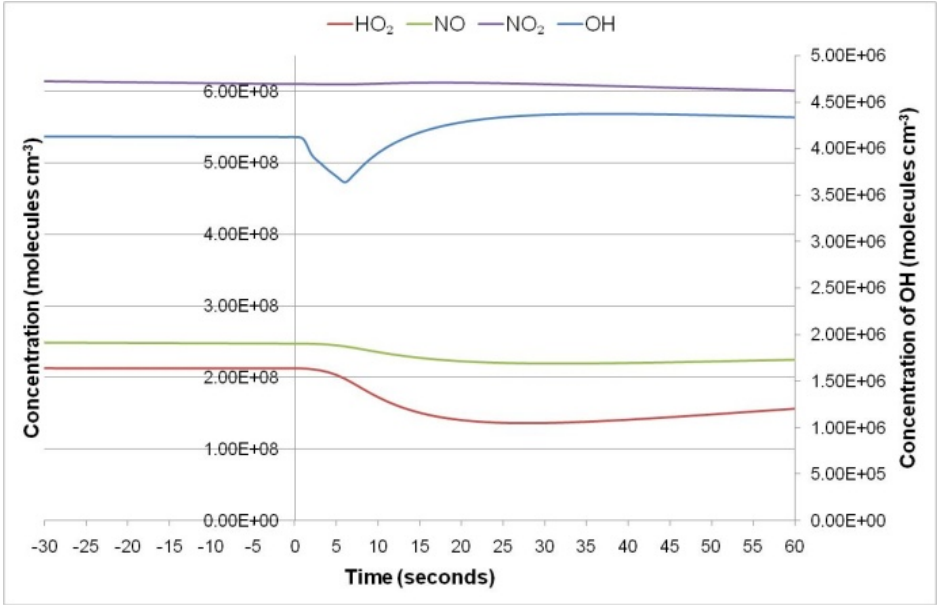

Figure 3.8: Modelled HO_x and NO_x Species Concentrations for Simulation A1.

Figure 3.8 shows that at 12 seconds, the point of observation, the concentrations of HO_x and NO_x species are lower than before the addition of I_2, but they are returning to their original concentrations. This suggests that these HO_x and NO_x species are reacting with iodine compounds. In the case of OH, after a rapid decrease in concentration, at 25-30 seconds OH levels are higher than before the introduction of iodine species, reflecting an increase in production (due to HOI photolysis) and the sink of OH resulting from I_2 is now much more reduced due to the fast photolysis of I_2.

Figure 3.9 supports the hypothesis that OH reacts rapidly with I_2 and as levels of I_2 decrease to negligible amounts, concentrations of OH return to higher than before any I_2 was added. When I_2 is released, it can react with OH to produce HOI and I. Hence, the production of OH is again apparent, when levels of I_2 decrease, due to HOI photolysis.

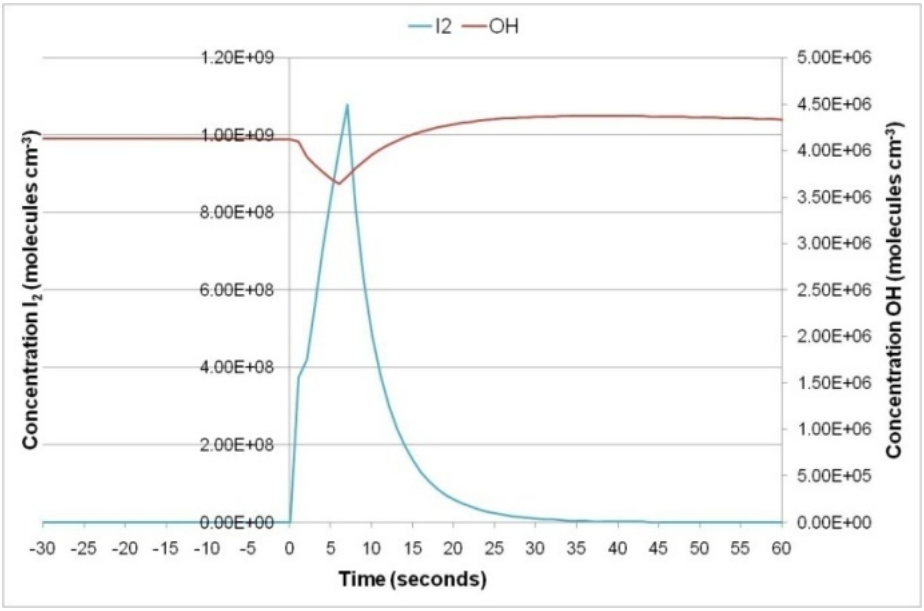

Figure 3.9: Modelled Data of OH and I_2 for Simulation A1.

Figure 3.10 shows that as HO_2 decreases with the addition of I_2, HOI is produced. The decrease of HO_2 is not as rapid as OH because HO_2 reacts with IO to produce HOI. It takes a few seconds for I_2 to photolyse, than for I atoms to react with O_3 yielding IO.

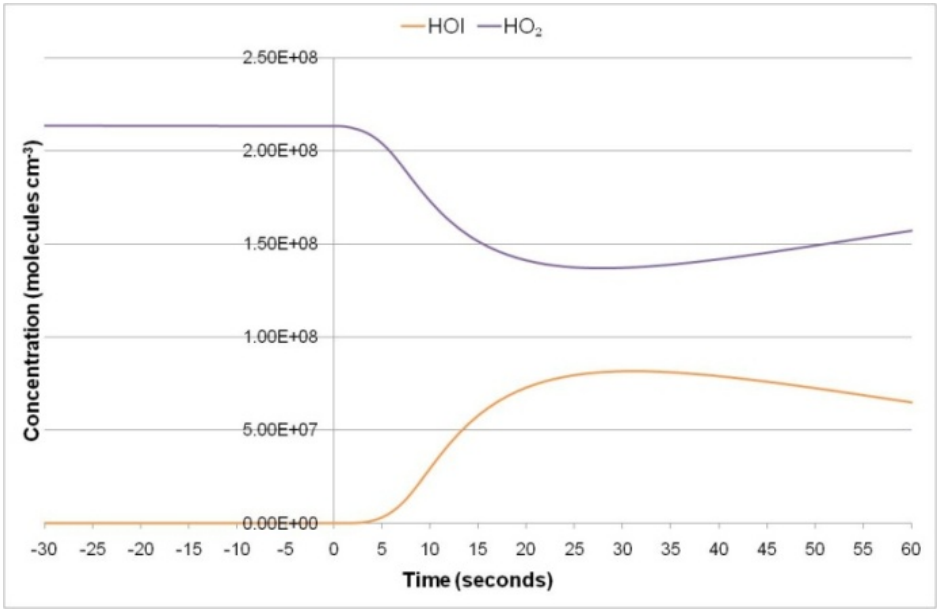

Figure 3.10: Modelled HO_2 and HOI Data for Simulation A1.

HOI can be formed *via* the reaction of OH and I_2 or the reaction of IO with HO_2. Figure 3.11 shows that the main production pathway for HOI, is the reaction of IO with HO_2. This has important implications for the HO_2 to OH ratio.

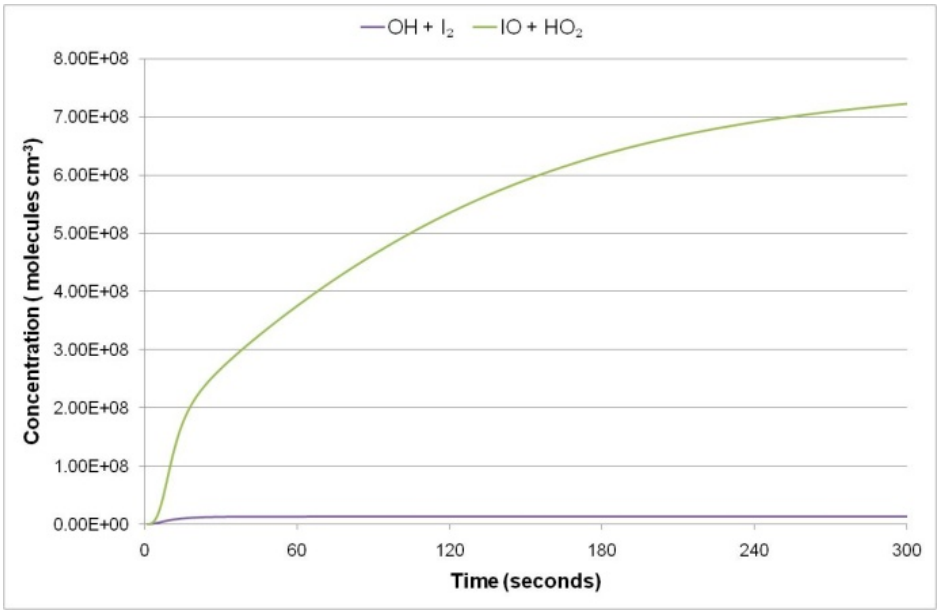

Figure 3.11: Modelled Data for the Production Pathway of HOI.

Figure 3.12 indicate the concentrations of other iodine species present as a result of I_2 addition. PI 1-4 are particulate matter iodine, iodine species in the aerosol phase. PI1 is I_3O_5 or equivalent, PI2 is I_3O_6 or equivalent, PI3 is I_2O_5 and PI4 is HIO_3 (see Appendix 8.2 for details).

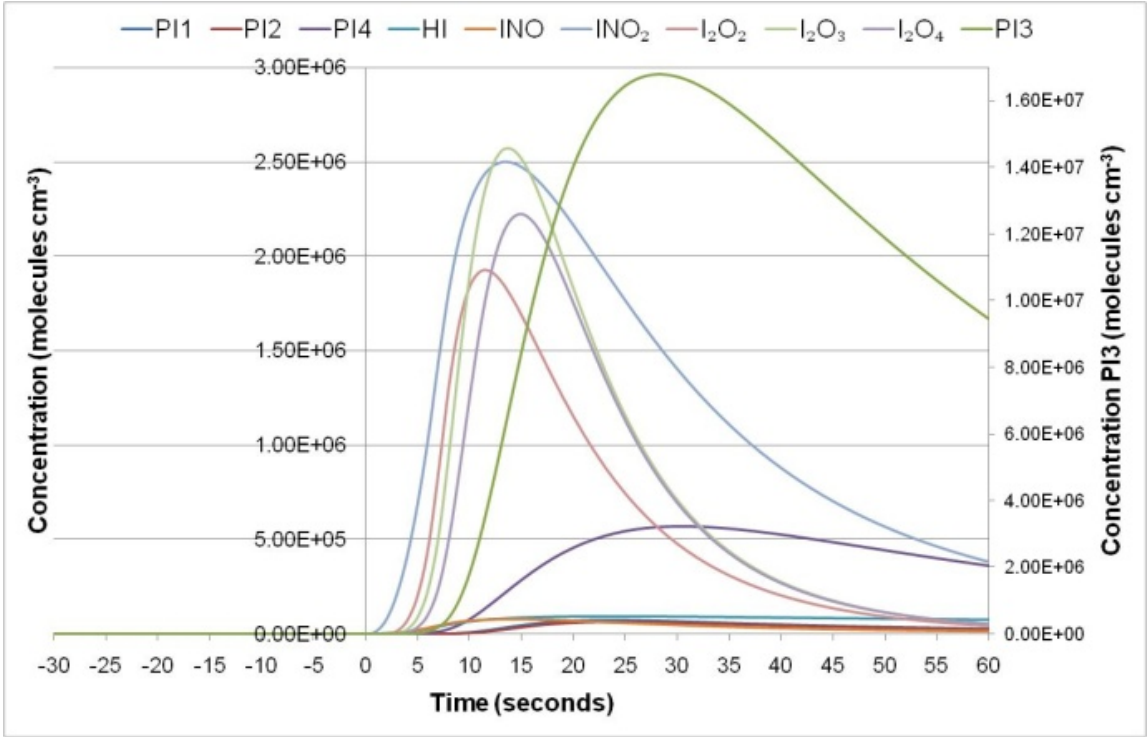

Figure 3.12: Modelled Iodine Species in the Aerosol Phase for Simulation A1.

3.1.2 Scenario A2: Low low tide, the Concentrated Emission Zone

For simulation A2 at low low tide, during the concentrated emission zone of 10 m, it would take 1 second for the box of air to travel over the I_2 emission source. Hence a 1 second I_2 addition window was incorporated within the model simulation. In order to replicate IO observations from POMORIS, it was necessary to add a total of 260ppt I_2. Figure 3.13 shows that there is a rapid decrease of I_2 after 10 seconds. This again confirms the fast photolysis of I_2. Figure 3.13 shows the concentration of iodine species at 12 seconds, the point at which the air parcel would reach the observation station. The observed levels of IO (Figure 3.5) have been replicated by design.

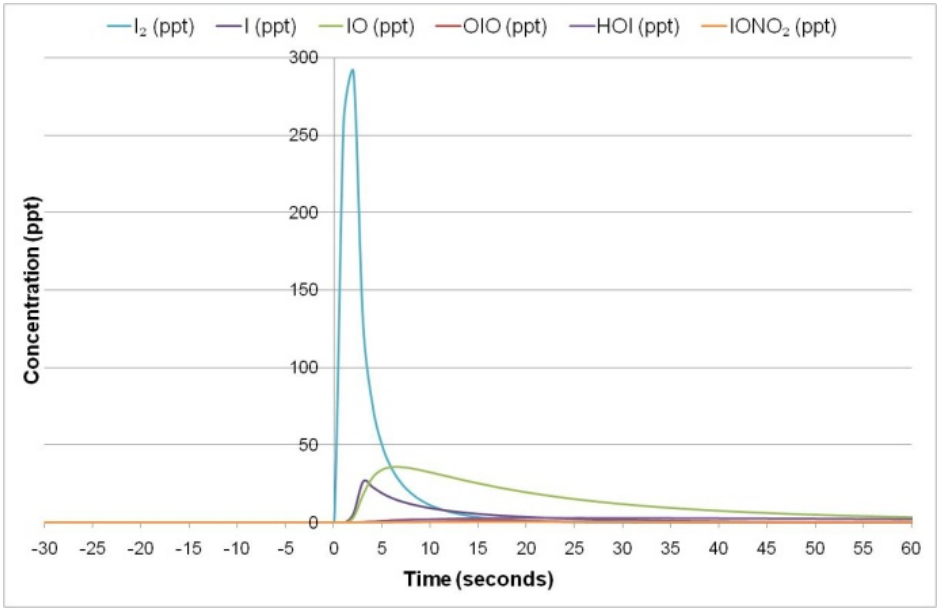

Figure 3.13: Modelled Iodine Species for Simulation A2.

Figure 3.14 again confirm that HO_x and NO_x species are affected by the presence of I_2 in the atmosphere. HO_x and NO_x concentrations decrease rapidly as I_2 is injected into the air parcel. Most noticeably OH decreases extremely rapidly within the first second, the point when I_2 is added.

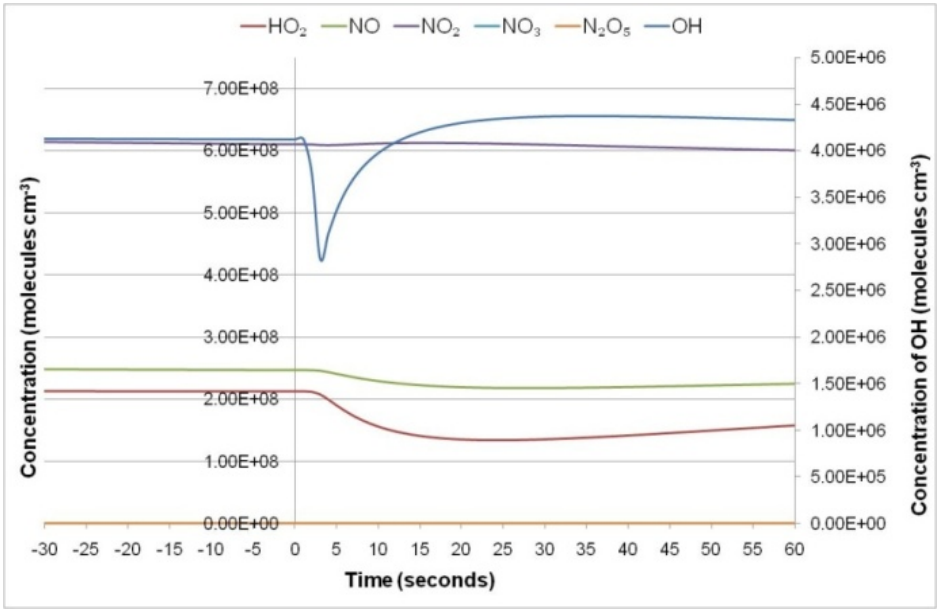

Figure 3.14: Modelled HO_x and NO_x Concentrations for Simulation A2.

Figure 3.15 shows that there is a greater impact upon OH initially with a smaller I_2 emission zone, however at the measurement point, there is no difference. There is no change on NO_2 with simulations A1 and A2, although there is a greater impact upon NO and HO_2 with a concentrated emission zone. It is small, yet would be observed at the measurement point.

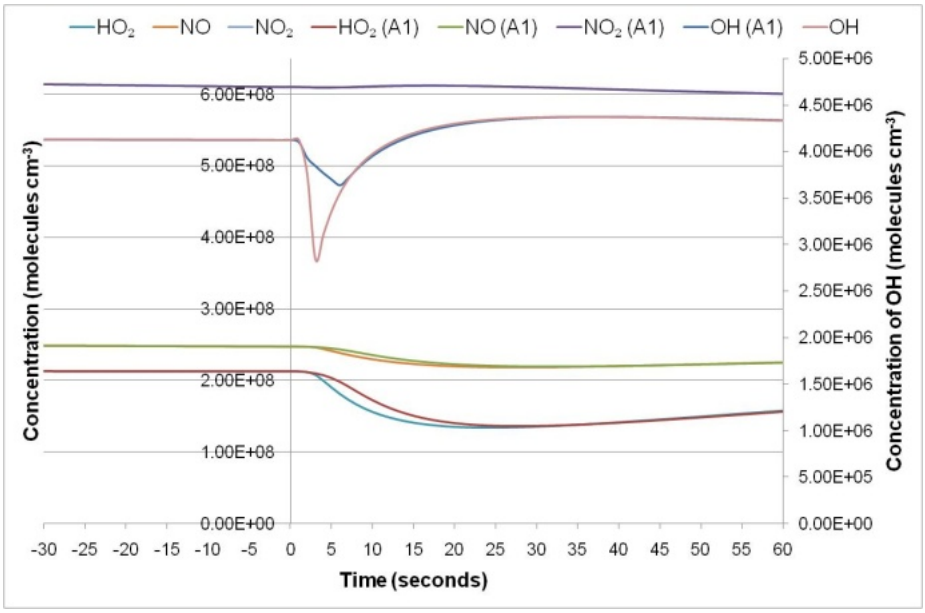

Figure 3.15: Comparing HO_x and NO_x Data for Scenarios A1 and A2.

Figure 3.16 shows the predicted concentrations of other iodine compounds including those in the aerosol phase. Compared to scenario A1, a concentrated emission zone has a much greater impact upon species P3. However, the remaining species show that a small emission zone has a much lower impact upon their concentrations.

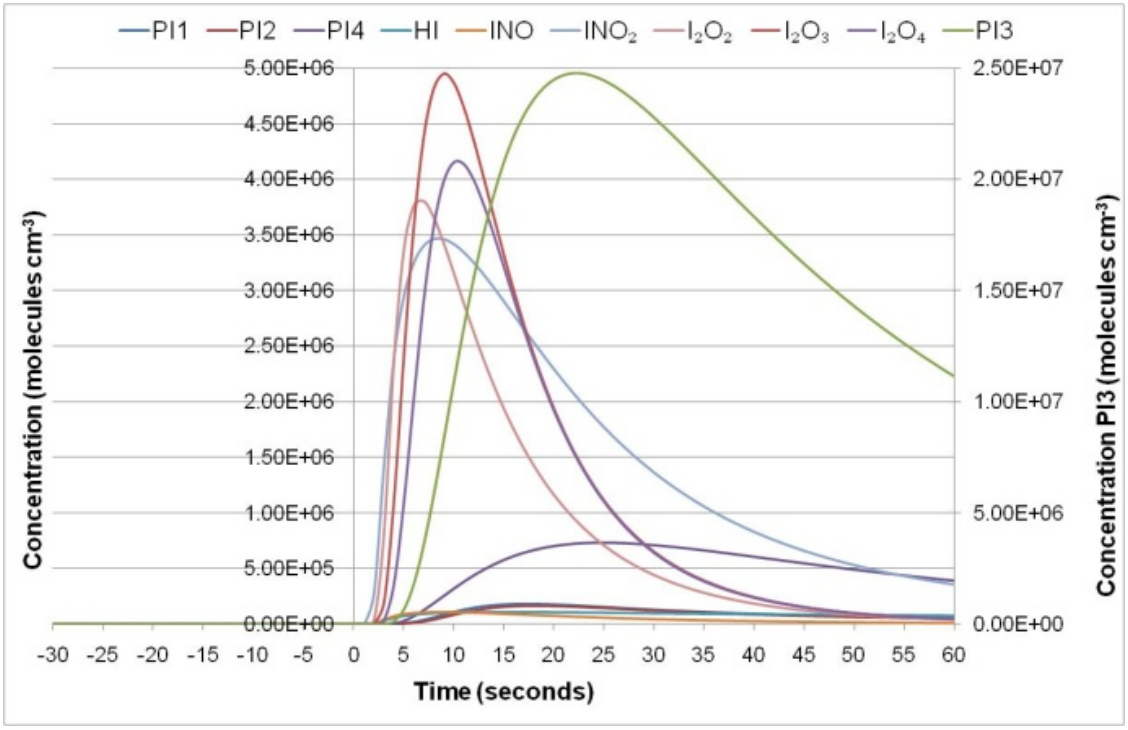

Figure 3.16: Modelled Data for Other Iodine Species.

3.1.3 Scenario B: High low tide, the Whole Emission Zone

Scenario B was used to replicate measurements of IO at a period of high low tide. A representative high low tide period from the measured data was selected: 15.00 on 20/08/07. The tide height at low low tide was measured at 0.2 m, compared with 1.3 m at high low tide. For simulation B, the emission zone of I_2 was estimated to be 20 m therefore a total of 30 ppt I_2 was added to the model to replicate observed levels of IO from POMORIS. At high low tide the seaweed would not be as exposed as low low tide therefore the emissions of I_2 may not be as high in concentration with high low tide periods. Figure 3.17 show the modelled data of iodine species and if compared with Figure 3.3 it can be seen that the IO data has been replicated.

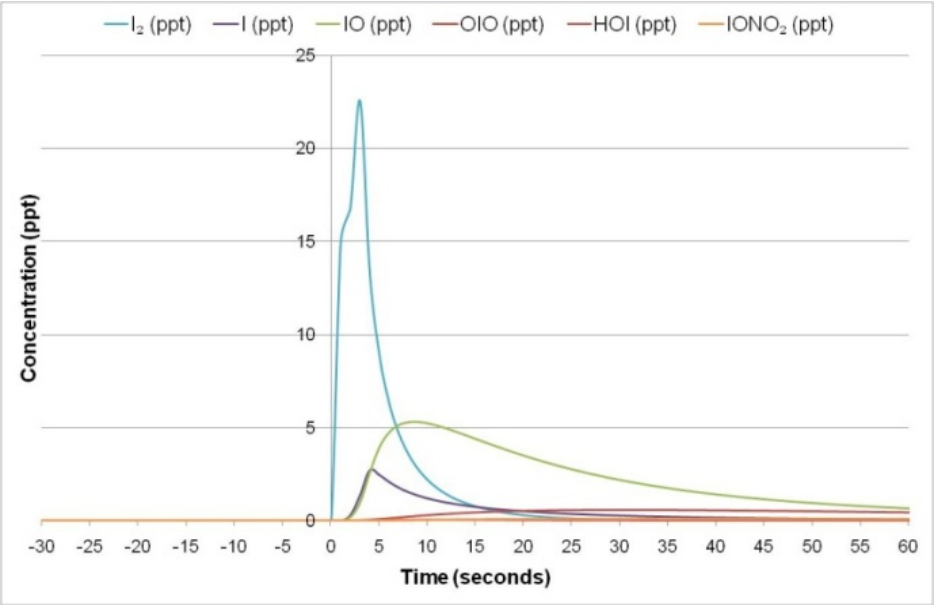

Figure 3.17: Modelled Iodine Species Concentrations.

The measurements of IO on this day were 3-5 ppt compared with 25-30 ppt measured on a low low tide day. This strongly supports the theory that seaweed, specifically those species only exposed at the lowest low tides, are a key source of I_2 to the atmosphere in the Mace Head Coastal environment.

Figure 3.18 again indicates the rapid decrease in concentration of OH, however, here, the change in concentration of NO, NO_2 and HO_2 is much more subtle than in case A1 and A2 described above (Figure 3.8 and Figure 3.14) and as Figure 3.18 shows, at 12 seconds the levels of these species are constant.

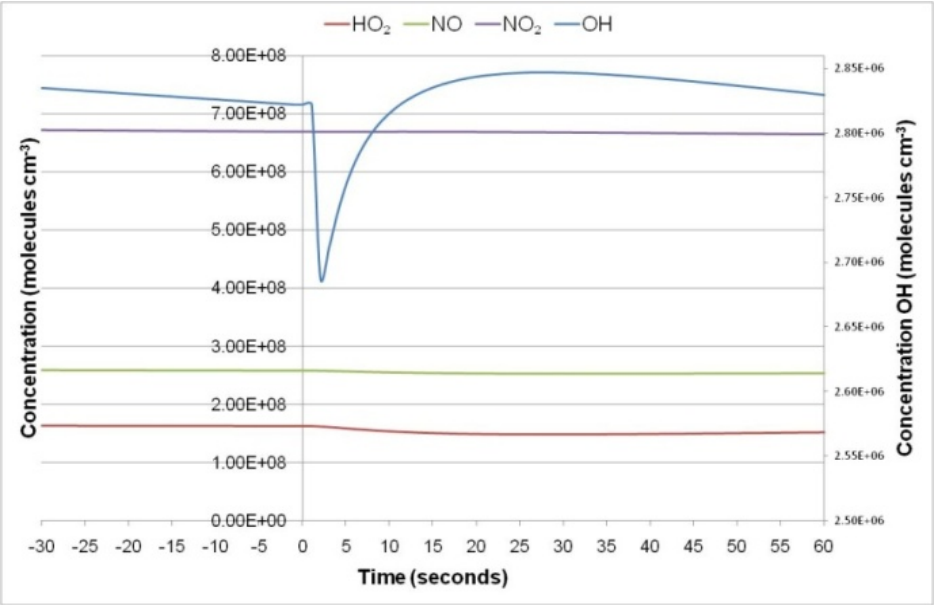

Figure 3.18: Modelled HO_x and NO_x Concentrations for Simulation B.

3.2 Modelled Data during the Night

3.2.1 Scenario C1: Low low tide, the Whole Emission Zone

Based on measurements taken during POMORIS, night time levels of I_2 at the Mace Head site reached 100 ppt. For simulation C1, the whole emission zone was considered, which was estimated to be 50 m (as with A1, this is the same tidal phase and the largest exposed area of the emission source). Therefore I_2 was added for 6 seconds because at the measured wind speed of 9 m s-1 it would take 6 seconds for the air parcel to travel over the emission source. This corresponded to a total of 360 ppt I_2 added, equivalent to 100 ppt of I_2 present where the observation station would be, that is 110 m inland at 12 seconds. The difference between the initial level of I_2 and the I_2 present at 12 seconds arises due to the vertical dilution of the iodine plume.

Figure 3.19 indicates that when modelled during hours of darkness no other iodine species are present at significant concentrations. During the NAMBLEX campaign a few ppt of iodine oxides were detected. However with I_2 not photolysing there are no other iodine species being formed. However, as Figure 3.19 clearly shows, at 12 seconds there is 125 ppt of I_2 and this level is decreasing supporting the vertical dilution of I_2.

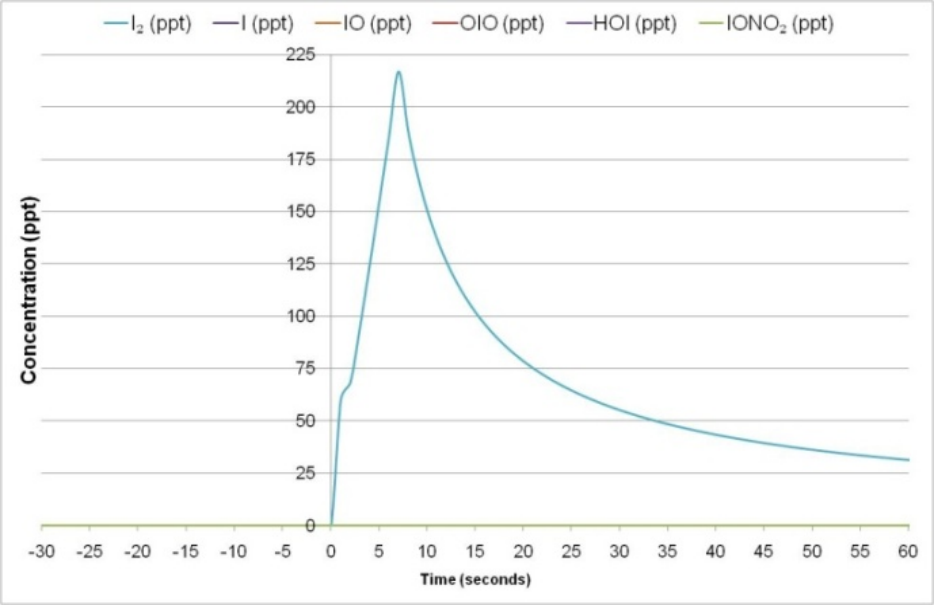

Figure 3.19: Modelled Iodine Concentrations for Simulation C1.

Even though NO_3 is the night time radical, Figure 3.20 clearly shows that as I_2 is added to the air parcel, OH is still rapidly reacting with iodine (although the night time levels of OH are extremely low)[53]. However, compared to the daytime simulations, OH does not decrease as much here. This could suggest that I_2 is also reacting with NO_3.[29] In simulation A2 where 260 ppt I_2 is added to the model, at the point of 1 second I_2 is present at less than 5 ppt, clearly I_2 is photolysed extremely rapidly during the day. Here however, the main loss of I_2 is from dilution. There is some reaction with NO_3, as shown by the NO_3 line on the graph, but presumably this is a minor contribution to the I_2 removal (which is dominated by dilution and mixing).

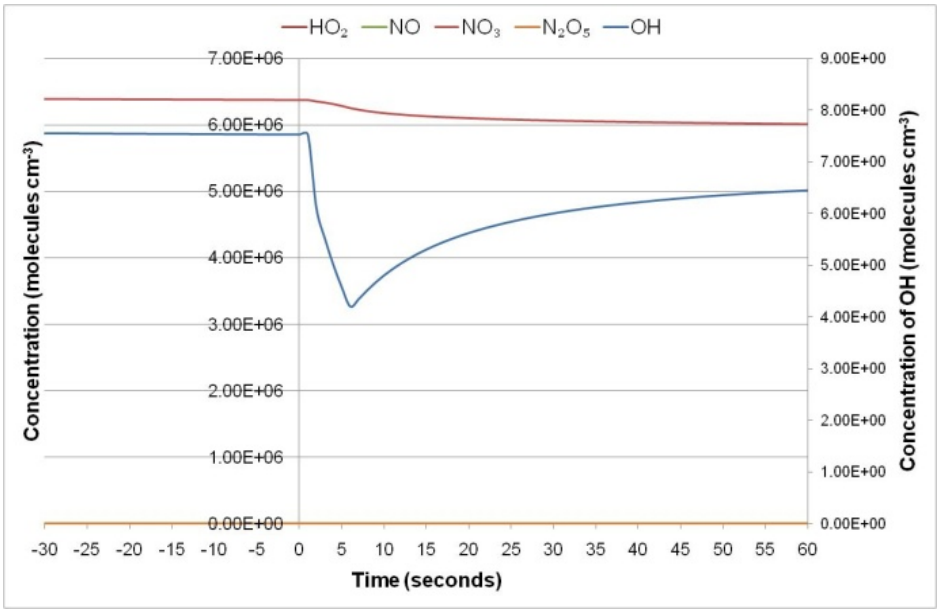

Figure 3.20: Modelled HO_x and NO_x Species Concentrations for Simulation C1.

In comparison with daytime simulations (A1 and A2), where PI3 was the most abundant iodine species, here, Figure 3.21 shows that particulate matter is rapidly decreasing in concentration whereas INO_2 is formed steadily and after around 120 seconds decreases very slowly. This is because during the night there is no photolysis of INO_2.

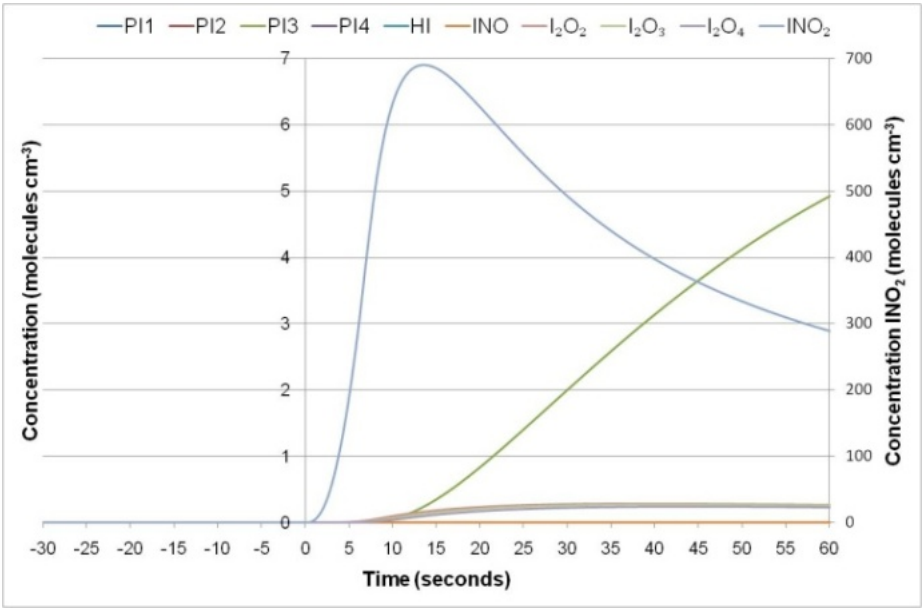

Figure 3.21: Modelled Data for Simulation C1.

3.2.2 Scenario C2: Low low tide, the Concentrated Emission Zone

Simulation C2 employs the estimation of the extent of the concentrated emission zone to be 10 m. This is the night time equivalent of scenario A2 as described above. Again the total concentration of I_2 added to the air parcel was 360 ppt as with C1. Note that this is in contrast to the daytime case, when the I_2 addition differed between the two scenarios (A1 and A2 respectively). The concentration of I_2 decreases more rapidly than in the previous scenario (C1) due to the dilution of I_2; but again I_2 is the only iodine species present at significant levels. This again supports the idea that I_2 has a short photolysis lifetime during the day.

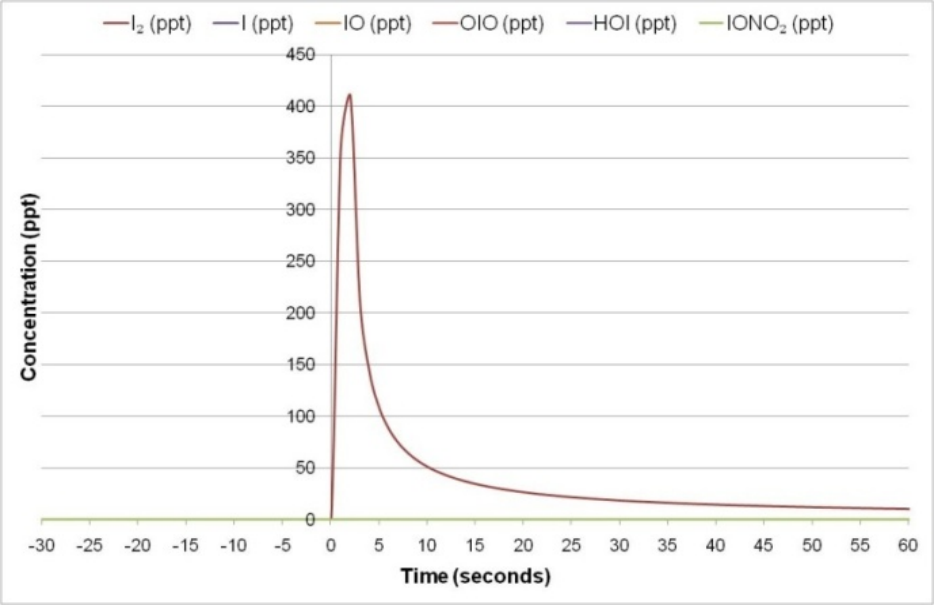

Figure 3.22: Modelled Concentrations for Iodine Species for Simulation C2.

The chemical lifetime of I_2 (with respect to reaction with NO_3) can be calculated from the modelled NO_3 concentration and the $I_2 + NO_3$ rate constant:

$k[NO_3] = k^1$

k = first order rate constant for the reaction between NO_3 and I_2 (yielding I and $IONO_2$) which is 1.5×10^{-12} cm^3 $molec^{-1}$ s^{-1} (personal communication, W. Bloss)

$[NO_3]$ = concentration of NO_3 which here will be 6.15×10^6 molecules cm^{-3} taken from the modelled data at 12 seconds.

Due to these conditions, the lifetime of I_2 for this reaction can be calculated (section 1.1.1 defines lifetime) using the following calculation:

$$\frac{1}{\left(1.5 \times 10^{-12}\right)\left(6.15 \times 10^{6}\right)} = 108401.084 \left(= 30 hours\right)$$

The chemical lifetime of I_2 at night, due to reaction with NO_3, is long (30 hours) and the main loss is dilution as the iodine plume expands, while during the day its lifetime is short (10-13 seconds) due to photolysis. This is because levels of NO_x are low (50 ppt) in these simulations to represent a remote coastal location, therefore there is not much NO_3 available.

In conjunction with Figure 3.20 for simulation C1, Figure 3.23 shows that as I_2 is added, there is some reaction with NO_3 as in the first 5 seconds after I_2 addition NO_3 decreases rapidly, although it only decreases by a small amount. This is a key difference to simulations A1 and A2.

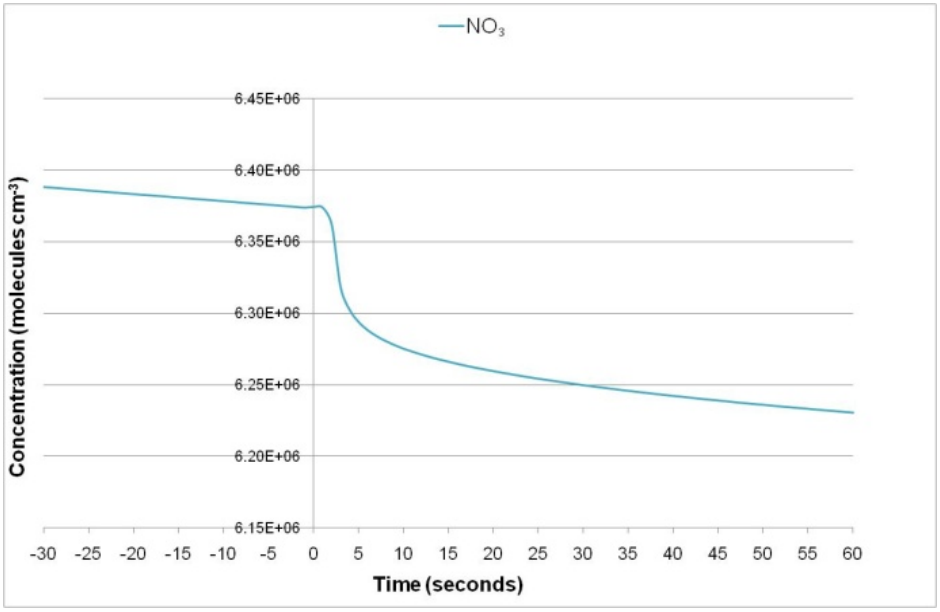

Figure 3.23: Modelled NO_3 Data for Simulation C2.

Another difference between the day time scenarios (A1 and A2) and the night time simulations is that INO_2 is formed steadily in the night as shown in Figure 3.24

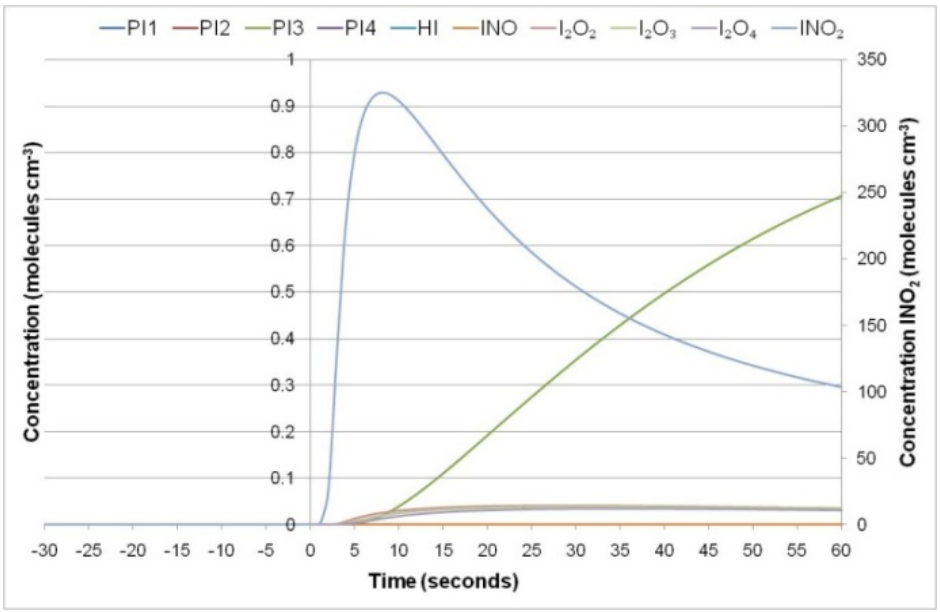

Figure 3.24: Modelled Iodine Species Concentrations for Scenario C2.

4 SENSITIVITY STUDY

A sensitivity study was carried out in order to investigate the potential impacts of those iodine kinetic and photochemical properties for which measurements are unavailable, and which were therefore estimated in constructing the iodine reaction mechanism (see Appendix 8.2). For this sensitivity study conditions from simulation A1 were used. These conditions as previously mentioned were midday, 29/08/07 with a total of 90 ppt of I_2 added to the air parcel over the whole emission zone estimated to 50 m. The same model run was repeated, with each individual parameter changed in turn. The effects were evaluated in terms of (changes in the) concentrations of I, IO, total PI (particulate matter, iodine in the aerosol phase) OH and HO_2 at a time of 12 seconds, the point of observations and at 60 seconds to see what happens to the evolution of these species downwind of the Mace Head observation point.

4.1 Additional Reactions used in the Sensitivity Study

It was hypothesised the reactions 20 to 23 may occur with the presence of iodine in the atmosphere. These are shown in Table 4 below. These reactions and corresponding rate constants were proposed due to measurements taken of OIO reported in 2007.[43] These measurements suggested that a high level of OIO can be observed in clean environments and the chemical lifetime of OIO is longer than previously thought. Model predictions by Stutz *et al.* suggest that iodine oxides may be reacting with NO_x species in the troposphere.[43] Reactions 20 and 21 were added individually, but reactions 22 and 23 were added together.

Reaction	Rate Constant (cm^3 $molecules^{-1}$ s^{-1})	Reaction Number
$I + IONO_2 \rightarrow I_2 + NO_3$	1×10^{-11}	Reaction 20
$O_3 + IONO_2 \rightarrow OIO + NO_2 + O_2$	1×10^{-13}	Reaction 21
$I + IO \rightarrow I_2O$	1.7×10^{-10}	Reaction 22
$I + I_2O \rightarrow I_2 + IO$	2.1×10^{-10}	Reaction 23

Table 4: Summary of Additional Reactions.

Figure 4.1 indicates how levels of I and IO have altered with the addition of these reactions.

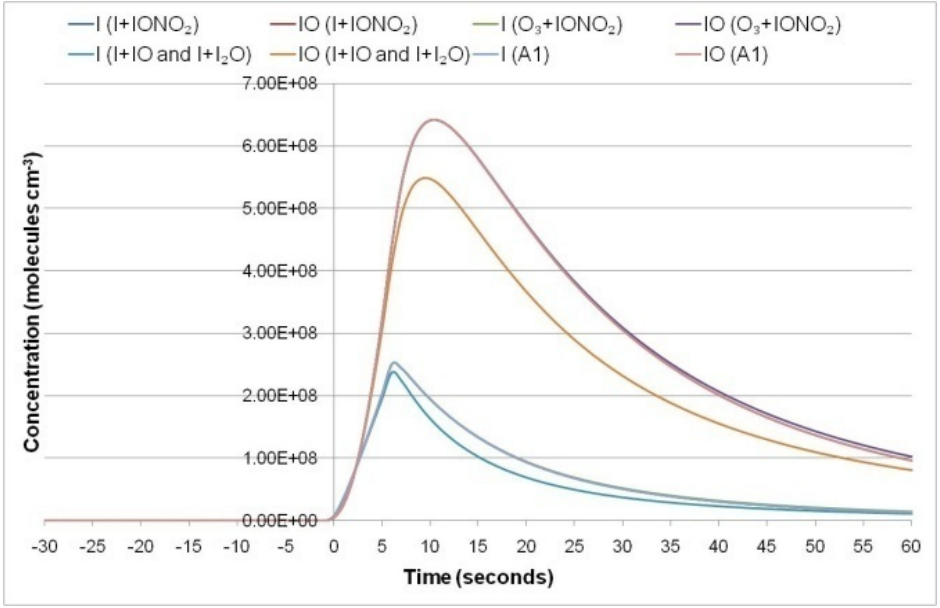

Figure 4.1: Modelled Concentrations of I and IO including addition reactions 20-23. I (A1) and IO (A1) show the original values without the addition of any reactions.

Figure 4.2 however, shows at 12 seconds, where these species would be observed, no significant change in HO_x and NO_x concentration is apparent. However, at 60 seconds reactions 22 and 23 have a slightly greater impact on OH concentration than the other addition reactions.

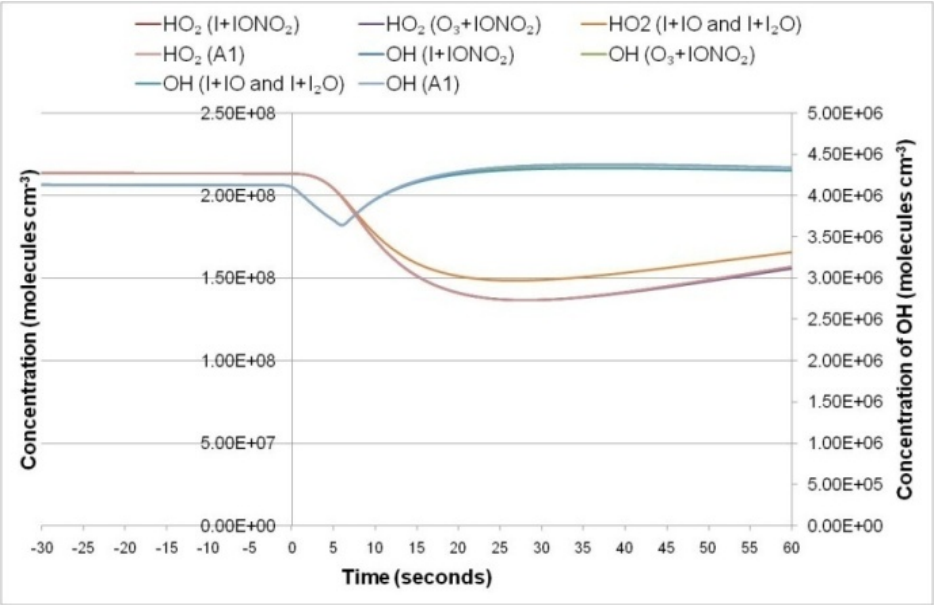

Figure 4.2: Modelled Concentrations of HO_x including addition reactions 20-23. (A1) indicate the original levels of HO_x.

Figure 4.3 shows that with the addition of reaction 21, there is a smaller impact upon the concentration of PI4 and PI3 species than without the addition of this reaction. With the addition of reactions 22 and 23 there is a much smaller impact upon PI4 and PI3 than without the addition of these reactions.

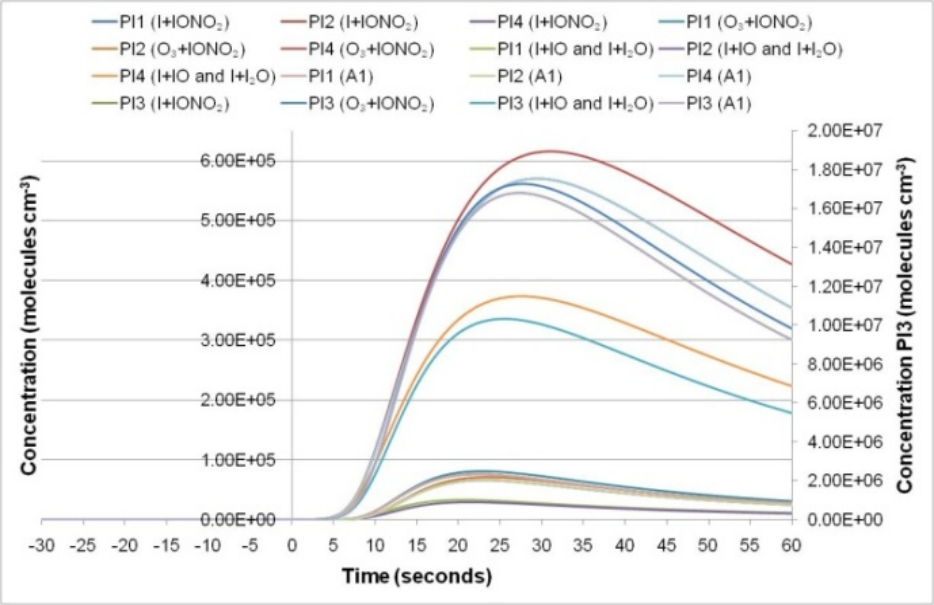

Figure 4.3: Modelled PI Data with Additional Reactions 20-23. (A1) indicate the original levels of PI.

4.2 Changes to the Total Aerosol Surface Area

A further point to investigate was the total aerosol surface area. The model used a value of 5 x 10^{-6} cm^2 cm^{-3} as measured during NAMBLEX.[31] which would be expected to be similar for POMORIS, but may not reflect the conditions on the actual measurement day. Figure 4.4 shows changes in the modelled concentration of I and IO when the aerosol surface area (ASA) was increased and decreased. When the surface area was increased by a factor of 5 in the model, I and IO concentrations reduce more rapidly than the previous (scenario A1) surface area. The surface area was also reduced by a factor of 5 in the model leading to a slight change in IO and I concentrations, from ~50 seconds onwards they do not decrease as rapidly.

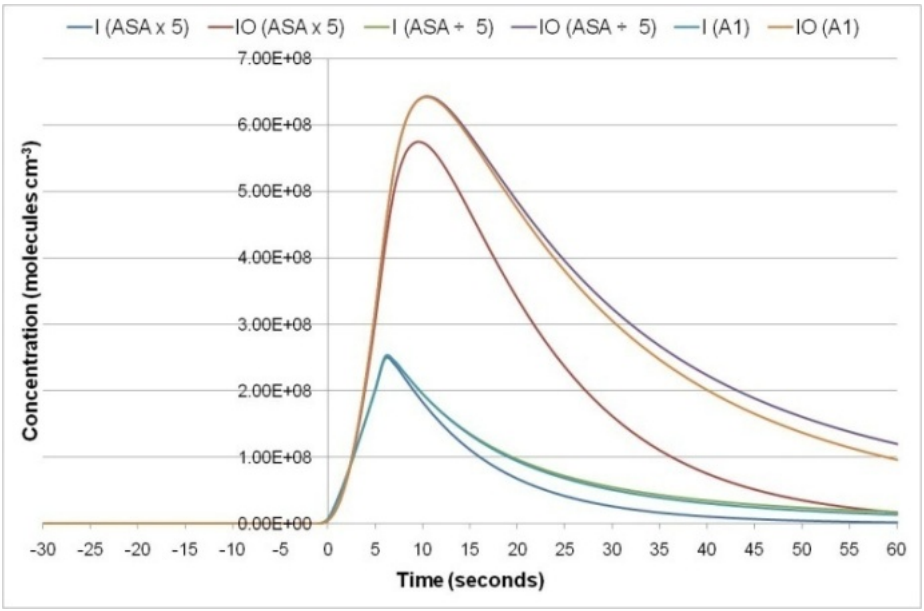

Figure 4.4: Modelled Concentration of I and IO with a change in Aerosol Surface Area. (A1) indicate the original levels of I and IO.

Figure 4.5 clearly indicates that a change in the aerosol surface area has significant impacts upon HO_x species. When the surface area is increased, the concentration of OH and HO_2 decrease considerably. In the case of HO_2, when iodine is injected into

the model and the concentration decreases rapidly, here with the surface area being increased, the concentration of HO_2 does not have such a rapid decrease upon the first addition. Whereas when the surface area is decreased, OH and HO_2 concentrations increase.

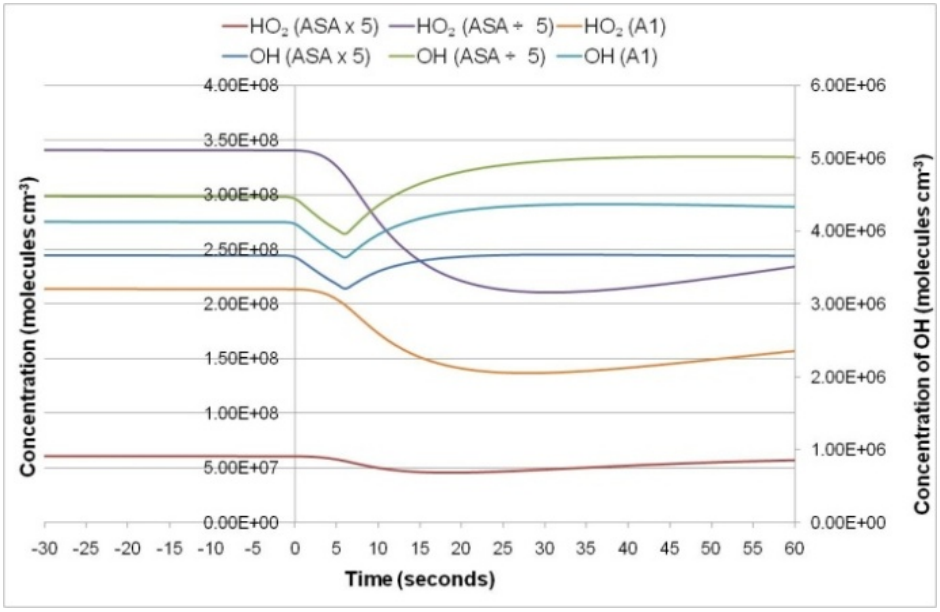

Figure 4.5: Modelled Concentration of HO_x with a change in Aerosol Surface Area. (A1) indicate the original levels of HO_x.

The large change in HO_x could be due to the direct heterogeneous loss of HO_2 and the removal of HOI by photolysis.[14, 52]

Figure 4.6 indicates that with the total aerosol surface area decreased by a factor of 5 there was much less impact upon PI3 and PI4 than when the total aerosol surface area had not been decreased. With an increase in surface area by a factor of 5, there was a much greater impact upon PI3 and PI4 than when the total aerosol surface area had not been increased.

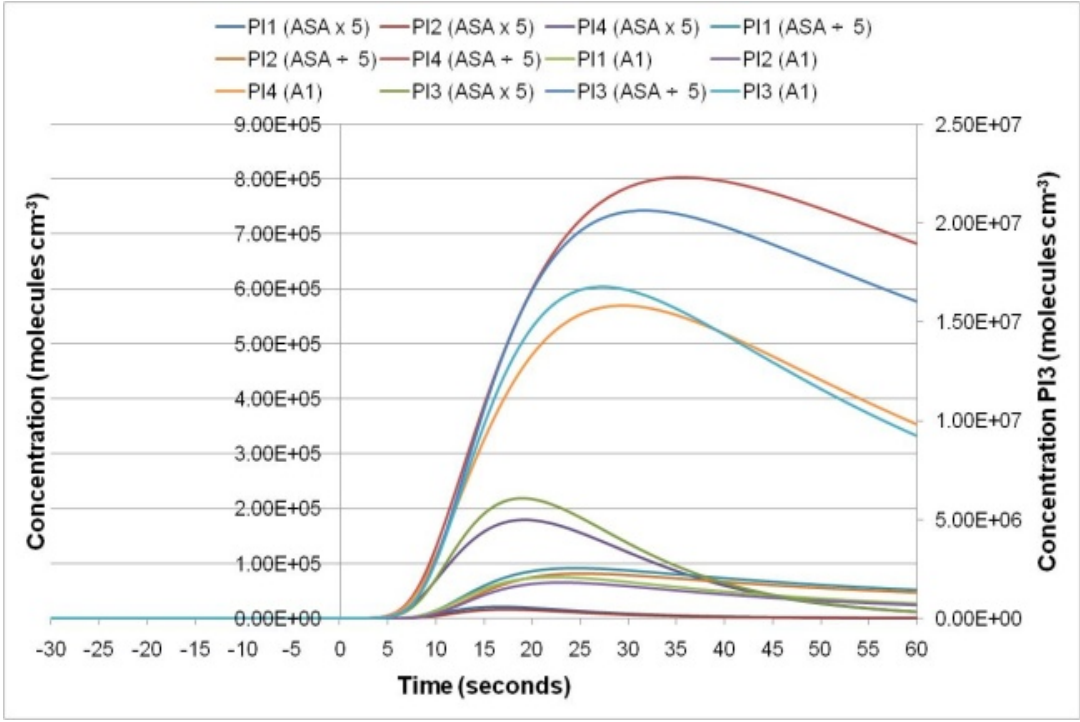

Figure 4.6: Modelled PI Data with a change in Aerosol Surface Area. (A1) indicates original levels of PI.

4.3 A Change in Photolysis Yield for the reaction of OIO

It was originally assumed that the reaction of OIO photolysis yields 100% I and O_2 as products. However, this photolysis yield was estimated and due to uncertainly, this was varied to a 5% photolysis yield.[54] The photochemistry of OIO has important implications for tropospheric chemistry in the marine boundary layer as it can influence its oxidising capacity and is involved in the formation of new particles. With the photolysis yield decreased to 5%, the resulting 95% does not dissociate OIO and the molecule is assumed to relax to the ground state. Figure 4.7 shows that this change does alter concentrations of I and IO slightly, which would be seen at the point of detection at the observation station.

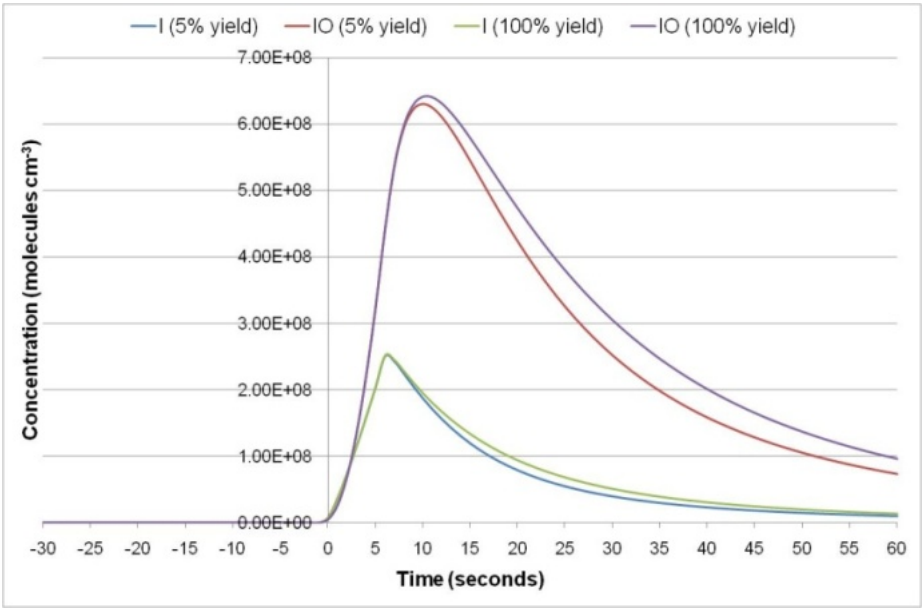

Figure 4.7: Modelled I and IO Concentrations with a Change on Photolysis Yield.

Figure 4.8 shows that at ~ 20 seconds onwards when reducing the photolysis yield of OIO to 5%, OH decreases slightly and HO_2 increases slightly. At the point of detection (12 seconds), this difference in the concentration of HO_x at 100% or 5% yield would only just about be detected whereas at 60 seconds there is a more noticeable difference in HO_2.

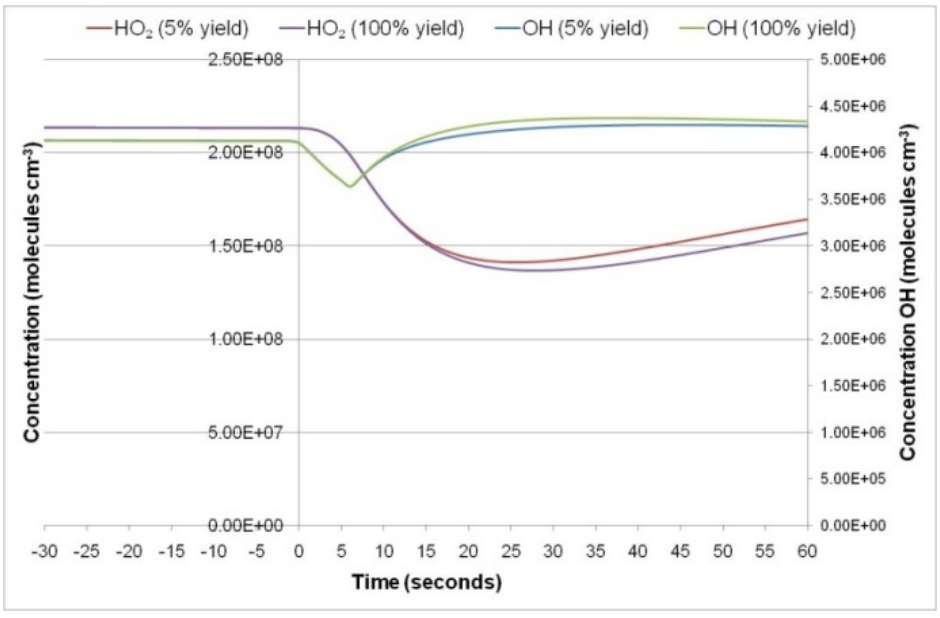

Figure 4.8: Modelled HO_x Concentrations for the Change in Photolysis Yield.

Figure 4.9 shows that with decreasing the photolysis yield of OIO, there is a much smaller impact upon PI species.

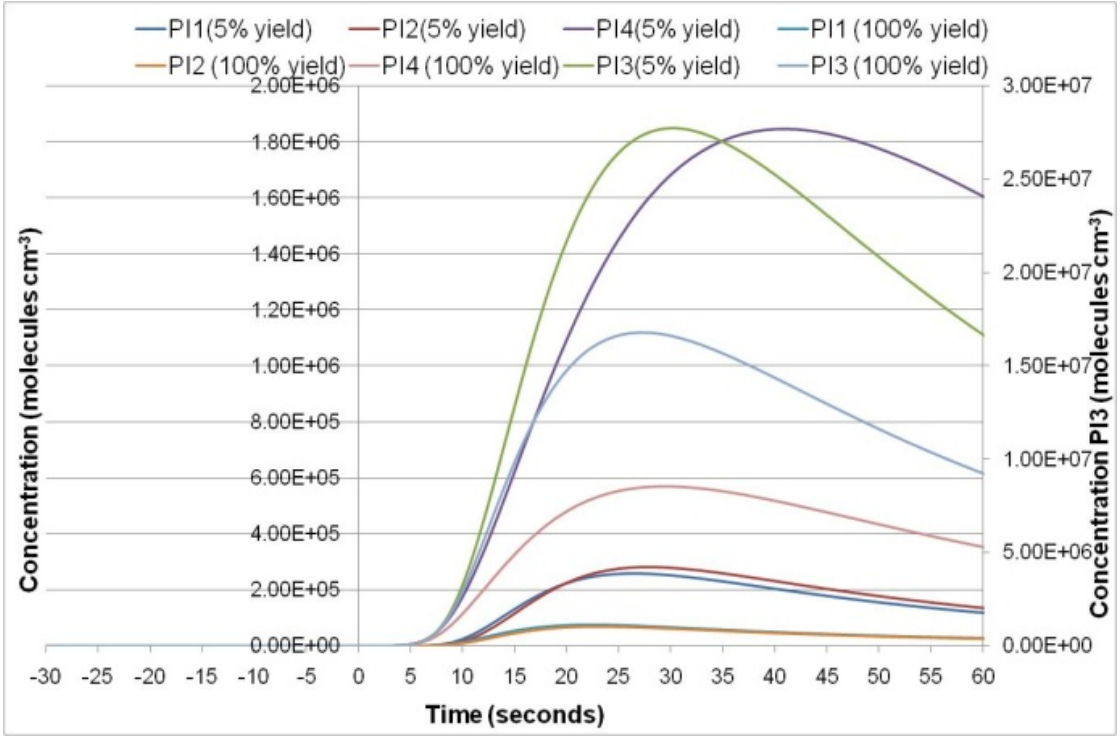

Figure 4.9: Modelled PI Data for the Change in Photolysis Yield.

4.4 Altering the Rate of Photolysis of $IONO_2$

The rate of photolysis of $IONO_2$ may be significant and is uncertain so this rate was considered. $IONO_2$ is formed by the reaction of IO with NO_2. There is a discrepancy in literature regarding the photolysis rate of $IONO_2$ and it has been suggested that it does not have a long enough lifetime (~1 minute) to be stable and provide a significant iodine reservoir during daylight.[55, 56] To investigate this, the photolysis rate of $IONO_2$ was increased by a factor of 5 and 10. However, as Figure 4.10 shows, this had no effect on the concentration of I and IO. There was also no change in the concentration of HO_x.

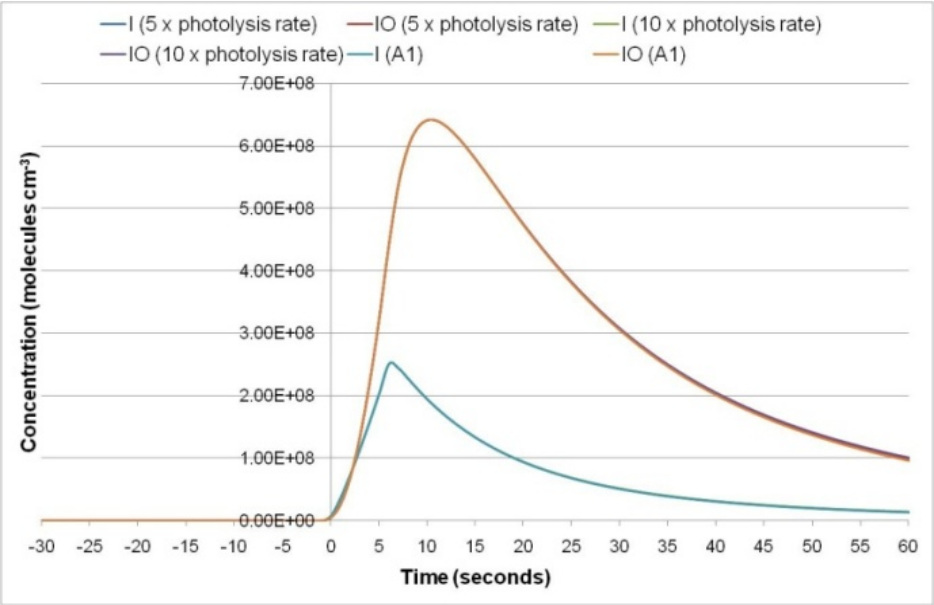

Figure 4.10: Modelled Data for I and IO Concentration with the Change in Photolysis Rate. (A1) indicate the original levels of I and IO.

This indicates that even the original "slow" $IONO_2$ photolysis was sufficiently rapid that little $IONO_2$ was formed (which was also affected by the low NO_x levels in these simulations).

4.5 Alternative Products for the Reaction IO + CH_3O_2

Due to a limited number of investigations into the reactions of iodine of relevance to the marine boundary layer, there is an uncertainty in the reactions and their rate constants (k) that have been predicted. Laboratory studies have shown that it is difficult to determine the products and rate constant for the reaction of IO + CH_3O_2 due to the effects of the self reaction of IO in laboratory studies.[30, 57] The products and value for k may be different to those which were estimated, shown in reaction 24. Reaction 25 is an alternative reaction that was used in the sensitivity study (replacing reaction 24). The ultimate products of this reaction (HCHO + HI + O_2) are what were

expected to form rapidly under marine boundary layer conditions. The addition of reaction 25 is compared to previous concentrations of I and IO (when reaction 24 was used).

$$IO + CH_3O_2 \rightarrow CH_3O + IOO \rightarrow HCHO + HO_2 + I \quad k = 2\times10^{-12}$$ Reaction 24

$$IO + CH_3O_2 \rightarrow CH_3O + IOO \rightarrow HCHO + HI + O_2 \quad k = 6\times10^{-11}$$ Reaction 25

Figure 4.11 shows that only a slight change in the concentration of I and IO, which would be apparent at the point of detection.

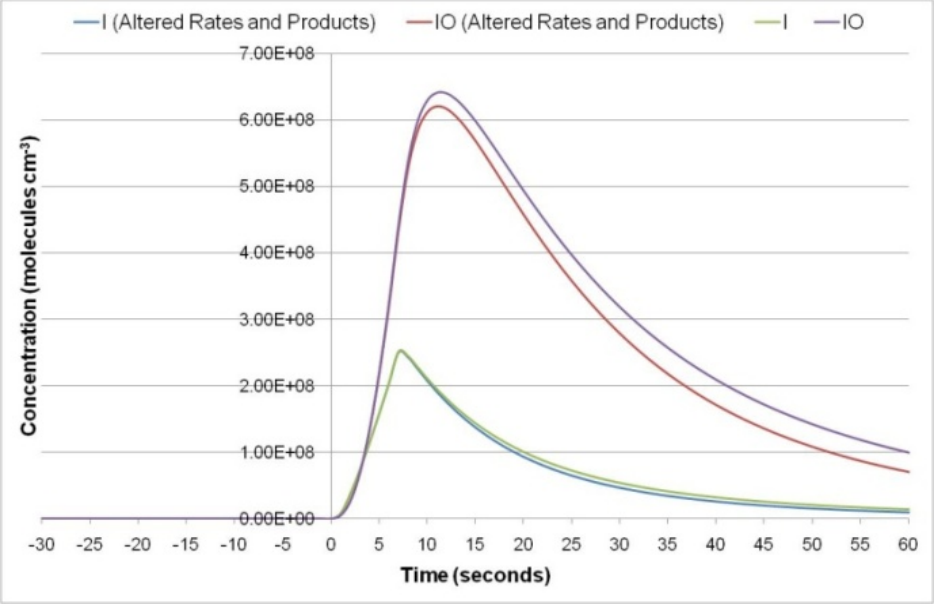

Figure 4.11: Modelled Concentrations for I and IO for the Alternative Rates and Products for the reaction IO + CH_3O_2.

There is also a slight change in concentration between HO_x species with the alternative products and this change is seen in Figure 4.12. However, Figure 4.12 displays this would not be detectable at the observation station but at 60 seconds the

change in concentration is apparent. With reaction 25, there is a smaller impact upon HO_2 but a larger impact upon OH.

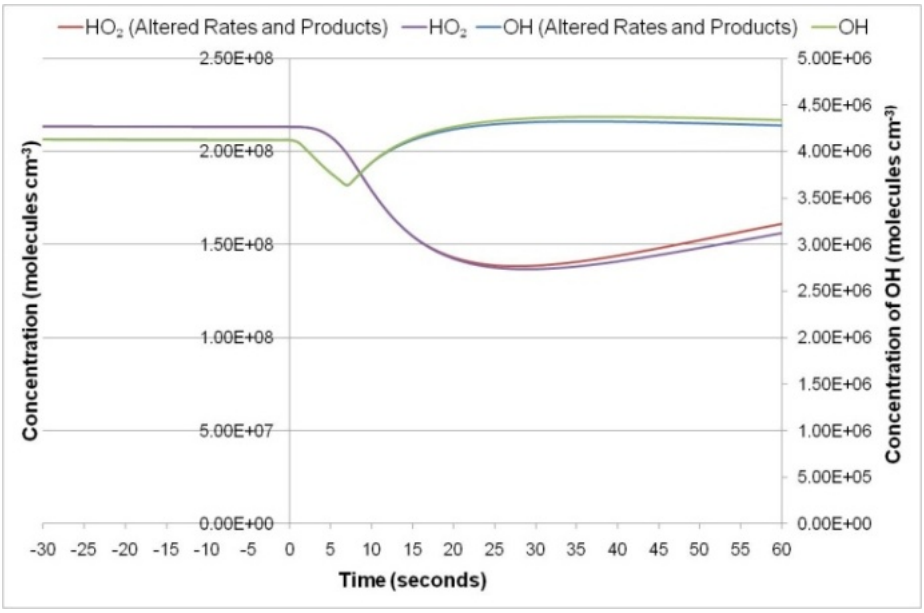

Figure 4.12: Modelled Concentrations for HO_x for the Alternative Rates and Products for the reaction IO + CH_3O_2.

Figure 4.13 shows that with the addition of reaction 25, at the point of detection (12 seconds) negligible changes in levels of PI would be observed, however at 60 seconds it can be seen that reaction 25 has a greater impact upon PI species compared to the use of reaction 24.

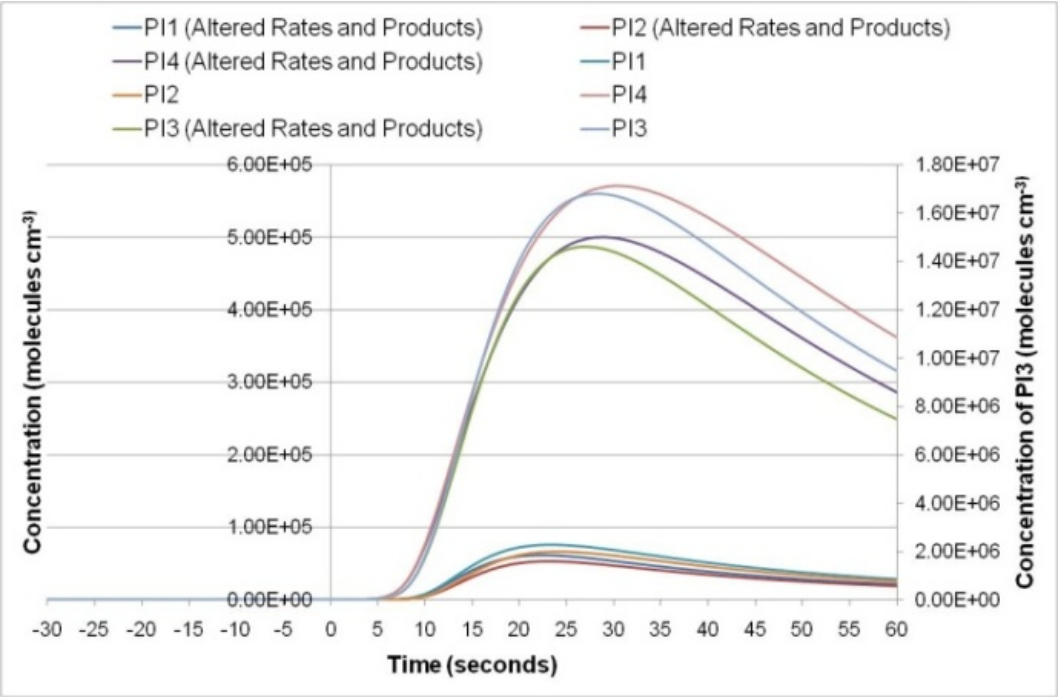

Figure 4.13: Modelled PI Data for the Alternative Rates and Products for the reaction IO + CH_3O_2.

4.6 Investigating the Thermal Stability of $IONO_2$

The final factor which was considered in the sensitivity study was the thermal stability of $IONO_2$. This can be produced when IO and NO_2 react together. $IONO_2$ will thermally decompose readily and its thermal stability is not well known. Therefore the loss rate of $IONO_2$ may be much faster than previously considered.[58] The decomposition rate constant was reduced to 10% of the original value and also multiplied to ten times the original value. However, there was no change on the concentration of iodine species (Figure 4.14) or HO_x species therefore this factor is not significant to the iodine reaction mechanism. It could be that photolysis of $IONO_2$ is dominating or that levels of $IONO_2$ are very low in these simulations due to the low levels of NO_x.

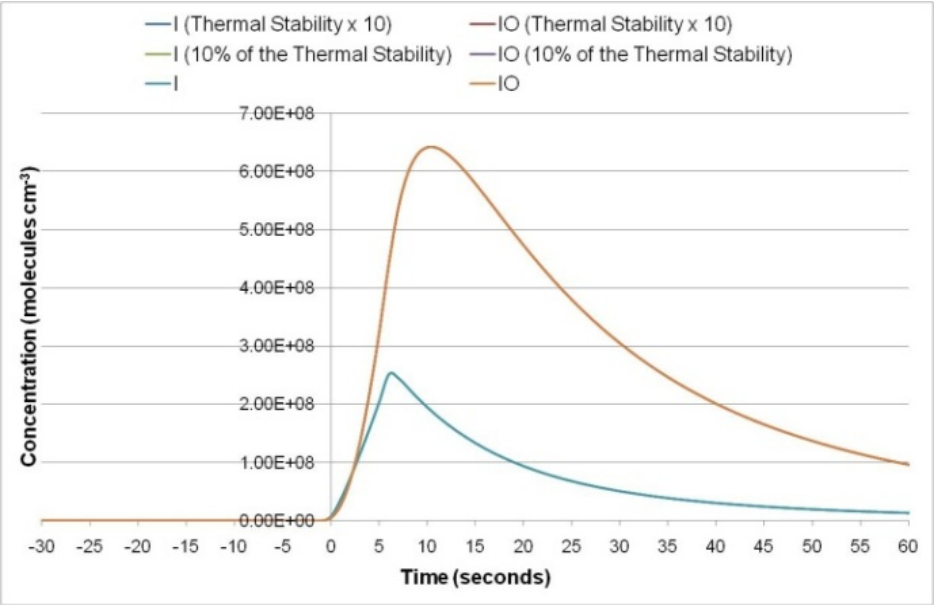

Figure 4.14: Modelled I and IO Data for the Investigation in Thermal Stability of $IONO_2$.

4.7 Summary of Sensitivity Study

Table 5 and Table 6 show the percentage change in I, IO, OH, HO_2 and total PI for the factors that were investigated during the sensitivity study. Table 5 shows the percentage change in these species at the time of 12 seconds corresponds to the point of observation for these species. Table 6 indicates how much these species have changed at a later period of 60 seconds.

Factor Changed	% Change in I	% Change in IO	% Change in OH	% Change in HO_2	% Change in Total PI
Additional Reactions					
$I + IONO_2 \rightarrow I_2 + NO_3$	-0.01	0.00	0.00	0.00	0.00
$O_3 + IONO_2 \rightarrow OIO + NO_2 + O_2$	0.19	0.07	-0.03	-0.01	0.90
$I + IO \rightarrow I_2O$ $I + I_2O \rightarrow I_2 + IO$	-19.72	-17.29	-0.20	3.29	-24.18
Total Aerosol Surface Area **(5 x 10^{-6} cm^2 cm^{-3})** Increased by a factor of 5	-10.15	-13.82	-13.34	-70.41	-37.11
Reduced by a factor of 5	0.41	0.40	10.63	58.92	5.98
Photolysis Yield for the reaction of OIO 5% photolysis yield	-6.70	-3.36	-0.97	0.35	21.34
Rate of Photolysis of $IONO_2$ Increased by a factor of 5	0.08	0.03	0.00	-0.01	0.03
Increased by a factor of 10	0.17	0.08	0.01	-0.01	0.07
Alternative Products for the Reaction IO + CH_3O_2 $\rightarrow HCHO + HI + O_2$	5.15	-2.33	-1.50	2.95	-29.10
Thermal Stability of $IONO_2$ Increased by a Factor of 10	0.00	0.00	0.00	0.00	0.00
Reduced to 10%	0.00	0.00	0.00	0.00	0.00

Table 5: Percentage Change in Modelled Species for Sensitivity Study at 12 Seconds.

The most significant difference which would be detected at 12 seconds is a -70% change in the concentration of HO_2 when the total aerosol surface area was

increased by a factor of 5. This was also significant, although to a lesser extent, to the other species modelled. Therefore this would need to be considered in future modelling.

The inclusion of reactions 22 and 23 (section 4.1) show a change in ~20-24% for species I, IO and total PI which is also significant and the remaining reactions that were added had a negligible effect.

The rate of photolysis and thermal stability of $IONO_2$ is not significant as the percent change in all species was ~0 therefore this is not an important consideration for these simulations.

Factor Changed (60 seconds)	% Change of I	% Change of IO	% Change of OH	% Change of HO_2	% Change of Total PI
Additional Reactions					
$I + IONO_2 \rightarrow I_2 + NO_3$	0.09	0.07	0.00	-0.01	0.02
$O_3 + IONO_2 \rightarrow OIO + NO_2 + O_2$	8.39	6.59	0.09	-0.81	6.89
$I + IO \rightarrow I_2O$ $I + I_2O \rightarrow I_2 + IO$	-15.01	-15.93	-0.78	5.48	-40.70
Total Aerosol Surface Area **(5×10^{-6} cm^2 cm^{-3})**					
Increased by a factor of 5	-83.21	-82.64	-15.59	-63.70	-96.39
Reduced by a factor of 5	28.95	24.68	15.59	49.15	74.50
Photolysis Yield for the reaction of OIO					
5% photolysis yield	-24.78	-23.87	-1.25	4.69	91.91
Rate of Photolysis of $IONO_2$					
Increased by a factor of 5	3.73	2.85	0.06	-0.32	0.99
Increased by a factor of 10	6.52	5.07	0.12	-0.60	1.93
Alternative Products for the Reaction IO + CH_3O_2					
$\rightarrow HCHO + HI + O_2$	-27.14	-26.96	-1.27	2.67	-19.28
Thermal Stability of $IONO_2$					
Increased by a Factor of 10	0.01	0.01	0.00	0.00	0.00
Reduced to 10%	-0.01	0.00	0.00	0.00	0.00

Table 6: Percentage Change in Modelled Species for Sensitivity Study at 60 Seconds.

At 60 seconds, which would be later than the point of detection, the situation looks quite different for some species. The increase in total aerosol surface area has a greater impact upon I, IO and total PI where the latter reaches 96% change. However, in contrast to the situation at 12 seconds, at 60 seconds, although the addition reactions 22 and 23 are significant (section 4.1), it is less significant here except for the total PI which the inclusion of these reactions has a greater impact. The addition of reaction 21 has much more of a significant impact upon I, IO and PI than the previous case at 12 seconds.

The photolysis yield for the reaction of OIO is much more significant at 60 seconds, in particular for the total PI which shows a percentage change of 91% compared to 20% at 12 seconds.

The alternative products for the reaction of IO + CH_3O_2 shows a more significant change for I and IO at 60 seconds than at 12. In conjunction with the results at 12 seconds, the thermal stability of $IONO_2$ shows no change and is insignificant in both cases.

In summary, the uncertainties in the physical conditions, such as the total aerosol surface area, do lead to significant changes in the predicted levels of iodine species and HO_x. The uncertainties in reactions such as OIO photolysis and the occurrence of the I + IO reactions (22 and 23) also lead to significant changes in the predicted levels of iodine and HO_x species. Agreement of modelled data with measured values to levels greater than 20-30% should be regarded as serendipitous rather than as

proof of the accuracy of the simulations. This sensitivity study has shown that further research into these processes is required.

5 DISCUSSION

The role of iodine and its effect on HO_x and NO_x species in the coastal marine boundary layer was studied using a box model which used aspects of the MCM and was constrained to measurements from NAMBLEX (Summer 2002) and POMORIS (Summer 2007). These campaigns both took place at Mace Head, Ireland. This thesis presents the results from the first lagrangian box-model study of the interaction of coastally emitted iodine species with short-lifetime atmospheric constituents such as HO_x and NO_x. Based on NAMBLEX data, VOCs were selected which accounted for ~95% of the total OH budget. Previous studies accounted for ~80% of the species contributing to OH loss (see section 2.1 for the list of VOCs used).[45]

This study uses the point measurements of IO, I_2 and I measured using the methods LIF, BBCEAS and RF respectively. These data were taken during POMORIS and the employment of these instruments allowed point measurements of iodine species to be made. These measurements represent more accurately the levels of iodine species emitted into our atmosphere in a coastal region than the measurements of iodine species during NAMBLEX. This is due to the point measurements of POMORIS representing actual iodine species emission directly over the coast, in contrast to the NAMBLEX measurements where DOAS instrumentation averaged the concentrations of iodine species over several kilometres from Mace Head to Croaghnakeela Island (i.e over the open ocean).

This study has incorporated the use of plume evolution in the model simulations. The emission of iodine from seaweed occurs at the lowermost region of the PBL. The volume of air that this initial iodine emission is affecting increases as the plume travels with the wind. Therefore, the volume of air affected by the emission of I_2 depends on the wind speed at that particular time. As the iodine plume travels with the wind, it grows by mixing and dispersion, rather like the evolution of smoke from a bonfire which is a point source (Figure 2.3 section 2.1 shows an exaggerated plume boundary as the air parcel travels over the emission source). This iodine plume effect was implemented into this modelling study which relied on wind speed data measured during POMORIS followed a gaussian dispersion model from (Seinfeld & Pandis) under Pasquill-Gifford stability class D.[50]

5.1 Previous Modelling Studies

A box model constrained to observations from Mace Head in Spring 1997 was used by Carslaw *et al.* to simulate measured levels of OH and HO_2. It was reported that the model over estimated levels of HO_x which could be due to their model not including chemical mechanisms for the reactions of iodine.[59] In this thesis, results have shown that the inclusion of iodine chemistry in the model is important in controlling OH and HO_2 levels at Mace Head.

Davis *et al.* conducted a global modelling study on the impacts of iodine chemistry upon tropospheric oxidants. It was suggested that iodine species could have a

significant impact upon the rate at which tropospheric ozone is destroyed.[32] In the modelling study for this thesis however, the ozone destruction rate at the time scale considered (12 seconds) is too slow for an appreciable ozone loss to occur on the timescale of these simulations.

Davis *et al.* also state that iodine chemistry influences the levels of HO_x and NO_x and this effect increases with higher levels of iodine. This effect is apparent in the modelling study conducted for this thesis. The limitations of the study conducted by Davis *et al.* are that there were no measurements to constrain the abundance of iodine species and a number of the reactions were (at that time) uncertain.[32]

McFiggans *et al.* used modelling studies to simulate IO observations which were measured using DOAS (April – May 1997 from Mace Head and June – July 1997 from Tenerife). McFiggans *et al.* noted that with the presence of iodine species, NO_x levels decrease as a result of the reaction of IO with NO_2. This effect can be seen in simulations A1-B where with the addition of iodine species, levels of NO_x decrease.[60]

Sommariva *et al.* (2006) conducted a modelling study which simulated levels of short lived species (OH and HO_2) using a model constrained to observed levels of longer-lived compounds (for example O_3 and NO_x) based upon observations during the NAMBLEX campaign. Sommariva *et al.* however, did not account for the spatial variation of iodine species across the coastal margin. I_2 was added to their model to bring the simulated IO levels up to the DOAS beam path average of a few ppt. However, this approach is not correct for the shoreline location of the observation

station. The DOAS beam path travelled from the coastal observation site at Mace Head to Croaghnakeela Island. DOAS measurements represent an average of the concentration of IO over several kilometres. Sommariva *et al.* recognised that point measurements of IO were needed.[52] Their results however did indicate that the presence of iodine species in the atmosphere (in a coastal marine environment) a significant change in the levels of HO_x and NO_x occur. A limitation of their study was that the model integrated a 15 minute time step (modelling atmospheric species every 15 minutes). The work in this thesis showed that the iodine species evolution, which occurs on a timescale of a few seconds, causes large changes in HO_x and NO_x over the intertidal region where iodine measurements were made during and POMORIS. The approach by Sommariva *et al.* does not incorporate the change at the intertidal region, or the affects experienced by HO_x and NO_x species in a few seconds. Therefore their comparisons between modelled and measured HO_x levels may have been inaccurate along with their prediction of iodine species concentrations in the coastal marine environment of Mace Head.

5.2 The Models Ability to Replicate Observations

The availability of data from the POMORIS campaign which was used in this study determined the date at which the model was constrained to. I atom data was only available for the date 29/08/07.[51] On this date, at low tide, I levels range from ~3-22 ppt, IO levels range from ~5-22 ppt and I_2 levels range from ~2-24 ppt. Figure 5.1 shows these measured concentrations along with tide height. It also shows the modelled I, IO and I_2 levels for scenario A1. The range of modelled data is in the region of the observations of IO (unsurprisingly as this was the constraint used). The

levels of modelled I and I_2 lie in the range of the measured data at around midday. Figure 5.2 shows measured iodine levels and modelled concentrations for simulation A2, compared with Figure 5.1 A2 shows that the estimated concentrated emission zone (used in A2) does not reproduce the levels of I_2 and I compared with A1. The model was manually adjusted to simulate observations of IO and with the whole emission zone the range of I and I_2 levels were also replicated. Measured levels of I_2 at around midday on 29/08/07 were 12-21 ppt. Modelled levels of I_2 at midday were 12 ppt during scenario A1 (whole emission zone and 7ppt during scenario A2 (concentrated emission zone). The measured levels of I on 29/08/07 at midday were 7-22 ppt. Scenarios A1 and A2 modelled I atoms to ~7ppt at midday.

The model's ability to replicate the measured concentrations of IO is strongly dependent on the time the air parcel takes to reach the observation station and this is dependent upon the wind speed. As the wind speed is uncertain, this is not a robust proof that measured concentrations are replicated by the model.

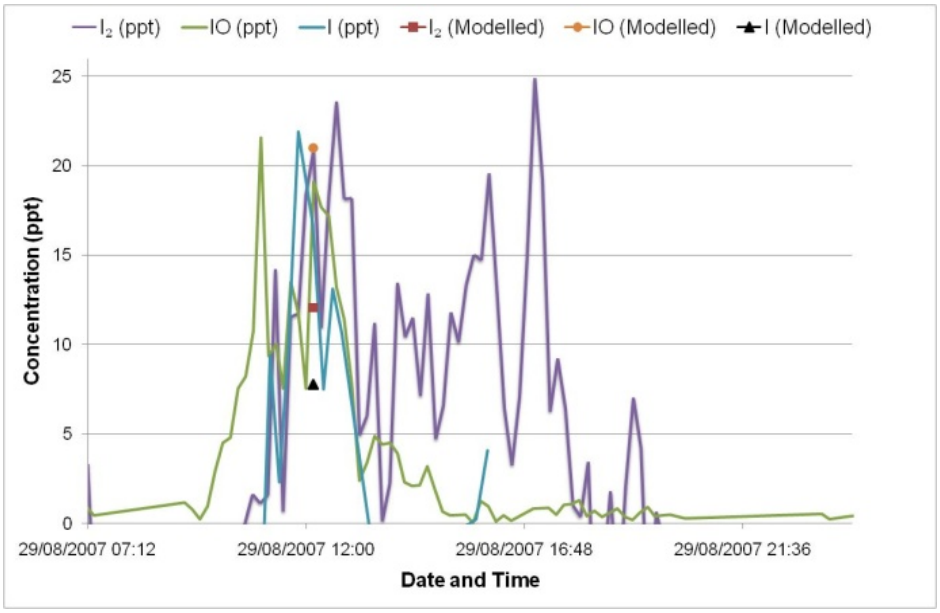

Figure 5.1: Measured I_2, IO and I atom data from POMORIS with Modelled Data for the Whole emission zone shown as a single point, (scenario A1).

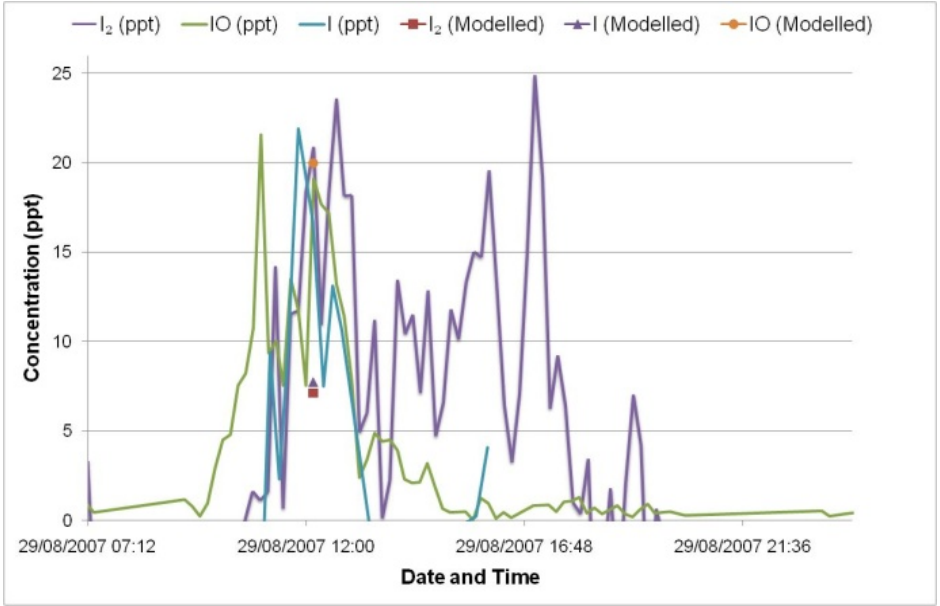

Figure 5.2: Measured I2, IO and I atom data from POMORIS with Modelled Data for the Concentrated emission zone shown as a single point, (scenario A2).

5.3 The Impact of Iodine Species on HO_x and NO_x

Compared to previous modelling studies, such as Sommariva *et al.*, the amount of I_2 injected into their air parcel during the model simulation greatly exceeded the level of I_2 used in this thesis. This is due to the model used by Sommariva incorporating a 15 minute time step. Results in this thesis have shown that HO_x and NO_x species experience the greatest impact as a result of the presence of iodine species only a few seconds after the emission of I_2. Sommariva would fail to see this effect and therefore their analysis of the iodine chemistry impacts may be inaccurate.[52]

The effect of iodine species on HO_x and NO_x species in a coastal marine environment is apparent in the first 20 seconds after the initial emission of I_2. In less than 10 seconds, in all scenarios modelled in this study (A1-C2), OH experiences a

rapid decrease in its concentration which quickly returns to 'normal' levels (those found in the base case, without any iodine) after the point of detection. Hence after the emission of I_2, HO_x and NO_x chemistry is dominated by their interaction with iodine species and in the first 20 seconds the greatest impact upon HO_x and NO_x due to the presence of iodine is apparent.

The HO_2 to OH ratio was altered when iodine species were present. IO can react with HO_2 to produce HOI and O_2. HOI can photolyse readily giving rise to I atoms and OH.[13] In agreement with previous modelling studies, the concentration of HO_2 decreased with the presence of iodine species. This occurred rapidly in the first 10 seconds and after 60 seconds levels of HO_2 were comparable to modelled levels without the presence of iodine (base case scenario).[52]

The modelled study by Sommariva *et al.* also states that there is an increase in the concentration of OH with the addition of IO reactions in the model. In the modelling study presented in this thesis, it was found that in the first 10 seconds (after the initial emission of I_2) the presence of iodine species had a much greater impact upon OH than without the presence of iodine. As previously mentioned, OH decreases extremely rapidly suggesting OH is reacting significantly with I_2. At 60 seconds the levels of modelled OH are greater than before the addition of iodine. This increase is due to the photolysis of HOI yielding OH and I atoms. In conjunction with Sommariva *et al.* this study therefore, suggests that the incorporation of iodine oxide chemistry into the model has a large and significant impact upon the local HO_x budget.[52]

Sommariva *et al.* used IO measurements taken by DOAS which were averaged IO concentrations taken over a 4 km beam path. It was suggested that point measurements of IO were needed to properly assess the impact of IO upon HO_x. Point measurements of IO (measured by LIF) taken from POMORIS were used in this modelling study giving a more accurate picture of the magnitude of the impact of IO upon HO_x. [52]

Bloss *et al.* conducted a study using calculations based on NAMBLEX data to assess the impact of iodine species upon HO_x. The conclusion of this study confirmed that the reaction of IO and HO_2 lead to a significant loss of HO_2 and that the photolysis of HOI yielded OH, which agrees with the results presented in this thesis. However, this study by Bloss *et al.* also recognised the disadvantage with using DOAS averaged measurements.[31] The results presented in chapter 3 of this thesis show the impact of iodine species upon HO_x and NO_x species considering point measurements and not measurements averaged over the open ocean.

Smith *et al.* also conducted a study using calculations based on NAMBLEX data to calculate the variation in HO_x levels with the addition of iodine species. Smith *et al.* increased the concentration of IO used in their calculations to get better agreement of calculated and measured HO_x data as DOAS underestimated the concentration of IO that would be found in a coastal environment.[14]

As indicated in the sensitivity study, the uncertainties in the iodine reaction mechanisms have a significant impact upon the simulated iodine species, HO_x and

NO_x. It is essential therefore to bear in mind that the results in this thesis are significantly dependent on the assumptions made in the chemical scheme. The distance for the emission zone of I_2 was estimated, which in conjunction with uncertainties in wind speed, lead to the results in this thesis being dependent upon these estimations. The vertical mixing of iodine species is unknown and therefore predictions in the chemical mechanisms of iodine reactions may be inaccurate based on this uncertainty. Further measurements need to be taken in order to reduce uncertainties.

5.4 The Evolution of Iodine Species

Figure 5.3 shows the evolution of I, IO, OIO and total PI when the time is extended to 35 minutes. At 10 minutes, total PI and IO have reached almost zero concentration. The rapid decrease and eventually very low levels of these iodine species would be as a result of dilution in the atmosphere. Hence in previous studies when a 15 minute time step was used, iodine species would still have been modelled (due to the model constraints) but at much lower levels than would have been be measured at 12 seconds, the detection point in scenarios A1-C2 in this study.

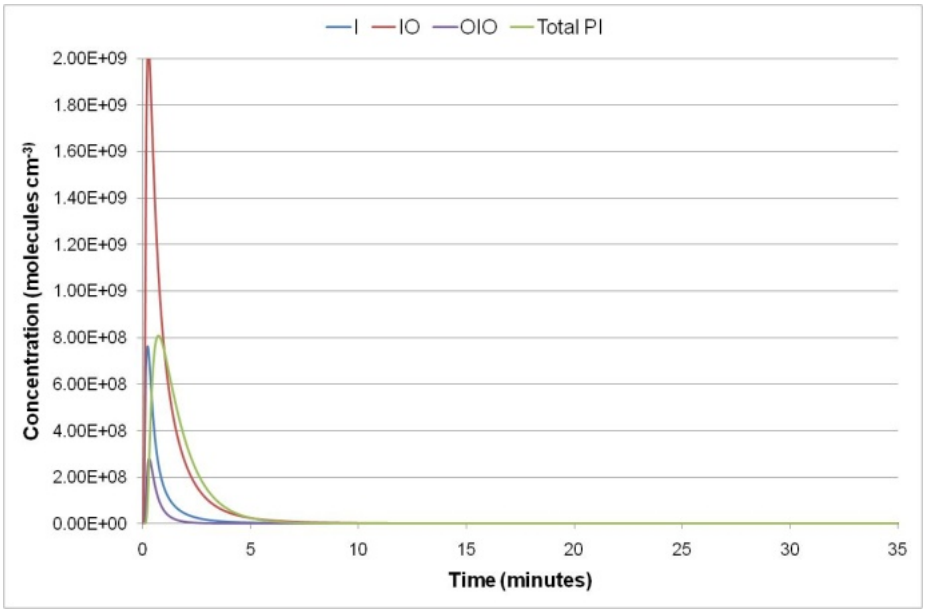

Figure 5.3: Extended Time of Scenario A1 to 30 minutes in order to see the evolution of IO_x and PI Species.

5.5 An Environment with Higher Concentrations of NO_x

Figure 5.4 shows the effect on iodine species of an increased level of NO_x. The scenarios presented earlier in chapters 3 and 4 used 50 ppt NO_x which is typical of levels found in coastal sites such as Mace Head. However, in a polluted environment typical of many more populated coastal locations, levels could be as high as 100 ppb. In a subsequent model run (scenario A1) with NO_x levels of 50 ppt, modelled concentrations of I_2 were ~10 ppt compared with ~35 ppt shown in Figure 5.4 with a higher NO_x concentration. In simulation A1 levels of IO reached 25 ppt whereas with a higher level of NO_x, Figure 5.4 shows that IO would be less than 1 ppt at the observation station (12 seconds). I was also modelled in scenario A1 to give levels of 10 ppt whereas in an environment with higher NO_x I reaches less than 5 ppt. $IONO_2$ levels rise steadily with additional NO_x. At the point of detection 8 ppt of $IONO_2$ would be measured whereas at 60 seconds the concentration of $IONO_2$ increases giving a

level of over 40 ppt. In scenario A1, $IONO_2$ would have been negligible at the point of detection and this level did not significantly rise.

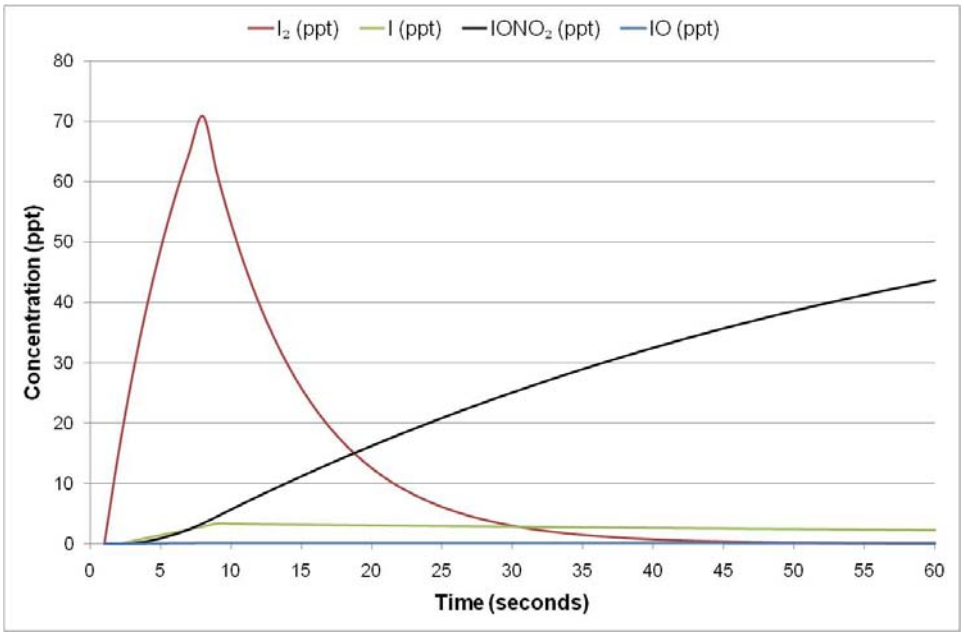

Figure 5.4: Modelled Data Showing the affect of an Increased level of NO_x (100 ppb) which would be found in Polluted Environments such as Cities and many more populated coastal locations.

Figure 5.5 shows modelled iodine species with lower levels of NO_x (50 ppt as used in scenarios A1-C2). Levels of I_2 are much lower with lower levels of NO_x, however there is a greater concentration of I atoms and a negligible amount of $IONO_2$ in contrast to Figure 5.4.

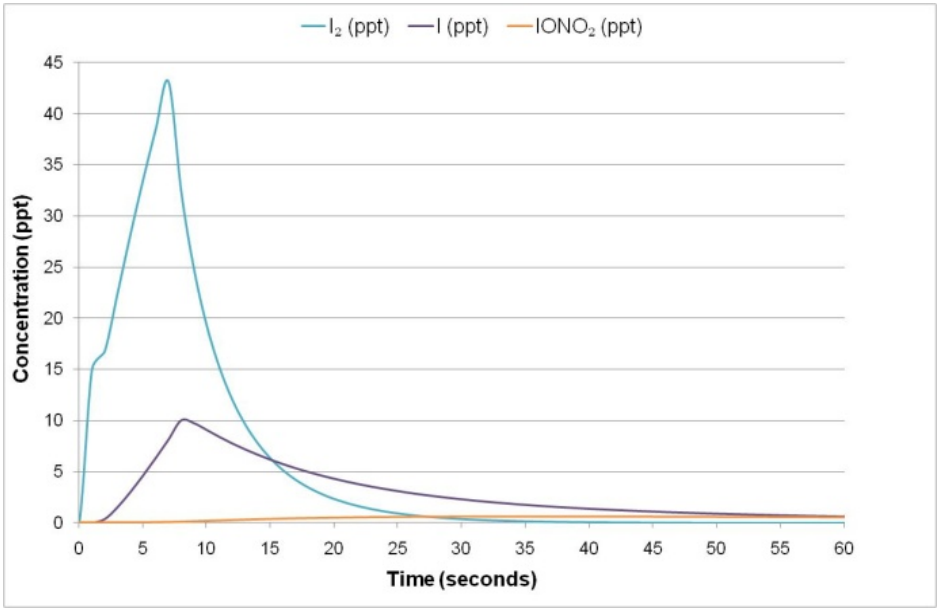

Figure 5.5: Modelled Data for Scenario A1 using 50 ppt NO_x.

5.6 Estimating the Global Iodine Emission

An estimate of the global iodine emission was obtained by using the optimised model simulations to determine how much I_2 was emitted, per unit coastline, per unit time. This was done by assuming that each 1 cm^3 box of air has either 90 or 260 ppt of I_2 (depending on whether simulation A1 or A2 is considered) is added over its transit time over the emission zone. This would be either 6 seconds or 1 second for scenario A1 and A2 respectively. The height of this box that I_2 is emitted into is from 0-32 m (as modelled) across the seaweed giving an average of 16 m. This estimation ranges from 0.2 kg per km, for scenario A1 where a total of 90 ppt I_2 was added to the model, to 3.5 per km, for scenario A2 where a total of 260 ppt I_2 was added to the model. Previous estimations by Saiz-Lopez *et al.* are much higher (1600 kg yr^{-1}) because they assumed that emission of I_2 occurred throughout the volume of air occupied by the DOAS path. The volume of the air parcel Saiz-Lopez *et al.* assumed to be full of iodine is 4.2×10^6 m^3, however the actual emission zone is much smaller

than this (as shown in the study presented in this thesis) as iodine emission only occurs at low tide along the coastal region.[40]

5.7 Iodine Species in the Aerosol Phase

Modelled results from this thesis (scenarios A1-B) indicate that the majority of iodine species in the aerosol phase exists as PI3 (I_2O_5). Figure 5.6 shows measurements of the density of aerosol particles from the NAMBLEX campaign 2002, which were measured as a volume so it has been assumed that the particle density is 1 g cm^{-3}. These data range from less than $1x10^{-9}$ to $2.25x10^{-7}$ g cm^{-3}. At 12 seconds, from scenario A1 in this thesis, the density of PI3 was $2.33x10^{-15}$ g cm^{-3}. This is a small fraction of the measurements taken during the NAMBLEX campaign. However, the majority of these observations could be sea salt. Further measurements need to be taken in order to identify the particulate matter iodine and compare these with modelled data.

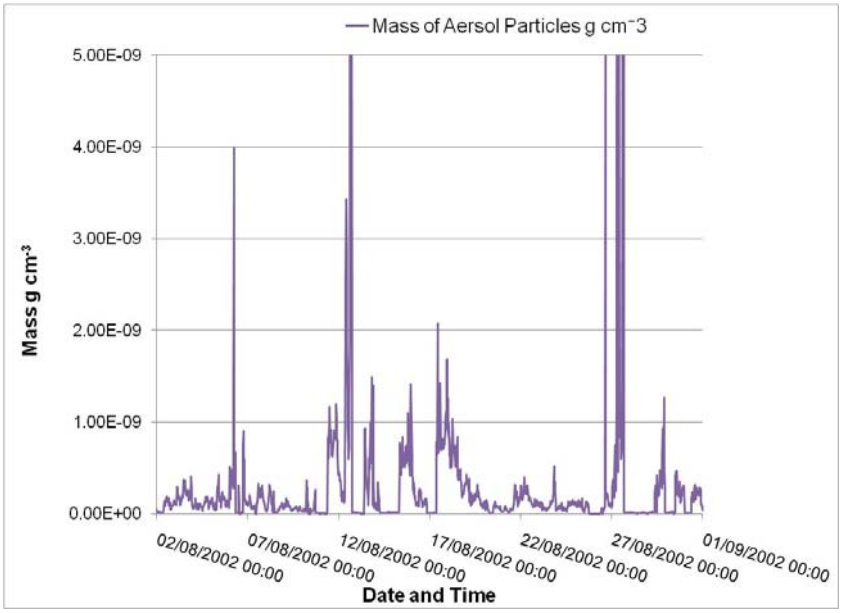

Figure 5.6: Density (g cm^{-3}) of Aerosol Particles from NAMBLEX 2002 (courtesy of W. Bloss).

5.8 Limitations of This Study

The limitations of this study are mainly that there are still uncertainties into the reaction mechanisms for iodine chemistry. The results presented in this thesis confirm that with the presence of iodine species, concentrations of HO_x and NO_x are altered significantly. However, these results are dependent on a number of assumptions and estimations used in the model. The emission zone of I_2 has been estimated in two cases, a concentrated emission zone of 10 m and a whole emission zone of 50 m. This needs to be measured in conjunction with the wind speed which at the moment remains uncertain. The magnitude of the impact of iodine upon important atmospheric radicals cannot be predicted unless further measurements are made. The observed concentrations of I_2 and IO during POMORIS (Summer 2007) vary daily, however this study mainly considered one date, 29/08/07, as this was the only date with available I atom data and further only one point in time during this day. Further measurements of I need to be made to compare more than one day of modelled data. From the sensitivity study (section 4) factors such as the total aerosol surface area need to be measured in order to simulate exact conditions for a particular day. As seen in the sensitivity study, slight changes in this value lead to significant changes in modelled levels of HO_x.

Although this study can confirm factors which affect levels of HO_x and NO_x species, the extent to which they are altered cannot be determined unless further measurements are taken.

5.9 Further Work

This study focuses on a remote location on the West coast of Ireland. Other locations could be considered in order to find out if iodine is emitted significantly over the open ocean, in which case its global MBL impact will be much greater.

The source of iodine in this study was assumed to be from littoral seaweed, it is not clear why iodine is produced in seaweed (although there are many proposed reasons in the literature) therefore any factors that affect this could affect its emission. This biological mechanism for the production of iodine within seaweed could be studied to help further knowledge of iodine emission and any potential variation with future environmental changes.

There are other potential sources of iodine such as from the pesticide methyl iodide. It appears to be the ideal replacement for CH_3Br, which was banned due to its role in stratospheric ozone depletion (see section 1.3.2), as it is capable of controlling insects and pests on just as efficiently. Degradation in soil is slightly slower than CH_3Br meaning it will be present in soil for longer periods of time.[37]

The most important difference between these two pesticides is that the average lifetime of CH_3I is 1.5 days compared to 1.7 years for CH_3Br. Therefore, CH_3I is not a stratospheric ozone depleting chemical.[37] However, it has been suggested that CH_3I is a carcinogenic and mutagenic compound, but the US EPA registered CH_3I in 2007 for one year despite receiving a letter from concerned scientists about the pesticide.

CH_3I is more expensive than CH_3Br but research has shown that 80-275 pounds per acre will be sufficient to control pests, which is half the amount of CH_3Br applied. However, if soil needs venting to reduce phytotoxicity there could be delays in planting. As CH_3I has a longer half life than CH_3Br (in soil) this could mean more CH_3I is emitted in to the atmosphere.[38] Therefore, iodine species may affect HO_x and NO_x species in other environments (ie. non-coastal arable regions) which could have different implications for the atmosphere.

6 CONCLUSION

This thesis used modelling studies constrained to data obtained from the NAMBLEX campaign which took place in the coastal marine environment of Mace Head, Ireland. The level of I_2 emission within the model was manually optimised in order to replicate observations of IO from the campaign POMORIS, which also took place at Mace Head.

The modelled results indicate that the presence of iodine species in an environment such as that found at Mace Head, has a significant effect on the levels of HO_x and NO_x species which in turn affects the oxidising capacity of the atmosphere. The changes experienced by HO_x and NO_x are apparent in the first few seconds after the emission of I_2.

However, the results presented in chapter 3 rely on the assumptions and estimations that have been made in the chemical scheme for iodine species. Further research needs to be done in order to confirm the accuracy of the magnitude of the affect of iodine species upon HO_x and NO_x.

7 REFERENCES

[1] R. C. Sommariva, The University of Leeds, **2004**.
[2] R. P. Wayne, Chemistry of Atmospheres, Oxford university press, Oxford, **2006**.
[3] L. J. Carpenter *American Chemical Society*. **2003**, 103, 4953-4967.
[4] L. Rosenfeld *Journal of Chemical Education* **2000**, 77 984-987.
[5] J. M. Plane, A. Saiz-Lopez, G. McFiggans, P.I. Williams, S.M. Ball, M. Bitter, R.L. Jones, C. Hongwei, and T. Hoffmann *Atmospheric Chemistry and Physics*. **2006**, 6, 883 - 895.
[6] V. M. Kerminen, H. Vuollekoski, T. Anttila, S.L. Sihto, M. Vana, M.Ehn, H. Korhonen, G. McFiggans, C. D. O'Dowd, M. Kulmala *Journal of Geophysical Research*. **2009**, 114, 13.
[7] J. J. Orlando, G.P. Brasseur, G.S.Tyndall, Atmospheric Chemistry and Global Change, OUP USA, **1999**.
[8] R. B. Stull, An Introduction to Boundary Layer Meteorology, Kluwer Academic publishers, **1998**.
[9] S. I. Rasool, Chemistry of The lower atmosphere, Plenum Pub. Co., **1973**.
[10] M. Z. Jacobson, Atmospheric Pollution: History, Science and Regulation, Cambridge University Press, **2002**.
[11] W. J. Bloss *Royal Society of Chemistry*. **2007**.
[12] www.metoffice.gov.uk/science
[13] P. Monks *Chemical Society Reviews*. **2005**, 34, 376-395.
[14] J. D. Lee, S. C. Smith, W. J. Bloss, G. P. Johnson, T. Ingham, and D. E. Heard *Atmospheric Chemistry and Physics*. **2006**, 6.
[15] M. Jenkins S. Saunders, C. Bloss in Master Chemical Mechanism, www.mcm.leeds.ac.uk/mcm/
[16] European Parliment and The Council of the European Union *Official Journal of the European Union*. **2004**, 143, 10.
[17] R. Harrison, Pollution: Causes and effects and Control, Royal Society of Chemistry.
[18] R. V. Glasow *Nature*. **2008**, 453, 1195-1196.
[19] J. M. C. Plane, R. W. Saunders *Environmental Chemistry*. **2005**, 2.
[20] P. Brimblecombe, Air Composition and Chemistry, Cambridge University Press, **1995**.
[21] S.M. Murphy, J.H. Kroll, R.C.Flagen, J.S. Seinfeld *Environmental Science Technology* **2006**, 40, 1869-1877
[22] J. Colls, Air Pollution: An Introduction.
[23] P. J. Crutzen, R. Von Glasow *Treatise on Geochemistry*. **2003**, 4, 21-64.
[24] C. E. Kolb *Nature*. **2002**, 417.
[25] C. D. O'Dowd, Jimenez, J. L., Bahreini, R., Flagan, R. C., Seinfeld, J. H., Hämeri, K., Pirjola, L., Kulmala, M., Jennings, S. G. and Hoffmann, T *Nature* **2002**, 417.
[26] Jacob, Introduction to Atmospheric Chemistry.
[27] J. Lelielveld, P. J. Crutzen *Earth Planet Science*. **2001**, 29, 17-45.
[28] G. McFiggans et al. *Atmospheric Chemistry and Physics* **2004**, 4.
[29] J. A. Shillito, A. Saiz-Lopez, H. Coe, J.M.C. Plane *Atmospheric Chemistry and Physics*. **2006**, 6, 1513-1528.
[30] M. E. Tucceri, T.J. Dillon, J.N. Crowley *Physical Chemistry Chemical Physics*, 10.

[31] J. D. Lee, W. J. Bloss, G. P. Johnson, R. Sommariva, D. E. Heard, A. Saiz-Lopez, J. M. C. Plane, G. McFiggans, H. Coe, M. Flynn, P. Williams, A. R. Rickard, and Z. L. Fleming *Geophysical Research Letters*. **2005**, 32.
[32] J. C. D. Davis, S. Liu, S. McKeen, A . Bandy, D. Thomton, F. Rowland, D . Blake *Journal of Geophysical Research*. **1996**, 101, 3135-2147.
[33] J. M. C. Plane, A. Saiz-Lopez, A.S. Mahajan, P.S. Anderson, S.J.B. Bauguitte, A.E. Jones, H.K. Roscoe, R.A. Salmon, W.J. Bloss, J.D. Lee, and D.E. Heard *Atmospheric Chemistry and Physics*. **2008**, 8, 887-900.
[34] P. S. Honaganahalli *Atmospheric Environment*. **2000**, 34, 3511-3523.
[35] J.N. Seiber, G. Honninger, U. Platt. **2002**.
[36] A. Camponogara M. L. Gullino, G. Gasparrini, V. Rizzo, C. Clini, A. Garibaldi *The American Phytopathological Society*. **2003**, 87, 1012-1021.
[37] L. O. Ruzo *Pest Management Science*. **2006**, 62, 99-113.
[38] D. Wang, S. R. Yates , F. F. Ernst and J. Gan *Environmental Science Technology*. **1997**, 31, 1136-1143.
[39] Oregon State University, Methyl Bromide Technical Fact Sheet, The National Pesticide Information Centre and the United States Environmental Protection Agency
[40] J. M. C. Plane, A. Saiz-Lopez *Geophysical Research Letters*. **2004**, 31, 4.
[41] K. A. Read, D. E. Heard, J. Methven, S. Al-Haider, W. J. Bloss, G. P. Johnson, M. J. Pilling, P. W. Seakins,, R. S. S. C. Smith, J. C. Stanton, T. J. Still, T. Ingham, B. Brooks, G. De Leeuw, A. V. Jackson,, R. M. J. B. McQuaid, M. H. Smith, L. J. Carpenter, N. Carslaw, J. Hamilton, J. R Hopkins, J. D. Lee,, R. M. P. A. C. Lewis, D. J. Wevill, N. Brough, T. Green, G. Mills, S. A. Penkett, J. M. C. Plane,, D. W. A. Saiz-Lopez, P. S. Monks, Z. Fleming, A. R. Rickard, M. R. Alfarra, J. D. Allan7, K. Bower,, M. C. H. Coe, M. Flynn, G. McFiggans, M. Gallagher, E. G. Norton, C. D. O'Dowd, J. Shillito,, G. V. D. Topping, P. Williams, M. Bitter, S. M. Ball, R. L. Jones, I. M. Povey, S. O'Doherty,, A. A. P. G. Simmonds, R. P. Kinnersley, D. C. S. Beddows, M. Dall'Osto, R. M. Harrison,, M. R. H. R. J. Donovan, S. G. Jennings, C. Noone, and G. Spain *Atmospheric Chemistry and Physics*. **2006**, 6, 2241-2271.
[42] M. Pilling, P. W. Seakins, *Reaction Kinetics*, Oxfor Science Publications, **1995**
[43] O. Pikelnaya, J. Stutz, S. C. Hurlock, S. Trick, S. Pechtl, R. Von Glasow *Geophysical Research Letters*. **2007**, 34.
[44] MCPA Software in Facsimile, www.mcpa-software.com/facsimileframe.html.
[45] J. R. Hopkins, A.C Lewis, L.J. Carpenter, J. Stanton, K.A. Read and M.J Pilling *Atmospheric Chemistry and Physics*. **2005**, 5, 1963-1974.
[46] R. R. Friedl, S.P Sander, D.M. Golden, M.J. Kurylo, G.K. Moortgat, H. Keller-Rudek, P.H. Wine, A.R. Ravishankara, C. E. Kolb, M.J. Molina, B.J. Finlayson-Pitts, R.E. Huie, V.L. Orkin *Jet Propulsion Laboratory, California Institute of Technology*. **2006**, Publication 06-2.
[47] D. L. Baulch, R.L. Atkinson, R.A. Cox, J.N. Crowley, R.F Hanson, R.G. Hynes, M.E Jenkin, M.J Rossi, J. Troe *Atmospheric Chemistry and Physics*. **2007**, 7, 981-1191.
[48] J. D. Lee, W.J. Bloss, D.E. Heard, A. Saiz-Lopez, J.M.C. Plane, S. Bauguitte, R. Salmon and A.E. Jones *Geophysical Research Abstracts*. **2006**, 8.
[49] A. M. Hough *AERE Report*. **1988**, R-13259.
[50] S. N. Pandis, J.H. Sienfeld, Atmospheric Chemistry and Physics, Wiley, **1998**.
[51] T. Ingham, C.S.E. Bale, R. Commane D.E. Heard, W.J. Bloss *Journal of Atmospheric Chemistry*. **2008**, 60, 51-70.
[52] W. J. Bloss, R. Sommariva, N. Brough, N. Carslaw, M. Flynn, A.L. Haggerstone, D. E. Heard, J. R. Hopkins, J. D. Lee, A. C. Lewis, G. McFiggans, P. S. Monks, S. A. Penkett, M. J. Pilling, J. M. C. Plane, K. A. Read, A. Saiz-Lopez, A. R. Rickard, and P. I. Williams *Atmospheric Chemistry and Physics*. **2006**, 6.

[53] M. J. Pilling, R. Sommariva, W. J. Bloss, D. E. Heard, J. D. Lee1, Z. L. Fleming, P. S. Monks, J. M. C. Plane, A. Saiz-Lopez, S. M. Ball, M. Bitter, R. L. Jones, N. Brough, S. A. Penkett, J. R. Hopkins, A. C. Lewis, and K. A. Read *Atmospheric Chemistry and Physics*. **2007**, 7, 587-598.
[54] S. H. Ashworth, J.C. Gómez-Martin, A.S Mahajan, J.M.C Plane *Geophysical Research Letters*. **2009**, 36.
[55] D. M. Rowley, J. C. Mossinger, and R. A. Cox *Atmospheric Chemistry and Physics*. **2002**, 2.
[56] S. H. Ashworth, J. M. C. Plane, D.M. Joseph *Physical Chemistry Chemical Physics*. **2007**, 9, 5599.
[57] C. E. Canosa-Mas, C.S.E. Bale, D.E. Shallcrossb, R.P. Wayne *Physical Chemistry Chemical Physics*. **2005**, 10.
[58] B. J. Allan, J. M. C. Plane *Journal of Chemical Physics*. **2002**, 106.
[59] D. J. Creasey, N. Carslaw, D. E. Heard, P. J. Jacobs, J. D. Lee, A. C. Lewis, J. B. McQuaid, and M. J. Pilling *Journal of Geophysical Research*. **2002**, 107, 4190.
[60] J. M. C. Plane, G. McFiggans, B.J. Allan, L.J. Carpenter, H.C.C. O'Dowd *Journal of Geophysical Research*. **2000**, 105, 14371-14385.

8 Appendices

8.1 DMS Oxidation

The DMS Oxidation Scheme developed by Carslaw *et al*. (1999) as used by Sommariva *et al*. (2006) was used (see below for reaction scheme), with the halogen monoxide-mediated DMS oxidation steps listed below added.

Rate Expression	Equation
1.2D-11*EXP(-260/TEMP)	DMS + OH = CH3SCH2O2 + FL203
(1.7D-42*EXP(7810/TEMP)*O2)/(1+5.5D-31*EXP(7460/TEMP)*O2)	DMS + OH = DMSOH + FL204
1.9D-13*EXP(500/TEMP)	DMS + NO3 = CH3SCH2O2 + HNO3
3.3d-10	DMS + Cl = CH3SCH2O2 + HCl
4.1D-12*EXP(180/TEMP)	CH3SCH2O2 + NO = CH3S + HCHO + NO2
1.5D-13*EXP(1250/TEMP)	CH3SCH2O2 + HO2 = CH3SCH2OOH
3.0E-13*RO2	CH3SCH2O2 = CH3S + HCHO
2.00E-12	CH3SCH2O2 + NO3 = CH3S + HCHO + NO2
J<41>	CH3SCH2OOH = CH3S + HCHO + OH
1.5D-11	CH3SCH2OOH + OH = CH3SCH2O2
6.10D-11	CH3SCH2O2 + CH3S = CH3S + HCHO + CH3SO
4.00D-12	CH3SCH2O2 + CH3SO = CH3S + HCHO + CH3SO2
2.50D-13	CH3SCH2O2 + CH3SO2 = CH3S + HCHO + CH3SO3
2e-12*O2	DMSOH = DMSO + HO2
1e-12*O2	DMSOH = CH3SOH + CH3O2
1e-12*O2	DMSOH = DMSOHOO
1.7D-17*O2	CH3SOH = CH3SO3H
1.1E-10	CH3SOH + OH = CH3SO + H2O
3.4E-12	CH3SOH + NO3 = CH3SO + HNO3
88	DMSOHOO = CH3SO3H + CH3O2
2.0D-12*EXP(290/TEMP)	CH3S + O3 = CH3SO
2.1D-11*EXP(320/TEMP)	CH3S + NO2 = CH3SO + NO
1.70D-16*EXP(1510/TEMP)*O2	CH3S = CH3SOO
6.40D-11	CH3S + NO3 = CH3SO + NO2
1.8D11*EXP(-3950/TEMP)	CH3SOO = CH3S
4.10D-12*EXP(180/TEMP)	CH3SOO + NO = CH3SO + NO2
8.00D-11	CH3SOO + CH3S = CH3SO + CH3SO
2.2D-11*EXP(0/TEMP)	CH3SOO + NO2 = CH3SO + NO3
6.00D-13	CH3SO + O3 = CH3SO2
8.0D-12	CH3SO + NO2 = CH3SO2 + NO
1.70D-16*EXP(1510/TEMP)*O2	CH3SO = CH3SOO2

8.00D-12	CH3SO + NO3 = CH3SO2 + NO2
1.8D11*EXP(-3950/TEMP)	CH3SOO2 = CH3SO
4.10D-12*EXP(180/TEMP)	CH3SOO2 + NO = CH3SO2 + NO2
5.00D13*EXP(-(8656/TEMP + 1))	CH3SO2 = SO2 + CH3O2
3.00D-13	CH3SO2 + O3 = CH3SO3
4.00D-12	CH3SO2 + NO2 = CH3SO3 + NO
1.70D-16*EXP(1510/TEMP)*O2	CH3SO2 = CH3SO2OO
1.8D11*EXP(-3950/TEMP)	CH3SO2OO = CH3SO2
4.10D-12*EXP(180/TEMP)	CH3SO2OO + NO = CH3SO3 + NO2
2.50D-13	CH3SO2 + HO2 = CH3SO3 + OH
2.50D-13	CH3SO2 + CH3O2 = CH3SO3 + CH3O
1.00D-14	CH3SO2 + NO3 = CH3SO3 + NO2
5.0D13*EXP(-(11071/TEMP+1))	CH3SO3 = SO3 + CH3O2
1.60D-15	CH3SO3 + HCHO = CH3SO3H + HO2 + CO
6.80D-14	CH3SO3 + DMS = CH3SO3H + DMSO2
5.00D-11	CH3SO3 + HO2 = CH3SO3H
3.00D-16	CH3SO3 + H2O2 = CH3SO3H + HO2
3.00D-16	CH3SO3 + CH3OOH = CH3SO3H + CH3O2
5.8E-11	DMSO + OH = DMSOHO
1.7E-13	DMSO + NO3 = DMSO2
1.5E7	DMSOHO = CH3SO2H + CH3O2
1.2E-12*O2	DMSOHO = DMSO2 + HO2
1.6E-11	CH3SO2H + OH = CH3SO2
1.00D-13	CH3SO2H + NO3 = CH3SO2 + HNO3
1.00D-12	DMSO2 + OH = DMSO2OO
4.1E-12*EXP(180/TEMP)	DMSO2OO + NO = CH3SO2 + HCHO + NO2
1.5D-13*EXP(1250/TEMP)	DMSO2OO + HO2 = DMSO2OOH
1.50D-11	DMSO2OOH + OH = DMSO2OO
J<41>	DMSO2OOH = CH3SO2 + HCHO + OH
3E-13*RO2	DMSO2OO = CH3SO2 + HCHO

8.2 Halogen Reaction Scheme

The model includes a detailed chemical scheme for iodine inorganic / organic reactions. Gas-phase kinetic parameters were taken from the literature, drawing upon the NASA/JPL and IUPAC evaluations (Sander *et al*., 2006; Atkinson *et al*., 2007) where possible. An issue is that a number of the kinetic and photochemical parameters are either poorly understood or simply unmeasured; we have estimated these where necessary, as detailed in the notes to Table 2, and considered potential variations in the rate and products of some of the key processes in a sensitivity study.

Supplementary Table S2: Halogen Scheme: Gas-Phase Kinetic Parameters

Reaction	*Rate Expression*	*Reference*	*Note*
$I + O_3 \rightarrow IO + O_2$	$k = 2.1\times10^{-11}\exp(-830/T)$	Atkinson *et al*., 2007	
$I + HO_2 \rightarrow HI + O_2$	$k = 1.5\times10^{-11}\exp(-1090/T)$	Atkinson *et al*., 2007	
$OH + HI \rightarrow I + H_2O$	$k = 1.6\times10^{-11}\exp(440/T)$	Atkinson *et al*., 2007	
$OH + I_2 \rightarrow HOI + I$	$k = 2.1\times10^{-10}$	Atkinson *et al*., 2007	
$NO_3 + I_2 \rightarrow I + IONO_2$	$k = 1.5\times10^{-12}$	Atkinson *et al*., 2007	1
$NO_3 + HI \rightarrow HNO_3 + I$	$k = 1.3\times10^{-12}\exp(-1830/T)$	Atkinson *et al*., 2007	
$I + NO_2 \rightarrow INO_2$	$k_0 = 3.0\times10^{-31}(T/300)^{-1.0}$ $k_\infty = 6.6\times10^{-11}$, $F_c = 0.6$	Sander *et al*., 2006	
$INO_2 \rightarrow I + NO_2$	k =0.14 s^{-1} (at 268 K)	Van den Bergh & Troe, 1976	2
$INO_2 + INO_2 \rightarrow I_2 + 2NO_2$	$k = 4.7\times10^{-13}\exp(-1670/T)$	Atkinson *et al*., 2007	
$I + NO \rightarrow INO$	$k_0 = 1.8\times10^{-32}(T/300)^{-1.0}$ $k_\infty = 1.7\times10^{-11}$, $F_c = 0.6$	Sander *et al*., 2006	
$INO \rightarrow I + NO$	k =0.087 s^{-1} (at 268 K)	Van den Bergh	2

		& Troe, 1976	
INO + INO → I_2 + NO + NO	$k = 8.4\times10^{-11}\exp(-2620/T)$	Atkinson *et al.*, 2007 or JPL	
IO + IO → 2I + O_2	$k = 0.11 \times 5.4\times10^{-11}\exp(180/T)$	Atkinson *et al.*, 2007	3
IO + IO → I + OIO	$k = 0.38 \times 5.4\times10^{-11}\exp(180/T)$	Atkinson *et al.*, 2007	3
IO + IO → I_2O_2	$k = 0.51 \times 5.4\times10^{-11}\exp(180/T)$	Atkinson *et al.*, 2007	3
IO + HO_2 → HOI + O_2	$k = 1.4\times10^{-11}\exp(540/T)$	Atkinson *et al.*, 2007	
OH + HOI → IO + H_2O	$k = 1.0\times10^{-10}$		4
IO + CH_3O_2 → CH_3O + IOO	$k = 2.0\times10^{-12}$	Dillon et al., 2006	5
IO + NO → I + NO_2	$k = 7.15\times10^{-12}\exp(300/T)$	Atkinson *et al.*, 2007	
IO + NO_2 → $IONO_2$	$k_0 = 6.5\times10^{-31}(T/300)^{-3.5}$ $k_\infty = 7.6\times10^{-12}(T/300)^{-1.5}$, $F_c = 0.6$	Sander *et al.*, 2006	
$IONO_2$ → IO + NO_2	$k = 2.1\times10^{15}\exp(-13670/T)$	Kaltsoyannis & Plane, 2008	6
IO + NO_3 → OIO + NO_2	$k = 9\times10^{-12}$	Dillon *et al.*, 2008	
I + NO_3 → IO + NO_2	$k = 1\times10^{-12}$	Dillon *et al.*, 2008	
IO + OIO → I_2O_3	$k = 5\times10^{-11}$	Gomez-Martin et al., 2007	7
OIO + OIO → I_2O_4	$k = 1.5\times10^{-10}$	Gomez-Martin et al., 2007	7.1
OIO + I_2O_3 → PI_1	$k = 1.5\times10^{-10}$	Gomez-Martin et al., 2007	7.1
OIO + I_2O_4 → PI_2	$k = 1.5\times10^{-10}$	Gomez-Martin et al., 2007	7.1

$I_2O_2 + O_3 \rightarrow I_2O_3 + O_2$	$k = 1.0\times10^{-12}$	Saunders & Plane, 2005	7.2
$I_2O_3 + O_3 \rightarrow I_2O_4 + O_2$	$k = 1.0\times10^{-12}$	Saunders & Plane, 2005	7.2
$I_2O_4 + O_3 \rightarrow PI_3$	$k = 1.0\times10^{-12}$	Saunders & Plane, 2005	7.2
$I_2O_2 \rightarrow IO + IO$	$k = 10\ s^{-1}$	Kaltsoyannis & Plane, 2008	7.3
$I_2O_4 \rightarrow OIO + OIO$	$k = 0.1\ s^{-1}$	Kaltsoyannis & Plane, 2008	7.3
$NO + OIO \rightarrow IO + NO_2$	$k = 1.1\times10^{-12}\exp(542/T)$	Plane *et al*., 2006	
$OH + OIO \rightarrow PI_4\ (HIO_3)$	$k = 2.2\times10^{-10}\exp(243/T)$	Plane *et al*., 2006	8
$IO + DMS \rightarrow I + DMSO$	$k = 1.2\times10^{-14}$	Sander *et al*., 2006	

Atkinson *et al*., 2007 = 2007 IUPAC Evaluation; Sander *et al*., 2006 = NASA/JPL Evaluation 15-06.

1: I_2+NO_3. Products assumed to be I+$IONO_2$ following Atkinson et al. (2007) on enthalpy arguments. Effect of alternative product channel (IO + INO_2, as adopted by Saiz-Lopez *et al*., 2008) considered in sensitivity study.

2: INO and INO_2 thermal decomposition calculated via the formation rate constants given, plus temeprature-dependent equilibrium constant expressions from van den Burgh & Troe, 1976: $K_{eq}(I + NO \leftrightarrow INO) = 10^{-5.70}\times\exp(9160/T)$ and $K_{eq}(I + NO_2 \leftrightarrow INO_2) = 10^{-6.43}\times\exp(9560/T)$, both in atm^{-1}.

3: IO + IO: Overall rate constant and OIO+I channel from Atkinson *et al*. (2007); branching ratio for $2I + O_2$ / I_2O_2 channels from Bloss *et al.* (2001). See also comments below (note 10.3).

4: OH + HOI – Rate constant estimated with reference to OH + HOCl, O + HOCl and O + HOBr.

5: Base-case for the IO + CH_3O_2 reaction is “slow” kinetics ($k = 2\times10^{-12}$; Dillon *et al*., 2006) and formation of CH_3O + IOO (*i.e.* the CH_3OOOI intermediate, likely decomposing to CH_3O + IOO and hence HCHO + HO_2 + I + O_2 in the atmospheric boundary layer) with unit yield. Sensitivity studies described in the text consider the potential impact of a higher rate constant (*e.g.* Bale *et al*., 2005) and alternative product channels, *e.g.* via the CH_3OOIO channel to CH_3O + OIO (Drougas & Kosmas, 2007).

6: Thermal decomposition rate reported by Kaltsoyannis & Plane (2008) adopted; this is based upon revised RRKM analysis coupled to laboratory kinetic data for the forward reaction obtained by Allen & Plane (2002), and supersedes the decomposition rate determined in a similar manner in the earlier paper.

7: *Higher Iodine Oxides*

In addition to thermal reactions with other chemical families (NO_x, BrO_x *etc*.) , iodine oxides are thought to polymerise through a series of addition reactions potentially involving IO, OIO, I_2O_2 and higher iodine oxides. Considerable laboratory evidence exists for the near-gas kinetic removal of OIO in fast iodine kinetics studies (*e.g.* Bloss *et al*., 2001; Ingham *et al*., 2000), and also for the formation of particles of bulk composition I_2O_5 / I_4O_9 (*e.g.* Burkholder *et al*., 2004; McFiggans *et al*., 2004), but details of the nucleation process are far from understood. In this paper, we adopt an iodine source selected to replicate the observed levels of IO subject to the chemical mechanism, which must therefore include a representation of the process for the removal of active iodine into the condensed phase. Whilst given our current level of understanding any specific mechanism is unlikely to be totally correct, the modelled effects of iodine chemistry upon HO_x and NO_x (the focus of the paper) should be robust as the levels of IO (which effectively constrains most of the other iodine-inorganic chemistry interactions) match those observed. The details of the mechanism adopted for removal of active iodine into the condensed phase will however impact upon the iodine source required to generate a given level of IO; this is considered further in the sensitivity studies.

Here we adopt a mechanism drawn from recent laboratory and theoretical studies, in which two routes to higher iodine oxides are considered: Sequential addition of ozone to I_2O_2/I_2O_3/I_2O_4 (Saunders & Plane, 2005), and polymerisation of OIO (Gomez-Martin *et al*., 2007). We consider any species above I_2O_4 to be thermally and photolytically stable on the timescale of these simulations, i.e. to irreversibly incorporate into particulate iodine: PI_1,PI_2 and PI_3, which may in reality be identified with I_3O_5 or I_2O_5 + I, I_3O_6 or I_2O_5 + IO, and I_2O_5+O_2 respectively. We also consider the thermal stability of I_2O_2, I_2O_3 and I_2O_4, based upon the calculations of

Kaltsoyannis and Plane (2008), and the photolysis of OIO, I_2O_2, I_2O_3 and I_2O_4 as described above. (These assumptions are explored further in the sensitivity study).

7.1 Gomez-Martin *et al*. (2007) infer limits for an association reaction between OIO and small (n = 1 - 4) OIO polymers of (1.2 – 3) $\times$ 10^{-10} $molec^{-1}cm^3s^{-1}$. Here we choose a mid-range value of 1.5 $\times$ 10^{-10} $molec^{-1}cm^3s^{-1}$, and apply this to the reaction of OIO with itself, I_2O_3 and I_2O_4.

7.2 : Oxidation of I_2O_2, I_2O_3 and I_2O_4 by ozone. The rate constant adopted (1×10^{-12} $molec^{-1}cm^3s^{-1}$) is based upon the analysis of Saunders & Plane (2005), although recent calculations (Kaltsoyannis & Plane, 2008) indicate that the reaction may be slower, and the calculated short thermal lifetime for I_2O_2 indicates that IO/OIO recombination is probably the dominant route to I_2O_3 / I_2O_4 in the atmosphere).

7.3 Kaltsoyannis & Plane calculate the lifetimes of I_2O_2, I_2O_3 and I_2O_4 with respect to thermal decomposition to be of the order of 0.1, 10^8 and 10 seconds respectively (293 K); appropriate (temperature-independent) decomposition rates for I_2O_2 and I_2O_4 are therefore included. I_2O_2 is assumed to be IOIO; IOOI is found to dissociate promptly.

8: The reaction of OIO with OH is assumed to form HIO_3, which is stable (Plane *et al*., 2006), and is assumed to contribute to particulate iodine: PI_4.

Other reactions considered, but discounted as their effects are negligible, were :

-Termolecular I atom recombination

-Oxygen atom / halogen reactions (O + I_2, O + IO)

-Halogen monoxide / ozone reactions (IO + O_3)

In addition to the standard MCM3.1 kinetic and photochemical schemes for HOx, NOx and VOC chemistry, the model included an iodine reaction mechanism, comprising photolysis reactions, thermal kinetic processes, heterogeneous uptake and deposition. Each section is briefly described below.

8.3 Photolysis rates

Photolysis rates for HOx/NOx/VOC species were calculated according to the algorithms of Hough *et al*. (1988) as implemented in the MCM (version 3.1). For species not included in the MCM (those listed in Table 1 - iodine compounds) photolysis rates were calculated from the measured values of $j(NO_2)$, using a scaling factor determined as the mean ratio of the photolysis rate in question to $j(NO_2)$, calculated using clear-sky actinic flux data from TUV (Madronich & Flocke, 1998) for conditions appropriate to the Mace Head measurements (local noon, SZA = xx), and absorption cross sections / photolysis quantum yields as described in Table 1.

Table 1: Photolysis rates for halogen species

Reaction	Quantum Yield Note	Mean $j(x)$ / $j(NO_2)$	Cross sections / Qm yields used	Note
I_2 + hv		20.3	Atkinson *et al*., 2007	
IO + hv		18.3	Bloss *et al*., 2001	
OIO + hv	Φ (I+O_2) = 1	51.6	Cox *et al*., 1999 / Joseph *et al*., 2005	9
$IONO_2$ + hv	Φ (I+NO_3) = 1	0.556	Joseph & Plane, 2007	10
I_2O_2 + hv	Φ (IO) = 2	0.556		11
I_2O_3 + hv	Φ (IO+OIO) = 1.0	0.556		11
I_2O_4 + hv	Φ (OIO+OIO) = 1.0	0.556		11
INO_2 + hv	Φ (I+NO_2) = 1	0.319	Sander *et al*., 2006	
INO + hv		3.71	Sander *et al*., 2006	
HOI + hv		1.12	Atkinson *et al*., 2007	
HI + hv		6.89×10^{-3}	Atkinson *et al*., 2007	

Atkinson *et al*., 2007 = 2007 IUPAC Evaluation; Sander *et al*., 2006 = NASA/JPL Evaluation 15-06.

Notes

9: OIO absorption spectrum from Cox *et al*. (1999) scaled to match 567 nm cross section determined by Joseph *et al*. (2005). Quantum yield for photolysis assumed to be 100 % production of I + O_2 following Gómez-Martin *et al*. (2009); alternative lower photolysis quantum yields (5% I + O_2) following Joseph *et al*. (2005) and Tucceri *et al*. (2006) were considered in the sensitivity study.

10: $IONO_2$ cross sections have been reported by Mossinger *et al*. (2002) and by Joseph *et al*. (2007). The latter data are significantly smaller at long (> 360 nm) wavelengths, corresponding to roughly one order of magnitude difference in photolysis rate. The more recent values of Joseph & Plane, taken from the table within their paper, are used here, with unit photolysis yield of I + NO_3 adopted; the magnitude of the $IONO_2$ cross sections is considered in the sensitivity study.

11: Definitive cross-sections are not available for I_2O_2, I_2O_3 or I_2O_4. Following the laboratory estimates of Bloss *et al*. (2001) and Gómez-Martín *et al*. (2005), and *ab initio* results (Kaltsoyannis & Plane, 2008) we assume the absorption spectrum is equal to that of $IONO_2$ – this corresponds to a midday photolysis rate of 8×10^{-3} s^{-1} for these species (corresponding $j(NO_2) = 1.85\times10^{-2}$ s^{-1}). The sensitivity of the model results to this assumption is evaluated in the sensitivity study section.

8.4 Heterogeneous Processes

Heterogeneous uptake of reactive gas-phase species is simulated using the free molecular approach, assuming an aerosol surface area of $5x10^{-6}$ cm^2 cm^{-3}, based upon the earlier observations during the NAMBLEX campaign (ref). Reaction probabilities used are summarised in Table 3 - uptake to the condensed phase is assumed to lead to permanent removal of the gas-phase species: reactions in the condensed phase are not incorporated. In reality the uptake and subsequent hydrolysis of species such as $IONO_2$ and HOI upon aqueous aerosol ultimately leads to re-release of molecular (inter)halogen molecules such as IBr and ICl (Vogt *et al*., 1999), in our model this process will be subsumed within the overall halogen source term; an estimate of its maximum potential magnitude is obtained by assuming that uptake to the aerosol is the rate-limiting step for iodine recycling, which then proceeds with unit efficiency. Dry deposition was included for all non-constrained species with a deposition velocity of 0.5 cms^{-1} : the calculated plume height was used for the boundary layer height term in the deposition loss calculation.

Supplementary Table S3: Heterogeneous reaction probabilities

Species	Reaction Probability γ	Reference
HONO	0.04	JPL 15-06
PNA	0.1	JPL 15-06
HNO_3	0.1	JPL 15-06
N_2O_5	0.04	JPL 15-06
HO_2	0.2	Jacob, 2000
CH_3O_2	0.04	Jacob, 2000
HI	0.2	JPL 15-06
HOI	0.5	Mossinger & Cox, 2001 / Braban et al. (2007) / JPL 15-06
$IONO_2$	0.2	Assumed as $BrONO_2$
INO_2	0.1	Assumed
IO	0.5	Assumed
OIO, I_2O_2, I_2O_3, I_2O_4	1	Assumed
PI_n	1	Assumed

Other Processes Incorporated (in addition to standard MCM3.1 kinetics / photochemistry):

Kinetic Adjustments

Minor adjustments have been made to the gas-phase kinetic scheme to account for revisions subsequent to the 2001 IUPAC evaluation upon which most of the MCM3.1 kinetics are based :

1. $O^1D + N_2/O_2/H_2O$: Current (MCM3.1) value is Same as IUPAC (2004). This does not include latest data from Boulder/Leeds groups => Use JPL 15-06 Kinetics:

$O(^1D) + O_2 \rightarrow O(^3P) + O_2$	$k = 3.3\times10^{-11}\exp(55/T)$	Sander *et al*., 2006
$O(^1D) + N_2 \rightarrow O(^3P) + N_2$	$k = 2.15\times10^{-11}\exp(110/T)$	Sander *et al*., 2006
$O(^1D) + H_2O \rightarrow OH + OH$	$k = 1.63\times10^{-10}\exp(60/T)$	Sander *et al*., 2006

References

Allan, B. J. And J. M. C. Plane, A Study of the Recombination of IO with NO_2 and the Stability of INO_3: Implications for the Atmospheric Chemistry of Iodine, J. Phys. Chem. A 106, 8634-8641, 2002.

Aranda, A., Le Bras, G., La Verdet, G., and Poulet, G. : The BrO + CH3O2 reaction : Kinetics and role in the atmospheric ozone budget, Geophys. Res. Lett. 24, 2745-2748, 1997.

Atkinson, R.L., Baulch, D.L., Cox, R.A., Crowley, J.N., Hampson, R.F., Hynes, R.G., Jenkin, M.E., Rossi, M.J., Troe, J.: Evaluated kinetic and photochemical data for atmospheric chemistry: Volume III – gas phase reactions of inorganic halogens. Atmos. Chem. Phys. **7**, 981-1191, 2007.

Bale, C. S. E., Canosa-Mas, C. E., Shallcross, D. E., and Wayne, R. P.: A discharge-flow study of the kinetics of the reactions of IO with CH_3O_2 and CF_3O_2, Phys. Chem. Chem. Phys., 7, 2164-2172, 2005.

Braban, C. F., J. W. Adams, D. Rodriguez, R. A. Cox, J. N. Crowley and G. Schuster, Heterogeneous reactions of HOI, ICl and IBr on sea salt and sea salt proxies, Phys. Chem. Chem. Phys. 9, 3136-3148, 2007.

W.J. Bloss, D.M. Rowley, R.A. Cox and R.L. Jones, Kinetics and Products of the IO Self-Reaction, J. Phys. Chem. A, 105, 7840-7854, 2001.

Burkholder, J. B., J. Curtuis, A. R. Ravishankara and E. R. Lovejoy, Laboratory studies of the homogeneous nucleation of iodine oxides, Atmos. Chem. Phys. 4, 19-34, 2004.

Carslaw, N., D. J. Creasey, D. E. Heard, A. C. Lewis, J. B. McQuaid, M. J. Pilling, P. S. Monks, B. J. Bandy and S. A. Penkett, Modeling OH, HO_2 and RO_2 radicals in the marine boundary layer 1. Model construction and comparison with field measurements, *J. Geophys. Res.* 104, 30241, 1999.

R.A. Cox, W.J. Bloss, R.L. Jones and D.M. Rowley, OIO and the Atmospheric Cycle of Iodine, Geophys. Res. Lett., 26, 1857-1860, 1999

Davison, B., Hewitt, C. N., O'Dowd, C., Lowe, J. A., Smith, M. H., Schwikowski, M., Baltensperger, U. and Harrison, R. M., Dimethyl sulphide, methane sulphonic acid and the physiochemical aerosol properties in Atlantic air from the United Kingdom to Halley Bay, J. Geophys. Res. 101, 22855-22867, 1996.

Dillon, T. J., Tucceri, M. E., and Crowley, J. N.: Laser induced fluorescence studies of iodine oxide chemistry, Phys. Chem. Chem. Phys., 8, 5185-5198, 2006.

Dillon, T. J., Tucceri, M. E., Sander, R. and J. N. Crowley, LIF Studies of Iodine Oxide Chemistry Part 3. Reactions IO + $NO_3 \rightarrow$ OIO + NO_2, I + $NO_3 \rightarrow$ IO + NO_2 and CH_2I + $O_2 \rightarrow$ (products): implications for the chemistry of the marine atmosphere at night, *Phys. Chem. Chem. Phys.* 10, 1540, 2008.

Drougas, E. And A. M. Kosmas, Ab Intitio Characterization of (CH_3IO_3) Isomers and the CH_3O_2 + IO Reaction Pathways, J. Phys. Chem. A 111, 3402-3408, 2007.

Enami, S., Yamanaka, T., Hashimoto, S., Kawasaki, M., Nakano, Y., and Ishiwata, T.: Kinetic Study of IO Radical with RO_2 (R = CH_3, C_2H_5, and CF_3) Using Cavity Rind-Down Spectroscopy, J. Phys. Chem. A, 110, 9861-9866, 2006.

Enami, S., Yamanaka, T., Nakayama, T., Hashimoto, S., Kawasaki, M., Shallcross, D. E., Nakano, Y., and Ishiwata, T.: A Gas-Phase Kinetic Study of the Reaction between Bromine Monoxide and Methylperoxy Radicals at Atmospheric Temperatures, J. Phys. Chem. A, 111, 3342-3348, 2007.

Gómez-Martin, J. C., Ashworth, S. H., Mahajan, A. S. and Plane, J. M. C., Photochemistry of OIO: Laboratory study and atmospheric implications, *Geophys. Res. Lett.* 36, doi:10.1029/2009GL037642, 2009.

Gómez Martin, J. C., P. Spietz and J. P. Burrows, Kinetic and Mechanistic Studies of the I_2/O_3 Photochemistry, *J. Phys. Chem. A*, 111, 306, 2007.

Hough A. M. The calculation of photolysis rates for use in global tropospheric modelling studies. AERE Report R-13259 (HMSO) London, 1988.

Ingham, T., M. Cameron and J. N. Crowley, Photodissociation of IO (355 nm) and OIO (532 nm): quantum Yields for $O(^3P)$ and $I(^2P_J)$ Production, J. Phys. Chem. A, 104, 8001-8010, 2000.

Jacob, D. J., Heterogeneous chemistry and tropsopheric ozone, Atmos. Environ. 34, 2131-2159, 2000.

D.M. Joseph, S.H. Ashworth and J.M.C. plane, The absorption cross-section and photochemistry of OIO, J. Photochem. Photobiol. A: Chemistry, 176, 68-77, 2005.

Joseph, D. M., S. H. Ashworth & J. M. C. Plane, On the photochemistry of $IONO_2$: absorption cross section (240-370 nm) and photolysis product yields at 248 nm, Phys. Chem. Chem. Phys. 9, 5599-5607, 2007.

Kaltsoyannis, N. And J. M. C. Plane, Quantum chemical calculations on a selection of iodine containing species (IO, OIO, INO_3, $(IO)_2$, I_2O_3, I_2O_4 and I_2O_5) of importance in the atmosphere, Phys. Chem. Chem. Phys. 10, 1723-1733, 2008.

Madronich, S. and S. Flocke, The role of solar radiation in atmospheric chemistry, in Handbook of Environmental Chemistry (P. Boule, ed.), Springer_Verlag, Heidelberg, pp. 1-26, 1998.

Maricq, M. M., J. J. Szente, E. W. Kaiser and J. Shi, Reaction of Chlorine Atoms with Methyl and Ethylperoxy Radicals, J. Phys. Chem. 98, 2083-2089, 1994.

Mössinger, J. C., and R. A. Cox (2001), Heterogeneous reaction of HOI

with sodium halide salts, J. Phys. Chem. A, 105, 5165– 5177.

Mössinger, J. C., D. M. Rowley and R. A. Cox, The UV-visible absorption cross-sections of $IONO_2$, Atmos. Chem. Phys. 2, 227-234, 2002.

Orlando, J. J. and G. S. Tyndall, Rate Coefficients for the Thermal Decomposition of $BrONO_2$ and the Heat of Formation of $BrONO_2$, J. Phys. Chem. 100, 19398-19405, 1996.

Plane, J. M. C., D. M. Joseph, B. J. Allan, S. H. Ashworth and J. S. Francisco, An Experimental and Theoretical Study of the Reactions OIO + NO and OIO + OH, J. Phys. Chem. 110, 93-100, 2006.

D.M. Rowley, W.J. Bloss, R.A. Cox and R.L. Jones, Kinetics and Products of the IO + BrO Reaction, J. Phys. Chem. A, 105, 7855-7864, 2001.

Sander, S. P., Friedl, R. R., Golden, D. M., Kurylo, M. J., Moortgat, G. K., Keller-Rudek, H., Wine, P. H., Ravishankara, A. R., Kolb, C. E., Molina, M. J., Finlayson-Pitts, B. J., Huie, R. E., and Orkin, V. L.: Chemical Kinetics and Photochemical Data for Use in Atmospheric Studies - Evaluation Number 15, NASA-JPL Publication 06-2, Jet Propulsion Laboratory, California Institute of Technology, Pasadena, CA, 2006.

Saunders, R. W. And J. M. C. Plane, Formation Pathways and Composition of Iodine Oxide Ultra-Fine Particles, Environ. Chem. 2, 299-303, 2005.

R. Sommariva, M. Pilling, W. Bloss, D. Heard, N. Carslaw, A. Lewis, G. McFiggans, J. Plane, A. Saiz-Lopez, P. Monks, OH and HO_2 chemistry during NAMBLEX: roles of oxygenates, halogen oxides and heterogeneous uptake, *Atmos. Chem. Phys.*, 6, 1135, 2006.

Tucceri, M. E., Hölscher, D., Rodriguez, A., Dillon, T. J., and J. N. Crowley, Absorption cross section and photolysis of OIO, Phys. Chem. Chem. Phys. 8, 834-846, 2006.

Van den Bergh, H. and J. Troe, Kinetic and thermodynamic properties of INO and INO_2 intermediate complexes in iodine recombination, J. Chem. Phys. 64, 736-742, 1976.

Vogt, R., R. Sander, R. Von Glasow and P. J. Crutzen, Iodine Chemistry and its Role in Halogen Activation and Ozone Loss in the Marine Boundary Layer: A Model Study, J. Atmos. Chem. 32, 375-395, 1999.

8.5 Sections of the Model Used in this Study

Iodine Emission

*Set time point for start and end of I2 emission zone ;

*And I2 source strength (top hat function) ;

?I2START=1800;

?I2END=1806;

?I2ADDITION=15*PPT;

?TIME = STTIME ;

?TIME1 = 0.00E+00 ;

* The Master Chemical Mechanism 3.1 (Oct 2003) ;

* 46 inorganic reactions 13523 organic reactions ; constructed by ;Sam Saunders - Leeds University/UWA ; Mike Jenkin - Imperial College ; Claire Bloss - Leeds University;

* Inorganic Chemistry IUPAC 2001

* thermal gas-phase reactions ;

% 5.60D-34*O2*N2*((TEMP/300)@-2.6) : O = O3 + FL1 ;

% 6.00D-34*O2*O2*((TEMP/300)@-2.6) : O = O3 + FL2 ;

% 8.00D-12*EXP(-2060/TEMP) : O + O3 = ;

% KMT01 : O + NO = NO2 + FL3 ;

% 5.50D-12*EXP(188/TEMP) : O + NO2 = NO + FL4 ;

% KMT02 : O + NO2 = NO3 + FL5 ;

% 3.20D-11*O2*EXP(67/TEMP) : O1D = O + FL6 ;

% 1.80D-11*N2*EXP(107/TEMP) : O1D = O + FL7 ;

% 1.40D-12*EXP(-1310/TEMP) : NO + O3 = NO2 + FL8 ;

% 1.40D-13*EXP(-2470/TEMP) : NO2 + O3 = NO3 + FL9 ;

% 3.30D-39*EXP(530/TEMP)*O2 : NO + NO = NO2 + NO2 + FL10 ;

% 1.80D-11*EXP(110/TEMP) : NO + NO3 = NO2 + NO2 + FL11 ;

% 4.50D-14*EXP(-1260/TEMP) : NO2 + NO3 = NO + NO2 + FL12 ;

% KMT03 % KMT04 : NO2 + NO3 = N2O5 + FL13 ;

% 2.20D-10*H2O : O1D = OH + OH + FL14 ;

% 1.70D-12*EXP(-940/TEMP) : OH + O3 = HO2 + FL15 ;

% 7.70D-12*EXP(-2100/TEMP) : OH + H2 = HO2 + FL16 ;

% 1.30D-13*KMT05 : OH + CO = HO2 + FL17 ;

% 2.90D-12*EXP(-160/TEMP) : OH + H2O2 = HO2 + FL18 ;

% 2.03D-16*((TEMP/300)@4.57)*EXP(693/TEMP) : HO2 + O3 = OH + FL19 ;

% 4.80D-11*EXP(250/TEMP) : OH + HO2 = ;

% 2.20D-13*KMT06*EXP(600/TEMP) : HO2 + HO2 = H2O2 + FL20 ;

% 1.90D-33*M*KMT06*EXP(980/TEMP) : HO2 + HO2 = H2O2 + FL21 ;

% KMT07 : OH + NO = HONO + FL22 ;

% KMT08 : OH + NO2 = HNO3 + FL23 ;

% 2.00D-11 : OH + NO3 = HO2 + NO2 + FL24 ;

% 3.60D-12*EXP(270/TEMP) : HO2 + NO = OH + NO2 + FL25 ;

% KMT09 % KMT10 : HO2 + NO2 = HO2NO2 + FL26 ;

% 1.90D-12*EXP(270/TEMP) : OH + HO2NO2 = NO2 + FL27 ;

% 4.00D-12 : HO2 + NO3 = OH + NO2 + FL28 ;

% 2.50D-12*EXP(-260/TEMP) : OH + HONO = NO2 + FL29 ;

% KMT11 : OH + HNO3 = NO3 + FL30 ;

% 4.00D-32*EXP(-1000/TEMP)*M : O + SO2 = SO3 + FL31 ;

% KMT12 : OH + SO2 = HSO3 + FL32 ;

% 1.30D-12*EXP(-330/TEMP)*O2 : HSO3 = HO2 + SO3 + FL33 ;

* photolysis reactions ;

% J<1> : O3 = O1D ;

% J<2> : O3 = O ;

% J<3> : H2O2 = OH + OH ;

% J<4> : NO2 = NO + O + FL34 ;

% J<5> : NO3 = NO ;

% J<6> : NO3 = NO2 + O ;

% J<7> : HONO = OH + NO + FL35 ;

% J<8> : HNO3 = OH + NO2 + FL36 ;

* Methane Subset;

% 9.65D-20*TEMP@2.58*EXP(-1082/TEMP) : OH + CH4 = CH3O2 + FL37 ;

% 9.60D-12*EXP(-1350/TEMP) : CL + CH4 = CH3O2 ;

% 1.82D-13*EXP(416/TEMP)*0.335*RO2 : CH3O2 = CH3OH ;

% 1.82D-13*EXP(416/TEMP)*0.335*RO2 : CH3O2 = HCHO ;

% 3.00D-12*EXP(280/TEMP)*0.001 : CH3O2 + NO = CH3NO3 ;

% 1.82D-13*EXP(416/TEMP)*0.33*RO2 : CH3O2 = CH3O ;

% 3.80D-13*EXP(780/TEMP) : CH3O2 + HO2 = CH3OOH ;

% KMT13 : CH3O2 + NO2 = CH3O2NO2 ;

% 3.00D-12*EXP(280/TEMP)*0.999 : CH3O2 + NO = CH3O + NO2 ;

% KRO2NO3*0.40 : CH3O2 + NO3 = CH3O + NO2 ;

% 6.01D-18*TEMP@2*EXP(170/TEMP) : CH3OH + OH = HO2 + HCHO ;

% J<12> : HCHO = H2 + CO ;

% 1.20D-14*TEMP*EXP(287/TEMP) : OH + HCHO = HO2 + CO ;

% 5.80D-16 : NO3 + HCHO = HNO3 + CO + HO2 ;

% J<11> : HCHO = CO + HO2 + HO2 ;

% 1.00D-14*EXP(1060/TEMP) : OH + CH3NO3 = HCHO + NO2 ;

% J<51> : CH3NO3 = CH3O + NO2 ;

% 7.20D-14*EXP(-1080/TEMP)*O2 : CH3O = HCHO + HO2 ;

% 1.90D-12*EXP(190/TEMP) : OH + CH3OOH = CH3O2 ;

% 1.00D-12*EXP(190/TEMP) : OH + CH3OOH = HCHO + OH ;

% J<41> : CH3OOH = CH3O + OH ;

% KMT14 : CH3O2NO2 = CH3O2 + NO2 ;

* End of Subset. No. of Species = 17, No. of Reactions = 22 ;

```
* MCM3.1 Subset generated for the following species:   ;
*   CH3OH HCHO CH3CHO ;
% 5.55D-12*EXP(311/TEMP) : OH + CH3CHO = CH3CO3 ;
% J<13> : CH3CHO = CH3O2 + HO2 + CO ;
% KNO3AL : NO3 + CH3CHO = HNO3 + CH3CO3 ;
% 1.00D-11*0.7*RO2 : CH3CO3 = CH3O2 ;
% 1.00D-11*0.3*RO2 : CH3CO3 = CH3CO2H ;
% KAPHO2*0.71 : CH3CO3 + HO2 = CH3CO3H ;
% KAPHO2*0.29 : CH3CO3 + HO2 = CH3CO2H + O3 ;
% KFPAN : CH3CO3 + NO2 = PAN ;
% KAPNO : CH3CO3 + NO = NO2 + CH3O2 ;
% KRO2NO3*1.60 : CH3CO3 + NO3 = NO2 + CH3O2 ;
% 1.82D-13*EXP(416/TEMP)*0.33*RO2 : CH3O2 = CH3O ;
% 8.00D-13 : CH3CO2H + OH = CH3O2 ;
% J<41> : CH3CO3H = CH3O2 + OH ;
% 3.70D-12 : CH3CO3H + OH = CH3CO3 ;
% KBPAN : PAN = CH3CO3 + NO2 ;
% 9.50D-13*EXP(-650/TEMP) : PAN + OH = HCHO + CO + NO2 ;
% 1.00D-14*EXP(1060/TEMP) : OH + CH3NO3 = HCHO + NO2 ;
% J<41> : CH3OOH = CH3O + OH ;

* Aerosol loss rates ;
% 0.04*CHONO*SURFAREA/4 :    HONO = LOSS + FL45 ;
% 0.1*CHO2NO2*SURFAREA/4 :  HO2NO2=LOSS + FL46 ;
% 0.1*CHNO3*SURFAREA/4 :      HNO3 = LOSS + FL47 ;
% 0.04*CN2O5*SURFAREA/4 :    N2O5 = LOSS + FL48 ;
% 0.2*CHO2*SURFAREA/4 :         HO2 = LOSS + FL49 ;
% 0.04*CCH3O2*SURFAREA/4 :  CH3O2 = LOSS + FL50 ;
% 0.15*CHI*SURFAREA/4 :           HI = LOSS + FL51 ;
```

% 0.15*CHBR*SURFAREA/4 : HBR = LOSS + FL52 ;

% 0.5*CHOI*SURFAREA/4 : HOI = LOSS + FL53 ;

% 0.6*CHOBR*SURFAREA/4 : HOBr = LOSS + FL54 ;

% 0.2*CIONO2*SURFAREA/4 : IONO2 = LOSS + FL55;

% 0.2*CBRONO2*SURFAREA/4 : BRONO2 = LOSS + FL56 ;

% 0.1*CINO2*SURFAREA/4 : INO2 = LOSS + FL57 ;

% 0.1*CBRONO*SURFAREA/4 : BRONO = LOSS + FL58 ;

% 0.5*CIO*SURFAREA/4 : IO = LOSS + FL59 ;

% 1*COIO*SURFAREA/4 : OIO = LOSS + FL60 ;

% 1*CI2O2*SURFAREA/4 : I2O2 = LOSS + FL61 ;

% 1*CI2O3*SURFAREA/4 : I2O3 = LOSS + FL62 ;

% 1*CI2O4*SURFAREA/4 : I2O4 = LOSS + FL63 ;

% 1*CPI*SURFAREA/4 : PI1 = LOSS + FL64 ;

% 1*CPI*SURFAREA/4 : PI2 = LOSS + FL65 ;

% 1*CPI*SURFAREA/4 : PI3 = LOSS + FL66 ;

% 1*CPI*SURFAREA/4 : PI4 = LOSS + FL67 ;

*Halogen Photochemistry ;

% JI2 : I2 = I + I + FL70;

% JIBR : IBR = I + BR + FL71;

% JBR2 : BR2 = BR + BR + FL72 ;

% JBRO : BRO = BR + O3 + FL73 ;

% JBRONO2 : BRONO2 = BR + NO3 + FL74 ;

% (JBRONO*0.5) : BRONO = BR + NO2 + FL75 ;

% (JBRONO*0.5) : BRONO = BRO + NO + FL76 ;

% JHOBR : HOBR = OH + BR + FL77 ;

% JHOI : HOI = OH + I + FL78 ;

% JIO : IO = I + O3 + FL79 ;

% JOIO : OIO = I + O2 + FL80 ;

*Base case for Mace Head is OIO+hv=I+O2 at 100 % ;

% JIONO2: IONO2 = I + NO3 + FL81 ;

% JINO2 : INO2 = I + NO2 + FL82 ;

% JINO : INO = I + NO + FL83 ;

% JI2O2 : I2O2 = IO + IO + FL84 ;

% JI2O3 : I2O3 = IO + OIO + FL85 ;

% JI2O4 : I2O4 = OIO + OIO + FL86 ;

% JHI : HI = HO2 + I + FL87 ;

*Halogen Kinetics ;

% 1.7E-11*EXP(-800/TEMP) : BR + O3 = BRO + FL90 ;

% 7.7E-12*EXP(-450/TEMP) : BR + HO2 = HBR + FL91 ;

% 6.7E-12*EXP(155/TEMP) : OH + HBR = BR + FL92;

% 2E-11*EXP(240/TEMP) : OH + BR2 = HOBR + BR + FL93;

% 7.7E-12*EXP(-580/TEMP) : BR + HCHO = HBR + HO2 + CO + FL94 ;

% 1.8E-11*EXP(-460/TEMP): BR + CH3CHO = HBR + CH3CO3 + FL95 ;

% KBRONO : BR + NO2 = BRONO + FL96 ;

% 2.7E-12 : BRO + BRO = BR + BR + FL97 ;

% 2.9E-14*EXP(840/TEMP) : BRO + BRO = BR2 + FL98 ;

% 4.5E-12*EXP(500/TEMP) : BRO + HO2 = HOBR + FL99 ;

% 5E-11 : OH + HOBR = BRO + FL100 ;

% 4.6E-13*EXP(798/TEMP) : BRO + CH3O2 = HOBr + CO + FL101 ;

*Nominal is HOBr + CH2O2 ie HOBr + CO (+H2O) ;

% 8.7E-12*EXP(260/TEMP) : BRO + NO = BR + NO2 + FL102 ;

% KBRONO2 : BRO + NO2 = BRONO2 + FL103 ;

% 2.8E13*EXP(-12360/TEMP) : BRONO2 = BRO + NO2 + FL104 ;

% 2.1E-11*EXP(-830/TEMP) : I + O3 = IO + FL107 ;

% 1.5E-11*EXP(-1090/TEMP) : I + HO2 = HI + FL108 ;

% 1.6E-11*EXP(440/TEMP) : OH + HI = I + FL109;

% 2.1E-10 : OH + I2 = HOI + I + FL110 ;

% 1.5E-12 : NO3 + I2 = IONO2 + I + FL111 ;

% 1.3E-12*EXP(-1830/TEMP) : NO3 + HI = HNO3 + I + FL112 ;

% (0.25*1e-10) : OH + IBR = HOBR + I + FL113 ;

% (0.75*1e-10) : OH + IBR = HOI + BR + FL114;

% KINO2 : I + NO2 = INO2 + FL115;

% 0.14 : INO2 = I + NO2 + FL116 ;

% 4.7E-13*EXP(-1670/TEMP) : INO2 + INO2 = NO2 + NO2 + I2 + FL117;

% KINO : I + NO = INO + FL118;

% 0.087 : INO = I + NO + FL119 ;

% 8.4E-11*EXP(-2620/TEMP) : INO + INO = I2 + NO + NO + FL120;

% 9E-12 : IO + NO3 = OIO + NO2 ;

% 1E-12 : I + NO3 = IO + NO2 ;

% (0.11*5.4E-11*EXP(180/TEMP)) : IO + IO = I + I + FL121 ;

% (0.38*5.4E-11*EXP(180/TEMP)) : IO + IO = OIO + I + FL122 ;

% (0.51*5.4E-11*EXP(180/TEMP)) : IO + IO = I2O2 + FL123 ;

% 1.4E-11*EXP(540/TEMP) : IO + HO2 = HOI + FL124;

% 1e-10 : OH + HOI = IO + FL125;

% 2E-12 : IO + CH3O2 = HCHO + HO2 + I + FL126 ;

*Nominal is 2e-12 and CH3 + IOO ie HCHO+HO2+I ;

% 7.15E-12*EXP(300/TEMP) : IO + NO = I + NO2 + FL127 ;

% KIONO2 : IO + NO2 = IONO2 + FL128 ;

% 2.1E15*EXP(-13670/TEMP) : IONO2 = IO + NO2 + FL129 ;

* 2.1E15*EXP(-13670/TEMP) is from Kaltsoyannis and Plane 2008 ;

% (0.2*1.5E-11*EXP(510/TEMP)) : IO + BrO = I + BR + FL130 ;

% (0.8*1.5E-11*EXP(510/TEMP)) : IO + BrO = OIO + BR + FL131 ;

% 5E-11 : IO + OIO = I2O3 + FL134 ;

% 1.5E-10 : OIO + OIO = I2O4 + FL135 ;

% 1.5E-10 : OIO + I2O3 = PI1 + FL136 ;

% 1.5E-10 : OIO + I2O4 = PI2 + FL137 ;

% 1.0E-12 : I2O2 + O3 = I2O3 + FL138 ;

% 1.0E-12 : I2O3 + O3 = I2O4 + FL139 ;

% 1.0E-12 : I2O4 + O3 = PI3 + FL140 ;

% 10 : I2O2 = IO + IO + FL141 ;

% 0.1 : I2O4 = OIO + OIO + FL142 ;

% 1.1E-12*EXP(542/TEMP) : OIO + NO = IO + NO2 + FL143 ;

% 2.2E-10*EXP(243/TEMP) : OIO + OH = PI4 + FL144;

% 1.4E-14*EXP(950/TEMP) : BRO + DMS = BR + DMSO + FL145 ;

% 9.0E-11*EXP(-2390/TEMP) : BR + DMS = HBR + CH3SCH2O2 + FL146 ;

% 1.2E-14 : IO + DMS = I + DMSO + FL147 ;

*Other SO2 Chemistry ;

% 4.00D-32*EXP(-1000/TEMP)*M : O + SO2 = SO3 +FL150 ;

% KMT12 : OH + SO2 = HSO3 + FL151 ;

% 1.30D-12*EXP(-330/TEMP)*O2 : HSO3 = HO2 + SO3 + FL152 ;

% 1.2D-15*H2O : SO3 = SLOSS + FL153 ;

*Additional iodine reactions to consider in sensit study ;

* % I + IONO2 = I2 + NO3 ;

* % O3 + IONO2 = OIO + NO2 ;

* % I + IO = I2O ;

* % I + I2O = I2 + IO ;

*Dry Deposition ;

% 0.5/BLH : O3 = LOSS + FL154 ;

% 0.5/BLH : HONO = LOSS + FL155 ;

% 0.5/BLH : HNO3 = LOSS + FL156 ;

% 0.5/BLH : HO2NO2 = LOSS + FL157 ;

% 0.5/BLH : N2O5 = LOSS + FL158 ;

% 0.5/BLH : HI = LOSS + FL159 ;

% 0.5/BLH : HBR = LOSS + FL160 ;

% 0.5/BLH : HOI = LOSS + FL161 ;

% 0.5/BLH : HOBR = LOSS + FL162 ;

% 0.5/BLH : IONO2 = LOSS + FL163 ;

% 0.5/BLH : INO2 = LOSS + FL164 ;

% 0.5/BLH : BRONO2 = LOSS + FL165 ;

% 0.5/BLH : BRONO = LOSS + FL166 ;

% 0.5/BLH : OIO = LOSS + FL167 ;

% 0.5/BLH : I2O2 = LOSS + FL168 ;

% 0.5/BLH : I2O3 = LOSS + FL169 ;

% 0.5/BLH : I2O4 = LOSS + FL170 ;

% 0.5/BLH : PI1 = LOSS + FL171 ;

% 0.5/BLH : PI2 = LOSS + FL172 ;

% 0.5/BLH : PI3 = LOSS + FL173 ;

% 0.5/BLH : PI4 = LOSS + FL174 ;

% 1/BLH : SO2 = LOSS + FL175 ;

% 1/BLH : HSO3 = LOSS + FL176 ;

% 1/BLH : SO3 = LOSS + FL177 ;